# INVESTIGATION OF MAGNETIC AND MAGNETOELASTIC PROPERTIES OF ORIENTED COBALT FERRITE

A thesis submitted in partial fulfillment of the requirements for the degree of

**Doctor of Philosophy** 

in

**MATERIALS ENGINEERING** 

By

**SRINIVAS INDLA** 

(11ETMM07)

*Under the supervision of* 

Prof. DIBAKAR DAS



# SCHOOL OF ENGINEERING SCIENCES AND TECHNOLOGY UNIVERSITY OF HYDERABAD

**HYDERABAD-500046** 

**INDIA** 

2021



#### **DECLARATION**

I, hereby declare that the thesis entitled "Investigation of magnetic and magnetoelastic properties of oriented cobalt ferrite" submitted to University of Hyderabad for the award of Doctor of Philosophy in Materials Engineering is original and was carried out by me during my tenure as a Ph.D. scholar under the supervision of Prof. Dibakar Das. I also declare that this thesis has not been submitted previously in part or in full to this University or any other University or Institution for the award of any degree or diploma.

Srinivas Indla

Reg. no.: 11ETMM07

School of Engineering Sciences and Technology

University of Hyderabad.



#### **CERTIFICATE**

This is to certify that the dissertation entitled, "Investigation of magnetic and magnetoelastic properties of oriented cobalt ferrite", submitted by Srinivas Indla, bearing registration number 11ETMM07 in partial fulfilment of the requirements for the award of Doctor of Philosophy in School of Engineering Sciences and Technology is a bonafide work carried out by him under my supervision and guidance.

This dissertation is free from plagiarism and has not been submitted previously in part or in full to this or any other University or Institute for the award of any degree or diploma.

#### Outcome of the dissertation

- A. Parts of this dissertation have published in the following publications:
- 1. S Indla et al., Journal of Alloys and Compounds, 779 (2019) 886-891
- B. Parts of this dissertation have presented at the following conferences:
- 1. Srinivas Indla et al., Poster presented in ICAFM-2014, NIIST, Kerala.
- 2. Srinivas Indla et al., Poster presented in ICC-2015, Bikaner, Rajasthan.
- Srinivas Indla et al., Oral and poster presentation in One day workshop on Advanced Sensor Materials and Devices-2019, ARCI

He was exempted from doing coursework (recommended by Doctoral Committee) on the basis of the following courses passed during his M.Tech. (Int M.Tech./ Ph.D) and the M.Tech. Degree was awarded:

Course No.	Title of the Course	Credits	Pass/Fail
MT401	Thermodynamics and Phase Equilibria	4	Pass
MT402	Concepts of Materials Science	4	Pass
MT403	Metal Forming: Science and Technology	4	Pass
MT404	Characterization of Materials	4	Pass

MT405	Seminar	2	Pass
MT406	Design and Selection of Engineering Materials	4	Pass
MT407	Advanced Engineering Mathematics	2	Pass
MT 408	Materials Processing and Characterization Laboratory	4	Pass
MT451	Materials & Technologies for Energy Systems	4	Pass
MT452	Diffusion, Phase Transformations and Kinetics	4	Pass
MT453	Modeling and Simulation	4	Pass
MT454	Powder Metallurgy and Ceramics	4	Pass
MT455	Surface Engineering	4	Pass
MT456	Polymer Science and Technology	2	Pass
MT457	Laboratory	4	Pass
MT458	Seminar	2	Pass
MT460	Dissertation	18	Pass
MT601	Research Methodology	4	Pass

Supervisor

(Prof. DIBAKAR DAS)
Prof. Dibakar Das
DEAN
School of Engineering Sciences and Technology
University of Hyderabad 500 046.

School of Engineering Sciences and Technology University of Hyderabad 500 046.

#### **ACKNOWLEDGEMENTS**

Ph.D. tenure had been a wonderful journey of my life with lot of surprise and delight. It not only taught me science through various experiments but also it provided me an opportunity to learn a lot from different people, tradition and culture. It provided me with an essence of research and life through various concepts and interesting people. So, it is my duty to thank each and every one, who was influential in this pivotal period of my life.

Das, for introducing the present topic of textured cobalt ferrite and for his valuable guidance, encouragement and continuous cooperation throughout my PhD tenure. His visionary thoughts, patience, trust and support rescued me from failure and despair in many occasions. He has been excellent supervisor and motivator throughout my Ph.D. and always provided me ample independency and freedom with his valuable directions and guidance. It was wonderful experience working under such noble person and dedicated and honest supervisor. A lot of thanks and gratitude for his all support and guidance.

I am also very thankful to Dean of SEST **Prof. Dibakar Das**, Former dean **Prof. M. Ghanshyam Krishna, Prof. R. Singh, Prof. M.Sundararaman Prof. Bhanu Shankar Rao** and all other SEST faculties for providing me the facilities and the guidance to carry out my research work.

In particular I am also thankful to **Prof. R. Chandrasekhar** (SOC), **Prof. Srinath** (SOP) for their constant encouragement and support during the doctoral committee meetings (DRC) and giving valuable suggestions.

I would like to acknowledge the (funding bodies) **DST-SERB** (sanction number SR/S3/ME/0012/2011) for providing the facilities for the project and the financial support (sanction number, ACK No:124454/2K17/1) obtained from council of scientific and industrial research (CSIR), in the form of senior research fellowship (SRF).

I would like to thank **Dr. Arout Chelvane**, for offering me help to utilize magnetic field press in advanced magnetic group, defense metallurgical research laboratory (DMRL). Thank all my lab mates Dr. Paul Praveen, Dr. Vinitha, Dr. Chandrakala, Dr. Swathi, Kranthi kumar, Dr. Jai Shree. K, Dr. Khushnuma Asghar, Dr. Mohd Qasim, P Parthiban, Sukhmoy, Masawir, and Mahfooz, Srinu, Subadeep Saha for their constant support and cooperation.

I would also like to thank the technicians and non-teaching staff of SEST Mallesh, Dinkar, Kranthi, Venu, Sridhar, Balakishan and Malathi.

I would like to thank all my batch mates Dr. Chandar Amgoth, Dr. Ravikiran, Dr. Parthu Yella and all other friends N Shama Rao, Raghu Rai, Srinivas Vemula, Mahipal Reddy, Srikanth reddy, Ramesh Madhire, Madhusoodhan, Mahipal Darugupally, Yellaiah Janapati, Praveen (SLS) especially for their support and encouragement.

The encouragement and support that I have received from my lab mates Dr. Khushnuma Asghar and Dr. Jai shree during writing of my thesis is highly valued.

I sincerely acknowledge the support and encouragement from my parents, which helped me to stay firm even through tough time.

I greatly appreciate the support and encouragement of my wife during the entire thesis period. She herself undertook the sole responsibility of my child vihan, thereby making me more focused on thesis writing. I value her patience, sacrifice and her enthusing words in odd days.

## **Contents**

	Page No.
DECLARATION	iii
CERTIFICATE	iv
ACKNOWLEDGEMENTS	vi
LIST OF FIGURES	xii
LIST OF TABLES	xvii
LIST OF PUBLICATIONS	xix
ABBERVATIONS	xxi
ABSTRACT	xxii
Chapter - 1	1
INTRODUCTION	1
1.1 BACKGROUND	2
1.2 FUNDAMENTALS	3
1.2.1 Types of magnetism	3
1.2.2 Ferrites	4
1.2.3 Ferrimagnetism in spinel ferrites	6
1.2.4 Magneto crystalline ansisotropy in cubic crystal	8
1.2.5 magnetostriction	9
1.3 TEXTURE	9
1.3.1 Templated grain growth (TGG) technique	10
1.3.2 Magnetic field assisted compaction(MAC) method	10
References	11
Chapter - 2	14
LITERATURE REVIEW	14

2.1 WHY COBALT FERRITE	15
2.2 METHODS OF PRODUCING ORIENTED CERAMICS	15
2.2.1 Synthesis of cobalt ferrite	15
2.3 OBJECTIVES OF THE WORK	18
References	19
Chapter - 3	22
EXPERIMENTAL PROCEDURE	22
3.1 MATERIALS	23
3.2 METHODS	23
3.2.1 Preparation of CFO by auto-combustion method	23
3.2.2 Preparation of CFO by solid state method	25
3.2.3 Magnetic field assisted compaction.	25
3.2.4 Molten salt synthesis of CFO	26
References	28
Chapter - 4	29
RESULTS & DISCUSSIONS	29
4.1 MAGNETIC FIELD ASSISTED COMPACTION OF CFO	30
4.1.1. Investigation of magnetic and magnetoelastic properties of	CoFe <sub>2</sub> O <sub>4</sub>
prepared by auto-combustion followed by parallel MAC	30
4.1.1.1 Characterization of CFO powder	31
4.1.1.2 Characterization of sintered AC-CFO pellets compacted under magnetic fiel	d 33
4.1.1.3 Conclusions	41
4.1.2. Investigation of magnetic and magnetoelastic properties of CoFe <sub>2</sub> prepared by solid state technique followed by parallel MAC	O <sub>4</sub>

4.1.2.1 Characterization of CFO powder	42
4.1.2.2 Characterization of sintered SS-CFO pellets compacted under magnetic field	44
4.1.2.3 Conclusions	52
4.1.3. Investigation of magnetic and magnetoelastic properties of CoFe <sub>2</sub>	$O_4$
prepared by auto-combustion followed by perpendicular MAC5	53
4.1.3.1 Characterization of sintered AC-CFO pellets compacted under perpendicular magne field	53
4.1.4. Investigation of magnetic and magnetoelastic properties of CoFe <sub>2</sub>	$O_4$
prepared by solid state technique followed by perpendicular MAC	<b>52</b>
4.1.4.1 Characterization of sintered SS-CFO pellets compacted under perpendicular magnet field	62
4.2 TEMPLATE GRAIN GROWTH OF CFO	71
4.2.1 Investigation of structural, morphological and magnetic properties	of
CFO template synthesized by molten salt synthesis	
4.2.1.1 Characterization of CFO nanoparticles used for molten salt synthesis	71
4.2.1.2 Characterization of CFO particles prepared in molten salt synthesis	73
4.2.1.3 Conclusions	84
4.2.2 Investigation of magnetic and magnetoelastic properties of textur	ed
CoFe <sub>2</sub> O <sub>4</sub> prepared by template grain growth (TGG) technique	5
4.2.2.1 Characterization of CFO pellets prepared from CFO templates synthesized at different conditions	
4.2.2.2 Conclusions	03
References	Ω4

Chapter – 5	105	
SUMMARY & CONCLUSIONS	105	
Summary and conclusions		
Future scope	107	

# **List of Figures**

Page No.

Figure 1.1 Crystal structure of cubic ferrites. The small filled circles represent metal ions, the large open or
shaded circles represent oxygen ions: (a) tetrahedral or A sites; (b) octahedral or B sites; and (c) one-fourth
of the unit cell of a cubic ferrite
Figure 1.2 (a) spin orientation in A and B sites; (b) the variation of saturation magnetization ( $\sigma_S$ ) with the
temperature
Figure 1.3 Domain orientations during magnetic field.
Figure 1.4 parallel magnetic field press and perpendicular magnetic field press used for parallel MAC and perpendicular MAC respectively
Figure 3.1 Synthesis of CFO by autocombustion method
Figure 3.2 Sintering protocol used for sintering of CFO at 1350°C for 12h
Figure 3.3 Flow chart for synthesis of CFO templates in various conditions
Figure 4.1.1.1 Powder X-ray Diffraction (XRD) pattern of as synthesized and calcined (800°C for 3 hrs CFO powder. The impurity phase of CoO (marked as # in the peak profile) in the as synthesized powder is shown in the inset of the figure.
Figure 4.1.1.2 TEM images of the powder particle sizes and their distribution of a) as-synthesized and by Calcined (800°C for 3 h) CFO powder
Figure 4.1.1.3 Room temperature magnetization (M-H) curve of CFO powder calcined at 800°C for 31
Figure 4.1.1.4 XRD of sintered AC–CFO Pellets compacted in parallel MAC at different magnetic fields
Figure 4.1.1.5 SEM micrographs of sintered AC–CFO Pellets compacted in parallel MAC at different magnetic fields
Figure 4.1.1.6 M–H curve of sintered AC–CFO Pellets compacted in parallel MAC at different magnetic fields
Figure 4.1.1.7 Magnetostriction data of sintered AC-CFO compacted in parallel MAC at different magnetic fields
Figure 4.1.1.8 Variation of magnetostriction of sintered AC–CFO samples with applied magnetic field during parallel MAC

Figure 4.1.1.9 Strain sensitivity data of sintered AC-CFO compacted in parallel MAC at different magnetic fields
Figure 4.1.1.10 Variation of strain sensitivity of sintered AC–CFO samples with applied magnetic field during parallel MAC
Figure 4.1.2.1 Powder X-ray Diffraction (XRD) pattern of CFO powder double calcined at 1000°C, 12h
Figure 4.1.2.2 SEM micrograph and particle size distribution of CFO powder double calcined at 1000°C, 12h
Figure 4.1.2.3 Room temperature magnetization (M-H) curve of CFO powder double calcined at 1000°C, 12h
Figure.4.1.2.4 XRD of sintered SS-CFO Pellets compacted in parallel MAC at different magnetic fields 44
Figure 4.1.2.5 SEM micrographs of sintered AC-CFO Pellets compacted in parallel MAC at different magnetic fields
Figure 4.1.2.6 M–H curve of sintered AC–CFO Pellets compacted in parallel MAC at different magnetic fields
Figure 4.1.2.7 Magnetostriction data of sintered SS–CFO compacted in parallel MAC at different magnetic fields
Figure 4.1.2.8: Variation of magnetostriction of sintered SS–CFO samples with applied magnetic field during parallel MAC
Figure 4.1.2.9 Strain sensitivity data of sintered AC-CFO compacted in parallel MAC at different magnetic fields
Figure 4.1.2.10 Variation of strain sensitivity of sintered SS-CFO samples with applied magnetic field during parallel MAC
Figure 4.1.3.1 XRD of sintered AC–CFO Pellets compacted in perpendicular MAC at different magnetic fields
Figure 4.1.3.2 SEM micrographs of sintered AC–CFO Pellets compacted in perpendicular MAC at different magnetic fields
Figure 4.1.3.3 M–H curve of sintered AC–CFO Pellets compacted in perpendicular MAC at different magnetic fields
Figure 4.1.3.4 Magnetostriction data of sintered AC–CFO compacted in parallel MAC at different

Figure 4.1.3.5 Variation of magnetostriction of sintered AC-CFO samples with applied magnetic field during perpendicular MAC
Figure 4.1.3.6 Strain sensitivity data of sintered AC–CFO compacted in parallel MAC at different magnetic fields
Figure 4.1.3.7 Variation of strain sensitivity of sintered AC–CFO samples with applied magnetic field during perpendicular MAC
Figure 4.1.4.1 XRD of sintered SS–CFO Pellets compacted in perpendicular MAC at different magnetic fields
Figure 4.1.4.2 SEM micrographs of sintered SS-CFO Pellets compacted in perpendicular MAC at different magnetic fields
Figure 4.1.4.3 SEM micrographs of sintered SS–CFO Pellets compacted in perpendicular MAC at different magnetic fields
Figure 4.1.4.4 Magnetostriction data of sintered SS-CFO compacted in perpendicular MAC at different magnetic fields
Figure 4.1.4.5 Variation of magnetostriction of sintered SS–CFO samples with applied magnetic field during perpendicular MAC
Figure 4.1.4.6 Strain sensitivity data of sintered SS-CFO compacted in perpendicular MAC at different magnetic fields
Figure 4.1.4.7 Variation of strain sensitivity of sintered SS–CFO samples with applied magnetic field during perpendicular MAC
Figure 4.2.1.1 XRD pattern of CFO particles
Figure 4.2.1.2 (a) TEM image of CFO particle and (b) size distribution of CFO nanoparticles
Figure 4.2.1.3 Room temperature magnetization (M-H) curve of CFO nanoparticles
Figure 4.2.1.4 XRD pattern of CFO powder prepared at different temperatures (700°C, 800°C, 900°C and 1000°C for 4h) with 1:1 salt to powder mass ratio
Figure 4.2.1.5 SEM micrographs of CFO powder prepared at different temperatures (700°C, 800°C, 900°C and 1000°C for 4h) with 1:1 salt to powder mass ratio
Figure 4.2.1.6 Room temperature M-H curve of CFO particles prepared at different temperatures (700°C, 800°C, 900°C and 1000°C for 4h) with 1:1 salt to powder mass ratio
Figure 4.2.1.7 XRD pattern of CFO powder prepared at 1000°C with different dwell time (4h, 12h, 24h) and 1:1 salt to powder mass ratio

Figure 4.2.1.8 SEM micrographs of CFO powder prepared at 1000°C with different dwell time (4h, 12h, and 24h) and 1:1 salt to powder mass ratio
Figure 4.2.1.9 Room temperature M-H curve of CFO particles prepared at 1000°C with different dwell time (4h, 12h, and 24h) and 1:1 salt to powder mass ratio
Figure 4.2.1.10 XRD pattern of CFO powder prepared at 1000°C, 24h with different salt to powder mass ratio (1:1, 3:1, 5:1)
Figure 4.2.1.11 SEM micrographs of CFO powder prepared at 1000°C, 24h with different salt to powder mass ratio (1:1, 3:1, 5:1)
Figure 4.2.1.12 Room temperature M-H curve of CFO particles prepared at 1000°C, 24h with different salt to powder mass ratio (1:1, 3:1, 5:1)
Figure 4.2.2.1 XRD pattern of sintered pellets prepared from CFO templates synthesized at different temperatures
Figure 4.2.2.2 SEM micrographs of sintered pellets prepared from CFO templates synthesized at different temperatures (700°C, 800°C, 900°C and 1000°C for 4h)
Figure 4.2.2.3 Room temperature M-H curve of sintered pellets prepared from CFO templates synthesized at different temperatures (700°C, 800°C, 900°C and 1000°C for 4h)
Figure 4.2.2.4 Magnetostriction curves of sintered pellets prepared from CFO templates synthesized at different temperatures (700°C, 800°C, 900°C and 1000°C for 4h)
Figure 4.2.2.5 Variation of magnetostriction with temperature at which CFO templates have been prepared
Figure 4.2.2.6 Strain sensitivity curves of sintered pellets prepared from CFO templates synthesized at different temperatures (700°C, 800°C, 900°C and 1000°C for 4h)
Figure 4.2.2.7 Variation of magnetostriction with temperature at which CFO templates have been prepared
Figure 4.2.2.8 XRD pattern of sintered pellets prepared from CFO templates synthesized at 1000°C with 1:1 salt to powder mass ratio and different dwell time (4h, 12h, and 24h)
Figure 4.2.2.9 SEM micrographs of sintered pellets prepared from CFO templates synthesized at 1000°C with 1:1 salt to powder mass ratio and different dwell times (4h, 12h, and 24h)
2.2.10 Room temperature M-H curve of sintered pellets prepared from CFO templates synthesized at 1000°C with 1:1 salt to powder mass ratio and different dwell times (4h, 12h, and 24h)
94

Figure 4.2.2.11 Magnetostriction curves of sintered pellets prepared from CFO templates synthesized at
1000°C with 1:1 salt to powder mass ratio and different dwell times (4h, 12h, and 24h)
Figure 4.2.2.12 Variation of magnetostriction with dwell time at which CFO templates have been prepared
Figure 4.2.2.13 Magnetostriction curves of sintered pellets prepared from CFO templates synthesized at 1000°C with 1:1 salt to powder mass ratio and different dwell times (4h, 12h, and 24h)
Figure 4.2.2.14 Variation of strain sensitivity with dwell time at which CFO templates have been prepared
Figure 4.2.2.15 XRD pattern of sintered pellets prepared from CFO templates synthesized at 1000°C, 24h with different salt to powder mass ratios (1:1, 3:1, and 5:1)
Figure 4.2.2.16 SEM micrographs of sintered pellets prepared from CFO templates synthesized at 1000°C, 24h with different salt to powder mass ratios (1:1, 3:1, and 5:1)
Figure 4.2.2.17 Room temperature M-H curve of sintered pellets prepared from CFO templates synthesized at 1000°C, 24h with different salt to powder mass ratios (1:1, 3:1, and 5:1)
Figure 4.2.2.18 Magnetostriction curves of sintered pellets prepared from CFO templates synthesized at 1000°C, 24h with different salt to powder mass ratios (1:1, 3:1, and 5:1)
Figure 4.2.2.19 Variation of magnetostriction with salt to powder mass ratio
Figure 4.2.2.20 Strain sensitivity curves of sintered pellets prepared from CFO templates synthesized at 1000°C, 24h with different salt to powder mass ratios (1:1, 3:1, and 5:1
Figure 4.2.2.21 Variation of strain sensitivity with salt to powder mass ratio

# **List of Tables**

Page No.
Table 1.2 Ion distribution and net moment per molecule of CoFe <sub>2</sub> O <sub>4</sub> and NiFe <sub>2</sub> O <sub>4</sub>
Table.4.1.1.1 lattice parameter values of sintered AC–CFO Pellets compacted in parallel MAC and different magnetic fields
Table 4.1.1.2 Magnetic properties of sintered AC-CFO Pellets compacted in parallel MAC at different magnetic fields
Table.4.1.2.1 lattice parameter values of sintered SS-CFO Pellets compacted in parallel MAC at different magnetic fields
Table 4.1.2.2 Magnetic properties of sintered SS-CFO Pellets compacted in parallel MAC at different magnetic fields
Table.4.1.3.1 lattice parameter values of sintered AC-CFO Pellets compacted in perpendicular MAC addifferent magnetic fields
Table 4.1.3.2 Magnetic properties of sintered AC–CFO Pellets compacted in perpendicular MAC addifferent magnetic fields
Table.4.1.4.1 lattice parameter values of sintered SS-CFO Pellets compacted in perpendicular MAC addifferent magnetic fields
Table 4.1.4.2 Magnetic properties of sintered SS-CFO Pellets compacted in perpendicular MAC and different magnetic fields
Table 4.2.1.1 crystallite size and lattice parameters of CFO powder prepared at different temperatures (700°C, 800°C, 900°C and 1000°C for 4h) with 1:1 salt to powder mass ratio
Table 4.2.1.2 Average particle size of bigger particles and smaller particles calculated from SEM micrographs of CFO powder prepared at different temperatures (700°C, 800°C, 900°C and 1000°C for 4h) with 1:1 salt to powder mass ratio
Table 4.2.1.3 magnetic properties of CFO particles prepared at different temperatures (700°C, 800°C 900°C and 1000°C for 4h) with 1:1 salt to powder mass ratio
Table 4.2.1.4 crystallite size and lattice parameters of CFO particles prepared at 1000 °C with different dwell time (4h, 12h, and 24h) and 1:1 salt to powder mass ratio

Table 4.2.1.5 Average particle size of bigger particles and smaller particles calculated from SEM micrographs of CFO powder prepared at 1000°C with different dwell time (4h, 12h, and 24h) and 1:1 salt to powder mass ratio
Table 4.2.1.6 magnetic properties of CFO particles prepared at 1000°C with different dwell time (4h, 12h, and 24h) and 1:1 salt to powder mass ratio
Table 4.2.1.7 Crystallite size and lattice parameters of CFO particles prepared at 1000 °C, 24h with different salt to powder mass ratio (1:1, 3:1, 5:1)
Table 4.2.1.8 Average particle size of bigger particles and smaller particles calculated from SEM micrographs of CFO powder prepared at 1000°C, 24h with different salt to powder mass ratio (1:1, 3:1, 5:1)
Table 4.2.1.9 magnetic properties of CFO particles prepared at 1000°C, 24h with different salt to powder mass ratio (1:1, 3:1, 5:1)
Table 4.2.2.1 magnetic properties of sintered pellets prepared from CFO templates synthesized at different temperatures (700°C, 800°C, 900°C and 1000°C for 4h)
Table 4.2.2.2 magnetic properties of sintered pellets prepared from CFO templates synthesized at different temperatures (700°C, 800°C, 900°C and 1000°C for 4h)
Table 4.2.2.3 magnetic properties of sintered pellets prepared from CFO templates synthesized at 1000°C, 24h with different salt to powder mass ratios (1:1, 3:1, and 5:1)

#### List of publications

#### A. List of peer-reviewed publications from the thesis work

 S Indla, A Chelvane, A Lodh, D Das\*, Enhancement in magnetostrictive properties of Cobalt ferrite by magnetic field assisted compaction technique, Journal of Alloys and Compounds, 779 (2019) 886-891.

#### B. Other peer reviewed publications

- S Indla, A Chelvane, D Das\*, Magnetic and Megnetoelastic properties of cobalt ferrite compacted through cold isostatic pressing, AIP Conference Proceedings, 1728 (2016) 020500
- VR Monaji, S Indla, S Rayaprol, S Sowmya, A Srinivas, D Das\*, Temperature dependent magnetic properties of Co<sub>1+x</sub>T<sub>x</sub>Fe<sub>2-2x</sub>O<sub>4</sub>, Journal of Alloys and Compounds, 700 (2017) 92-97.
- 3. JP Praveen, VR Monaji, E Chandrakala, **S Indla,** D Das\*, Enhanced magnetoelectric coupling in Ti and Ce substituted CFO-BCZT Lamainate composite, Journal of Alloys and Compounds, 750 (2018) 392-400.

#### C. List of oral and poster presentations

- Srinivas Indla, Vinitha Reddy M, Arout Chelvane and Dibakar Das, Effect of magnetic field assisted compaction on magnetostrictive properties of cobalt ferrite synthesized by combustion method, poster presented in ICAFM-2014,NIIST, Thiruvananthapuram., Kerala, India.
- Srinivas Indla, Arout Chelvane, Dibakar Das, Magnetic and Megnetoelastic properties of cobalt ferrite compacted through cold isostatic pressing, poster presented in ICC-2015, Bikaner, Rajasthan, India.
- Srinivas Indla, Tanjore V Jayaraman, Arout Chelvane, Dibakar Das, Influence of magnetic
  field assisted compaction on magnetic and magnetostrictive properties of cobalt ferrite for
  torque sensor application, oral and poster presented in ASMD 2019, ARCI, Hyderabad,
  India.

#### D. Participation in workshop

- 1. Participated in One day workshop on "Advanced Ceramic Processing and Fabrication" CGREI-2016 held at ARCI, Hyderabad.
- 2. Participated in the one-day workshop on "Advanced Engineering Materials: An Industry Perspective" held on Nov 2016 at School of Engineering Sciences and Technology, UOH.
- 3. Participated in the "New Advance methods in the OIM 8.0 Analysis Tool and the new techniques used to improve the EBSD Maps by using the NPAR technology", held on 12-13 October 2017 at ARCI, Hyderabad.
- Participated in the one day workshop on "Advanced Ceramics: Powder to product" held on 16<sup>th</sup> February 2018 at ARCI, Hyderabad.

#### **ABSTRACT**

In polycrystalline materials texture is developed due to orientation of grains. There are several texturing techniques, but templated grain growth (TGG) and magnetic field assisted compaction (MAC) have been used in the present work. CFO has been synthesized by conventional solid state method and autocombustion method at different fuel ratios. Phase pure CFO prepared in both solid-state method and autocombustion method has been pressed into pellets using parallel MAC and perpendicular MAC at different magnetic fields (0T, 0.5T, 1T, 1.5T, 2T). These pellets have been characterized for XRD, SEM, PPMS, and magnetostriction set up for structural, morphological, magnetic and magnetoelastic properties. Pure cubic spinel of AC-CFO, SS-CFO has been prepared in different magnetic fields of both parallel and perpendicular magnetic field assisted compaction. Average grain size of 3 µm to 5 µm has been observed for all AC-CFO samples prepared at different magnetic fields of both parallel and perpendicular magnetic field assisted compaction. Enhancement in magnetostriction, 33% (139 ppm to 185 ppm) and strain sensitivity, 40% (0.5×10<sup>-9</sup> m/A to 0.7×10<sup>-9</sup> m/A) have been observed for AC-CFO samples prepared by parallel magnetic field assisted compaction. Enhancement in magnetostriction, 22% (137 ppm to 167 ppm) and strain sensitivity, 40% (0.5×10<sup>-9</sup> m/A to 0.7×10<sup>-9</sup> m/A) have been observed for AC-CFO samples prepared by parallel magnetic field assisted compaction. A significant enhancement in magnetostriction, 89% (110 ppm to 207 ppm) and strain sensitivity, 141% (1.1×10<sup>-9</sup> m/A to 2.8×10<sup>-9</sup> m/A) have been observed for SS-CFO samples prepared by parallel magnetic field assisted compaction. A significant enhancement in magnetostriction, (113 ppm to 209 ppm) ~85% and strain sensitivity, 185% (0.9×10<sup>-9</sup> m/A to 2.5×10<sup>-9</sup> m/A) have been observed for SS-CFO samples prepared by parallel magnetic field assisted compaction. Texture Coefficient of 2.2has been observed for (511) plane in cobalt ferrite sintered sample prepared at 1T parallel field. Texture Coefficient of 1.6 has been observed for (440) plane in cobalt ferrite sintered sample prepared at 1.5T parallel field. CFO templates have been synthesized at different temperatures (700°C, 800°C, 900°C, 1000°C for 4h), different dwell time (4h, 12h and 24h) at 1000°C, and different ratios (1:1, 3:1, 5:1) for 1000°C, 24h. Particle size, saturation magnetization of CFO has been increased with increase in temparature, dwell time and salt to powder ratio. CFO particle morphology has been changed from distorted spherical to traingualr and octahedron shape with increase in temparature, dwell time and salt

topowder ratio. Numbers of particles with triangular and octahedral shapes has been increased with increase in temperature, dwell time and powder to salt ratio. Phase pure CFO pellets have been prepared from CFO powder synthesized at different conditions such as different temperature, dwell time, and salt to powder ratio. Preferential orientation has been observed for (511) peak for SPr1, SPr3 and SP24h samples. A small variation in magnetic properties has been observed for CFO pellets prepared at different conditions.  $\lambda_r$  values suggest that samples are not isotropic and some grain orientation might be possible for the pellets prepared at different temperatures, dwell time and salt to powder ratio.

# CHAPTER 1 INTRODUCTION

### **Chapter 1**

#### Introduction

In this chapter general background of the work, introduction to magnetostriction, giant magnetostrictive materials, ferrites, texturing, and methods of producing textured ceramics have been discussed.

#### 1.1) BACKGROUND

Change in dimension of a material in presence of applied magnetic field is called magnetostriction [1]. Because of its bidirectional exchange of energy between elastic and magnetic states this magnetostrictive effect is useful in many sensor, actuator and transducer applications. Giant magnetostrictive materials such as Terfenol-D [2] and SmFe<sub>2</sub> [3] were developed for magnetostrictive applications.

Need for contactless toque sensors have sparked considerable interest in developing magneto mechanical sensors having more strain sensitivity and high chemical stability. Because of high magneto crystalline anisotropy giant magnetostrictive materials such as Terfenol-D and SmFe<sub>2</sub> exhibited poor sensitivity to stress and high cost of production limited them in using contactless torque sensor applications. But because of low cost, non-corroding nature and high chemical and mechanical stability oxide materials were considered for this application. Among all oxides cobalt ferrite and metal bonded cobalt ferrite were considered as promising material for contactless torque sensor application [4].

In polycrystalline materials texture is developed due to orientation of grains. There are several texturing techniques, but templated grain growth (TGG) and magnetic field assisted compaction (MAC) have been used in the present work. Templated grain growth (TGG) has been used for synthesis of oriented ceramics, which can exhibit single crystal like properties [5]. Magnetic field assisted compaction (MAC) is a well known technique to align magnetic powders in applied magnetic field. Not many reports are available in the open literature on processing of cubic ferrites by MAC even though this technique is capable of producing oriented magnets. Hence magnetic field assisted compaction and templated grain growth techniques have chosen to

produce oriented CFO. Structural, morphological, magnetic and magnetoelastic properties of oriented CFO have been investigated in this thesis.

#### 1.2) FUNDAMENTALS

#### 1.2.1) Types of Magnetism

In a crystalline solid atoms are arranged in a periodic array. Magnetic properties of atoms are due to both of its orbital and spin motion of electrons. Magnetic moment is related with each of this motion and it is a vector. This magnetic moment of electron is in the direction of spin axis and perpendicular to the plane of orbit. The total magnetic moment of atom is the vector sum of all moments of its constituent electrons. The different types of magnetism include diamagnetism, paramagnetism, ferromagnetism, anti-ferromagnetism and ferrimagnetism.

#### 1.2.1.1) Diamagnetism

In diamagnetic materials, magnetic moment of electrons of an atom is oriented such that their net magnetic moment is zero. In presence of magnetic field they show negative magnetism. Atoms or molecules which have closed shell electronic structure such as rare earth gases He, Ne, Ar, etc., and molecules like  $N_2$ ,  $H_2$ , etc, rock salt show the diamagnetism.

#### 1.2.1.2) Paramagnetism

In presence of magnetic field if magnetic moments of electrons are partially aligned in direction of external magnetic field, orbital and spin moments of electrons are not fully cancelled out and left with small net magnetic moment. But all moments of these electrons are so oriented that their net magnetic moment becomes zero in absence of magnetic field. This category of magnetism is called para magnetism. Thermal agitation prevents alignment of magnetic moments in direction of applied field hence show low positive susceptibility. Dependence of mass susceptibility  $(\chi_m)$  with temperature is given by curie Weiss-law as follows

$$\chi_{\rm m} = \frac{C}{(T-\theta)}$$

Here C is curie constant per gram, T is absolute temperature and  $\theta$  is a constant, with the dimensions of temperature. Transition metal complexes, salts and oxides of actinides and

lanthanides and elements of lanthanides and actinides are good examples for paramagnetic substances.

#### 1.2.1.3) Ferromagnetism

Some elements like Fe, Co, Ni shows permanent magnetic moment even in absence of the external magnetic field. This is because of uncancelled magnetic moments of electrons present in atom as a consequence of electronic structure. Furthermore, in a ferromagnetic material, electron spins are aligned in same direction because of exchange forces present between them. The region of space where this spin alignment exists is called domain. The boundary separating two domains is called domain wall. In ferromagnetic materials spontaneous magnetization takes place by domain wall motion.

#### 1.2.1.4) Anti-ferromagnetism

An anti-ferromagnetic material has two interpenetrating identical ion sub lattices whose spontaneous magnetization is equal but in opposite directions as a result it shows zero net magnetic moment in absence of field but shows moment when strong fields are applied to it. Most of the anti-ferromagnetic substances are ionic compounds such as oxides (MnO, FeO, CoO etc.), sulphides ( $\alpha$ -MnS,  $\beta$ -MnS) and chlorides (FeCl<sub>2</sub>, CoCl<sub>2</sub>, NiCl<sub>2</sub>).

#### 1.2.1.5) Ferrimagnetism

The idea of ferrimagnetism is similar to anti-ferromagnetism. Ferromagnetic materials have two interpenetrating unidentical ion sub lattices whose spontaneous magnetization is not equal and opposite in direction as a result shows net magnetic moment even in absence of field. These ferrimagnetic materials exhibit substantial saturation magnetization at room temperature.

#### **1.2.2) Ferrites**

Based on crystal structure magnetic ferrites are divided into two groups such as cubic and hexagonal and garnet. The spinel cubic ferrites have molecular formula of MFe<sub>2</sub>O<sub>4</sub>, where M is a divalent metal ion such as Fe, Co, Zn, Cd, and Mn. Hexagonal ferrites have molecular formula of MFe<sub>12</sub>O<sub>19</sub>, where M is a divalent metal ion such as Ba and Sr, Garnet has molecular formula of MFe<sub>2</sub>O<sub>12</sub> where M is a trivalent metal ion such as Y, Sm, Gd, Eu, Sm, Tb and Lu, As an

4

important member in the family of spinel ferrites, cobalt ferrite (CoFe<sub>2</sub>O<sub>4</sub>) materials have been chosen as material of research contender for a wide variety of applications such as high chemical stability, low cost, non-corroding nature, moderate magnetization, high magnetostriction and high strain sensitivity[6-8].

#### 1.2.2.1) Structure of Spinel Ferrites

The general chemical formula of spinel ferrite is MFe<sub>2</sub>O<sub>4</sub> where M represents divalent ion, this crystal structure is closely related to MgAl<sub>2</sub>O<sub>4</sub>. Spinel ferrite structure contains eight formula units. In spinel ferrite structure, 32 oxygen ions are arranged in cubic shape and metal ions are occupied the interstitial spaces between the oxygen ions. The large oxygen ions are packed in a cubic arrangement and smaller metal ions occupy spaces between them. These interstitial spaces are of two kinds. One is called tetrahedral site or A-site, because it is surrounded by four oxygen ions in tetrahedral manner and this site present at the middle of the tetrahedron. The other kind is called octahedral site or B-site, because it is surrounded by eight oxygen ions in octahedral manner and the site is present at the centre of octahedron. Therefore crystallographic environments of both sites are different. Crystal structure of cubic ferrite is shown in fig 1.1

The unit cell contains 64 tetrahedral (A) sites and 32 octahedral (B) sites, and only 8 A sites and 16 B sites are occupied by metallic ions [9]. Significant variation of composition of metal ions in interstitial sites has been observed in spinel ferrites and thus the composition of the spinel ferrites can be described as [9-10]

$$[M^{II}_{1-\delta}Fe^{III}_{\delta}]_{tetra}[M^{II}_{\delta}Fe^{III}_{2-\delta}]_{octa}O_4$$

If  $\delta$ =0, all divalent metal ions occupy A site and trivalent Fe<sup>+3</sup> ions occupy B sites, and then it is called as "spinel" ferrite. If  $\delta$ =1, the trivalent Fe<sup>+3</sup> ions are evenly distributed on both A and B cation sites and all divalent metal ions occupy B sites, and then it is called as "inverse spinel" ferrite. Here  $\delta$  is defined as the inversion parameter. Metal ion size, interstitial size, charge on metal ion and electronic configuration of metal ions determine the distribution of metal ions in tetrahedral and octahedral sites of spinel and inverse spinel ferrites.

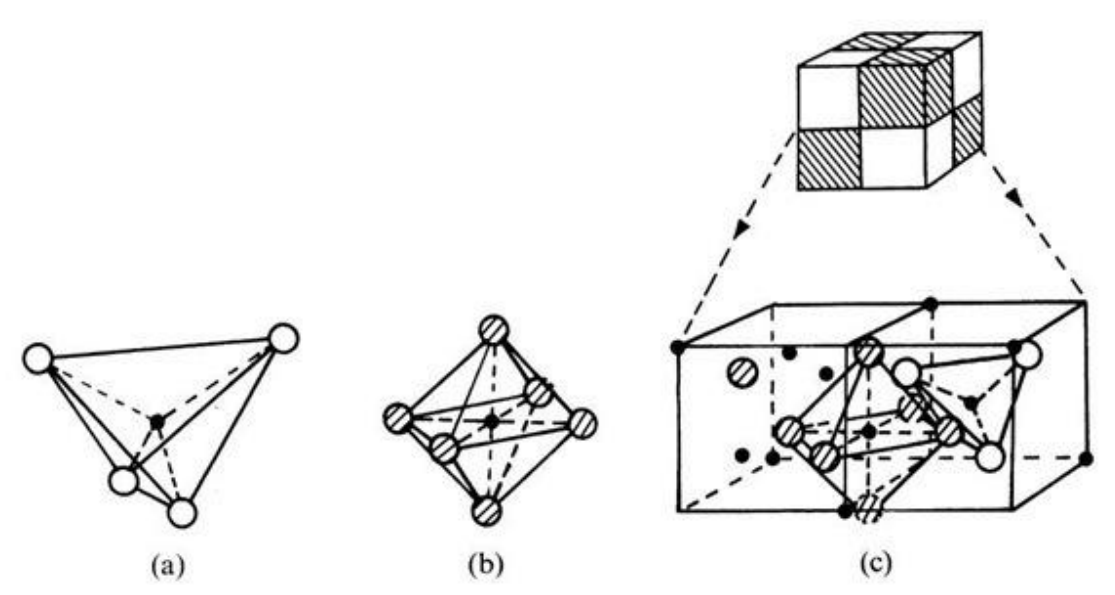


Figure 1.1. Crystal structure of cubic ferrites. The small filled circles represent metal ions, the large open or shaded circles represent oxygen ions: (a) tetrahedral or A sites; (b) octahedral or B sites; and (c) one-fourth of the unit cell of a cubic ferrite.

A typical spinel with a normal structure is cadmium ferrites (CdFe<sub>2</sub>O<sub>4</sub>) in which tetrahedral sites are filled by all divalent Cd ions and octahedral sites are filled by trivalent iron ions. An example of inverse structure is nickel ferrite (NiFe<sub>2</sub>O<sub>4</sub>), where octahedral sites are filled by divalent nickel ions and trivalent iron ions are evenly distributed in both octahedral and tetrahedral sites. Cobalt ferrite (CoFe<sub>2</sub>O<sub>4</sub>) has partially inverse spinel structure, i.e., both divalent cobalt and trivalent iron ions are distributed in both tetrahedral and octahedral sites. The distribution of cobalt and iron ions in interstitial sites is dependent on external processing parameters such as the sample preparation method and the heat treatment processes. Since Co<sup>+2</sup> has a major contribution to the magnetocrystalline anisotropy of cobalt ferrites, the distribution of cobalt in tetrahedral and octahedral sites severely impact the magnetic properties of cobalt ferrite.

#### 1.2.3) Ferrimagnetism in Spinel Ferrites

Ferrimagnetism in ferrites was explained by Neel. According to Neel, metal ions occupy tetrahedral (A-site) and octahedral (B-site) interstitial sites in ferrites. The exchange interactions between two sites are negative [5, 7]. Hence, Ions in A-site magnetized in one direction and Ions in B-site magnetized in opposite direction as shown in Fig.1.2 (a).

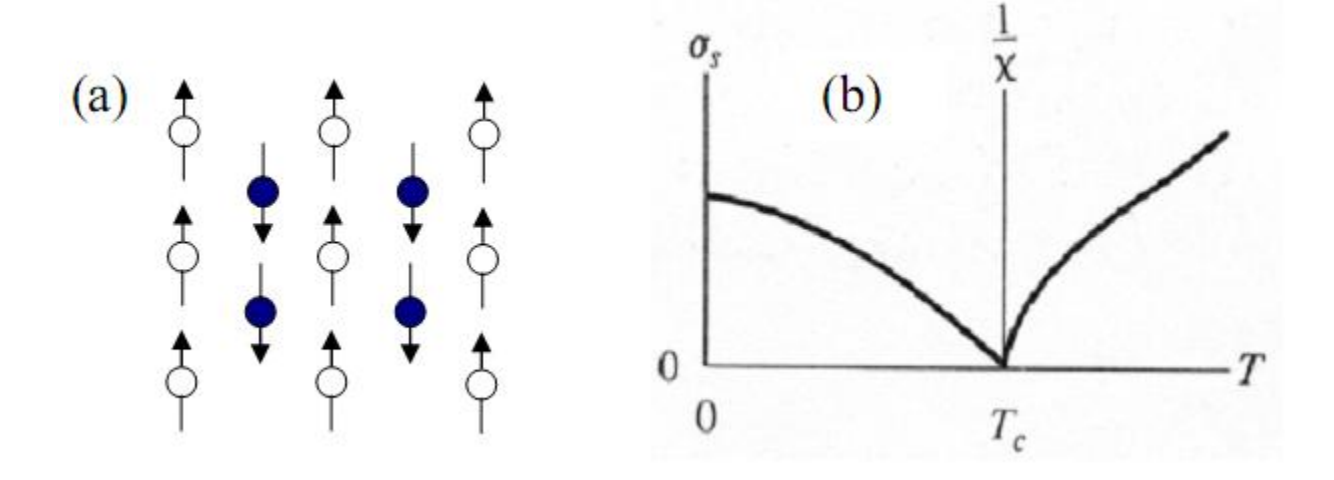


Figure 1.2. (a) spin orientation in A and B sites; (b) the variation of saturation magnetization ( $\sigma_S$ ) with the temperature.

However, due to difference in magnitudes of magnetic moments of A site and B site ferrite material shows net magnetic moment without external magnetic field [10]. Therefore, ferrimagnetic materials show spontaneous magnetization similar to ferromagnetic materials at room temperature, which makes them industrially important. As temperature increases spin randomness increases as a result spontaneous magnetization decreases, at a particular temperature spontaneous magnetization vanishes completely. This temperature is known as Curie temperature ( $T_C$ ), as shown in Fig.1.2 (b). Above the Curie point ( $T_C$ ), the ferrimagnetic material exhibits paramagnetic behavior, and the susceptibility ( $\chi$ ) decreases with increase in temperature.

Saturation magnetization of ferrite materials can be calculated from the magnetic moment of metal ion and the distribution of metal ions in both tetrahedral and octahedral sites at  $0^{\circ}$ K based on the Neel ferrimagnetism. Some examples are shown in Table 1.2. Magnetic moments of  $\text{Co}^{+2}$ , Fe<sup>+3</sup> are taken as  $3\mu_B$  and  $5\mu_B$  respectively

Substance	Structure	Tetrahedral A sites	Octahedral B sites	Net moment (µB)
NiFe <sub>2</sub> O <sub>4</sub>	Inverse	$Fe^{3+}(5\downarrow)$	Fe <sup>3+</sup> (5↑), Ni(2↑)	2
CoFe <sub>2</sub> O <sub>4</sub>	Inverse	$Fe^{3+}(5 \!\!\downarrow)$	Fe <sup>3+</sup> (5↑), Co(3↑)	3
CoFe <sub>2</sub> O <sub>4</sub>	Partially inverse	Fe3+(5↓)δ $Co(3↓)1-δ$	Fe <sup>3+</sup> (5 $\uparrow$ )2- $\delta$ Co(3 $\uparrow$ ) $\delta$	7-4δ

However, some discrepancies are always there between the experimental and the calculated values. Unquenched orbital momentum, inversion parameter (distribution of ions in A site and B site), exchange interaction direction are responsible for the deviations in magnetic moment values.

#### 1.2.4) Magnetic Crystalline Anisotropy in Cubic Crystal

Magneto crystalline anisotropy is also known as crystalline anisotropy. It is an intrinsic property of a ferromagnetic material. Spin-orbit coupling is responsible for crystal anisotropy. In presence of external field spins of electrons reorient in the applied field. Along with spins the orbits of those electrons also tend to reorient in that direction. But orbits are strongly coupled to lattice restricts the rotatation of spin axis. The energy required to orient the spin away from easy axis direction is called crystal anisotropy energy, is just the energy needed to overcome the spin – orbit coupling.

In a cubic crystal, such as a spinel ferrite, let magnetization vector make angles a, b, c with the crystal axes, and let  $\alpha_1$ ,  $\alpha_2$ ,  $\alpha_3$  be the direction cosines of these angles, then

$$E = K_0 + \ K_1 \ ({\alpha_1}^2 \ {\alpha_2}^2 + {\alpha_2}^2 \ {\alpha_3}^2 + {\alpha_3}^2 \ {\alpha_1}^2) + K_2 \ ({\alpha_1}^2 \ {\alpha_2}^2 \ {\alpha_3}^2) + \ldots \ldots$$

Where  $K_0$ ,  $K_1$ ,  $K_2$  ... are anisotropy constants for particular material at a particular temperature. The initial term  $(K_0)$  is independent of angle and is usually ignored, because normally we interested only in the change in anisotropic energy E when the magnetization vector oriented from one direction to another. The magnitudes of  $K_1$ ,  $K_2$ , etc. give the strength of the crystal anisotropy in a specific crystal.

#### 1.2.5) Magnetostriction

When magnetic field is applied dimensions of the material get changed, this phenomenon is called magnetostriction [1]. It is denoted by  $\lambda$ .

$$\lambda = \frac{\triangle L}{L}$$

The value of  $\lambda$  measured at magnetic saturation is called saturation magnetostriction  $\lambda_s$ .

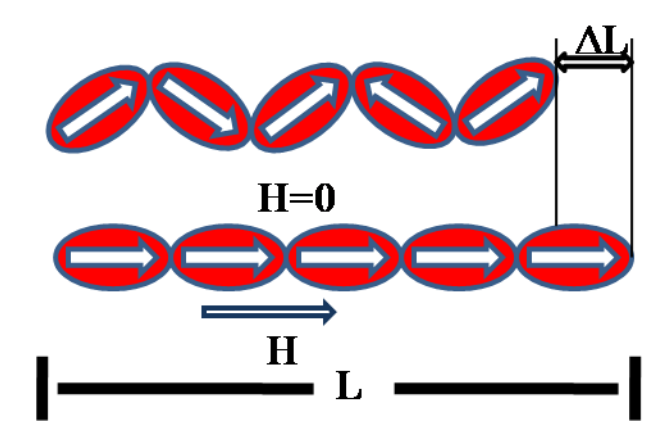


Figure 1.3 Domain orientations during magnetic field

This change in length is the result of the orientation of small magnetic domains in the direction of applied magnetic field. This orientation of domains is responsible for internal strains in the material structure. The strains in the material structure are responsible for increase in length in the case of positive magnetostriction, in the direction of the external magnetic field. During this stretching process the cross-section of material is decreased in a way that the volume is kept nearly constant. As strength of magnetic field increases, orientation of domains increases in the direction of the magnetic field. The magnetic saturation is achieved in material when all the domains are aligned in the direction of external magnetic field.

#### 1.3) TEXTURE

In a polycrystalline material each grain posses its own orientation. Some of the individual grains may have nearly the same orientation, while the others may have different orientations. Preferred orientation of grains in a polycrystalline material is referred to as texture [11]. Texture has been developed in ceramic materials by various techniques such as slip casting, tape casting, pressure filtration, dry pressing, extrusion and centrifugal casting [12-19], templated grain growth [20–26] and magnetic field assisted compaction techniques [27-34]. Physical, mechanical and chemical

properties of materials are influenced by crystallographic texture. Effect of texture on elastic modulus [35], yield strength [36], toughness [37], fracture [38], fatigue [39], magnetic properties [40], magnetoelastic properties [41], electric properties [42], corrosion [43] and oxidation properties [44] have been studied in literature.

#### 1.3.1) Templated grain growth (TGG) technique

Templated grain growth technique (TGG) is used to prepare textured ceramics with better properties compared to corresponding polycrystalline ceramics. In TGG, template and matrix particles are combined with each other, resultant powder mixture is pressed into compacts, these compacts are sintered to get textured product. Surface free energy difference between matrix grain and advancing crystal plane of template is responsible for TGG. In TGG process template particles grow at the expense of matrix particles during heating. This phenomenon is called Ostwald ripening. Orientation of grains in the sintered pellet depends on initial alignment of template particle in green compact, nucleation and growth of desired phase on the template particles during sintering.

#### 1.3.2) Magnetic field assisted compaction (MAC)

Magnetic field assisted compaction technique is a versatile method to improve the alignment of magnetic particles and magnetic properties in permanent sintered magnets. In magnetic field assisted compaction magnetic field is applied simultaneously with applied pressure during compaction in magnetic field press. Depending on the direction of applied magnetic field during compaction it is two types such as parallel magnetic field assisted compaction and perpendicular magnetic field assisted compaction is done in parallel magnetic field press and perpendicular magnetic field assisted compaction is done in perpendicular magnetic field press. In parallel magnetic field assisted compaction magnetic field is applied in the direction of applied pressure where as in perpendicular magnetic field assisted compaction. In parallel magnetic field assisted compaction domains are oriented in the direction of applied field where as in perpendicular magnetic field assisted compaction domains are oriented perpendicular to the applied pressure direction. Oriented state of particles is disturbed in parallel magnetic field assisted compaction where as it is not disturbed in perpendicular magnetic field assisted compaction.

# Press Direction Magnetic Field Direction

Figure 1.4 parallel magnetic field press and perpendicular magnetic field press used for parallel MAC and perpendicular MAC respectively.

#### **References:**

- 1. B. D. Cullity, C. D. Graham, Introduction to magnetic materials, Adision-Wisley, USA, (2009).
- 2. A. E. Clark, "Ferromagnetic Materials", Vol. I, edited by E. P. Wohlfarth, North-Holland. Amsterdam. (1980). ppS31-89.
- 3. F. E. Pinkerton, T. W. Capehart, J. F. Herbst, E. G. Brewer and C. B. Murphy, Appl. Phys Lett. 70 (1997) 2601.
- 4. Y. Chen, J. E. Snyder, C.R. Schwichtenberg, K. W. Dennis, R. W. McCallum, D. C. Jiles, IEEE Trans. Magn. 35 (1999) 3652.
- 5. G. L. Messing, S. Trolier-McKinstry, E. M. Sabolsky, C. Duran, S. Kwon, B. Brahmaroutu,
- P. Park, H. Yilmaz, P. W. Rehrig, K. B. Eitel, E. Suvaci, M. Seabaugh & K. S. Oh, Crit. Rev. Solid State Mater. Sci. 29 (2004) 45-96.
- F. X. Cheng, J. T. Jia, Z. G. Xu, B. Zhou, C. S. Liao, C. H. Yan, L. Y. Chen, and H. B. Zhao,
   J. Appl. Phys. 86 (1999) 2727.
- 7. J. Ding, T. Reynold, W. F. Miao, P. G. McCormick, and R. Street, Appl. Phys. Lett. 65 (1994) 7074.
- 8. J. Ding, Y. J. Chen, Y. Shi, and S. Wang, Appl. Phys. Lett. 77 (2000) 3621.

9. B. Viswanathan and V. R. K. Murthy, Ferrite materials science and technology. Springer verlag, Narosa Publishing House, (1990).

- 10. D. J. Craik and J. Derek, Magnetic Oxides, Wiley, London, NewYork (1975), pp327.
- 11. S. K. Suwas, R. K. Ray, Crystallographic texture of materials, Springer, London, Heidelberg, New York, Dordrecht, (2014).
- 12. E. Suvaci, G. L. Messing, Euro. Ceramics. Vii (2002) Pt 1–3.
- 13. T. S. Suzuki, Y. Sakka, Chem. Lett. 12 (2002) 1204-1205.
- 14. T. S. Suzuki, Y. Sakka Jpn, J. Appl. Phys. 41 (2002) L1272–L1274
- 15. T. S. Suzuki, T. Uchikoshi, Y. Sakka, J. Ceram. Soc. Jpn. 114 (2006) 59-62
- 16. I. Stubna, V. Trnovcova, Ceram-Silik. 42 (1998) 21-24
- 17. M. Wu, Y. Li, D. Wang, Q. Yin, Ceram. Inter. 34 (2008) 753-756
- 18. J. L. Ning, D. M. Jiang, K. B. Shim, Adv. Appl. Ceram. 105 (2006) 265-269.
- 19. D. L. West, D. A. Payne, J. Am. Ceram. Soc. 86 (2003) 1132-1137.
- 20. S. D. Bhame, P. A. Joy, Sens. Actuators, A, 137 (2007) 256.
- 21. K. K. Mohaideen, P. A. Joy, Appl. Phys. Lett., 101 (2012) 072405.
- 22. Z. H. Zhou, J. M. Xue, J. Wang, H. S. O. Chan, T. Yu, Z. X. Shen, J. Appl. Phys. 91 (2002) 6015.
- 23. L. A. Garcia-Cerda, V. A. Torres-Garcia, J. A. Matutes-Aquino, J. Alloy Compd. 369 (2004) 148.
- 24. T. Yamamoto, T. Sakuma, J. Am. Ceram. Soc. 77 (1994) 1107–09.
- 25. P. W. Rehrig, G. L. Messing, S. Trolier-McKinstry, J. Am. Ceram. Soc. 83 (2000) 2654–2660.
- 26. A. Khan, E. P. Gorzkowski, A. M. Scotch, E. R. Leite, T. Li, H. M. Chan, and M. P. Harmer,
- J. Am. Ceram. Soc. 86 (2003) 2176–2181.
- 27. D. B. Hovis, K.T. Faber, Scripta Mater. 44 (2001) 2525–2529
- 28. J. Wang, X. Gao, C. Yuan, J. Li, X. Bao, J. Magn. Magn. Mater. 401 (2016) 662-666
- 29. A. Srinivas, T. Karthik, R. Gopalan, V. Chandrasekaran, Mater. Sci. Eng. B. 172 (2010) 289–293
- 30. T. Karthik, A. Srinivas, V. Kamaraj, V. Chandrasekeran, Ceram. Inter. 38 (2012) 1093–1098
- 31. M. V. Reddy, A. Lisfi, S. Pokharel, D. Das, Sci. Rep. 7 (2017) 7935

32. N. Ouar, F. E. Schoenstein, S. Mercone, S. Farhat, B. Villeroy, B. Leridon, N. Jouini, J.

Appl. Phy. 114 (2013) 163907

33. N. P. Kumar, K. A. Chary, B. Sumana, K. S. Rao, M. B. Suresh, M. M. Raja, A. Srinivas,

Mater. Res. Express 6 (2019) 086112

- 34. C. Rong, V. V. Nguyen, J. P. Liu, J. Appl. Phys. 107 (2010) 09A717
- 35. R. K. Ray, J. J. Jonas, R. E. Hook Inter. Mater. Rev 39 (1994) 129–172
- 36. H. Inagaki, Z. Metallkd 83 (1992) 40-46
- 38. P. I. Welch, G. J. Davies, Textures Microstruct 6 (1983) 21–37
- 39. M. Mineur, P. Villechaise, J. Mendez, J. Mater. Sci. Eng. A. 286 (2000) 257–268
- 40. D. T. Zhang, R. Zhu, M. Yue, W.Q. Liu, Rare Met. 39 (2020) 1295–1299
- 41. D. N. Fager, W. F. Spurr Trans. ASM. 61 (1968) 283-292.
- 42. J. K. Gregory, H. G. Brokmeier, Mater. Sci. Eng. A. 203 (1995) 365–372.
- 43. F. Czerwinski, J. A. Szpunar, Corros. Sci. 41 (1999) 729–740

Chapter 2 Literature Review

# **CHAPTER 2**

# LITERATURE REVIEW

# Chapter 2

### **Literature Review**

Chapter 2 focuses on the literature review of methods of producing textured ceramics and the objectives of the present work have been discussed.

#### 2.1. WHY COBALT FERRITE?

Magnetostriction is the change of dimensions of a material when magnetic field is applied on the material [1]. Magnetostrictive materials can convert energy between magnetic and elastic states vice-versa, and therefore magnetostrictive materials are used for sensor and actuator applications [2-3]. Apart from magnitude the slope of the magnetostriciton, strain derivative  $(\frac{d\lambda}{dH})$  is also an essential property for different applications such as sensors and actuators. Gaint magnetostrictive materials such as terfenol-D, SmFe<sub>2</sub>, even though they are having high magnetostriction because of their high anisotropy these materials exhibits low sensitivity to stress [4, 5] and thus limits their usage for magneto mechanical sensors.

Due to high cost of production, low sensitivity to stress, poor mechanical properties and poor corrosion resistance of single crystal rare earth materials, scientist have tested different materials and came to the conclusion that oxide materials can be used as viable alternative. But because of low cost, non-corroding nature and high chemical and mechanical stability oxide materials were considered for this application. Among all oxides cobalt ferrite and metal bonded cobalt ferrite were considered as promising material for contactless torque sensor application [4].

To invent new smart materials and improving properties of already existing materials is always a matter of interest for researchers. Equally important thing is that materials should be synthesized with simple synthetic procedures. Recently many studies have been done on cobalt ferrite to improve the magnetoelastic properties by varying processing parameters, magnetic field annealing, gel casting and substituting different metal ions in Cobalt and iron sites [6-12].

#### 2.2 METHODS OF PRODUCING ORIENTED CERAMICS

#### 2.2.1 Synthesis of Cobalt ferrite

Synthesis of cobalt ferrite could be achieved by either ceramic method or chemical route. Higher magnetostriction is observed for cobalt ferrite pellet which is made from nano powders rather than bulk powders [13-14]. Conventionally CoFe<sub>2</sub>O<sub>4</sub> nano powder was fabricated from

coprecipitation method [15-18], sol-gel method [19-22] and hydro thermal method [23-24]. In recent years, due to inexpensive starting materials and relatively simple processing method auto combustion synthesis method has gained attention in synthesizing homogeneous, multi component metal oxide ceramic powders [25-27]. Metal oxides are prepared in autocombustion by heating reactant mixture of metal nitrates and fuels like glycine, oxalyldihydrazide, carbohydrazide and urea. Enthalpy of flame temperature during reaction determines the powder size, surface area, and agglomeration of particles. Nature of fuel and fuel to powder ratio used in combustion reaction determines the enthalpy of flame temperature in autocombustion synthesis [28-29]. Rapid evolution of large amount of gaseous products during the combustion dissipates the heat of combustion and restricts the rise of temperature. Various metal oxides such as alumina, zirconia, cerium oxide, barium titanate, lead zirconium titanate zinc oxide, cobalt ferrite, and nickel ferrite etc. have been prepared in autocombustion synthesis. Complex metal oxides have been produced in molten salt synthesis (MSS) method [30-48]. In this method constituent metal oxides and metal salts have been used as reactants. In MSS, reactants are heated with salt above the melting temperature of the salt. During heat treatment process, salt undergoes melting and required products are formed. This product mixture is treated with water to remove salt and to obtain pure product. Typically salts of chlorides and sulphates are used in MSS. Eutectic mixtures of salts have been used widely in MSS because of their lower melting temperatures, different single phase materials such as SrTiO<sub>3</sub> [30, 31], BaTiO<sub>3</sub> [31,32], ZnTiO<sub>3</sub> [33],  $Pb_{1-x}La_xTiO_3$  [34],  $PbTiO_3$  [35,36],  $KSr_2Nb_5O_{15}$  [37, 38],  $La_2Ti_2O_7$  [39], ,  $Nb_2O_5$  and ANbO<sub>3</sub> (A=Na, K) [40], ZnFe<sub>2</sub>O<sub>4</sub> [41], CoFe<sub>2</sub>O<sub>4</sub> [42], MgFe<sub>2</sub>O<sub>4</sub> [43], NiFe<sub>2</sub>O<sub>4</sub> [44], Ni<sub>0.5</sub>Zn<sub>0.5</sub>Fe<sub>2</sub>O<sub>4</sub> [45], and HT-LiCo<sub>0.8</sub>M<sub>0.2</sub>O<sub>2</sub> (M=Al, Ni) [46] have been prepared in different shapes in MSS.

In MSS molten salts are used to control the powder characteristics such as size, shape and etc.  $SrTiO_3$  of different sizes and different shapes have been prepared in MSS using different precursors and different molten salt used in MSS. Tabular or plate like  $Sr_3Ti_2O_7$  has been prepared in MSS using  $SrCO_3$ ,  $TiO_2$  as precursors and KCl as molten salt [30]. An edge length of 8–18  $\mu$ m and a thickness of 2–5  $\mu$ m have been observed for tabular  $Sr_3Ti_2O_7$  particles prepared at  $1300^{\circ}$ C reaction temperature. Plate like  $SrTiO_3$  has been prepared by reaction of plate like  $Sr_3Ti_2O_7$  with  $TiO_2$  in KCl molten salt at  $1200^{\circ}$ C. Nanorods of (80 nm diameter and 1.5 to 10  $\mu$ m length)  $SrTiO_3$  has been prepared using strontium oxalate,  $TiO_2$ , NaCl , NP9 (Nonyl phenyl

ether) precursors at appropriate stoichiometric ratios at 820°C for 3.5h [31]. Kuan et al. [32] have been prepared various shapes of BaTiO<sub>3</sub> (spherical, cubic and rod like) using distinct barium precursors and Titanium precursors in NaCl-KCl molten salt. It has been observed that besides the shape of the precursor's, dissolution rate of precursors in molten salt also determine the shape of the BaTiO<sub>3</sub> in MSS [32]. Xianran et al. [33] synthesized pure ZnTiO<sub>3</sub> plate like particles of 1-3 µm size using ZnO, TiO<sub>2</sub> and eutectic mixture of NaCl-KCl salt in MSS. Decrease in size of ZnTiO<sub>3</sub> has been observed with increasing molten salt. Zongying et al. have synthesized rod like, spherical, cubic and 1-D rod shape PbTiO<sub>3</sub> using different lead and titania precursors in NaCl-KCl molten salt. Spherical and rod like PbTiO<sub>3</sub> is formed when spherical and rod like TiO<sub>2</sub> is used as titanium precursor. Cubic shape PbTiO<sub>3</sub> is formed when K<sub>2</sub>Ti<sub>4</sub>O<sub>9</sub> is used as titanium oxide source.1D rod like PbTiO<sub>3</sub> is formed by reacting spherical PbTiO<sub>3</sub>, NaCl and the liquid nonionic surfactant polyoxyethylene (9) nonylphenolether (NP-9) in molar ratio of 1:5:10 and annealed at 900°C for 2h. Sonali et al. [41] have reported ZnFe<sub>2</sub>O<sub>4</sub> nanoparticles in MSS route for H<sub>2</sub>S gas sensing application. They have prepared ZnFe<sub>2</sub>O<sub>4</sub> nanoparticles of 15-20 nm using zinc sulphate, iron (iii) nitrate Fe(NO<sub>3</sub>)<sub>3</sub>, sodium hydroxide and sodium chloride in molar ratio of 1:2:8:10 respectively. The sensor based on ZnSO<sub>4</sub> exhibits a marked response toward H<sub>2</sub>S gas. Guangbin et al. [42] have synthesized CFO octahedral crystals in MSS using CFO nanoparticles prepared from hydrothermal method. Effect of different sodium salts, reaction temperature, dwelling time and salt to powder mass ratio on formation of octahedral CFO crystals have been discussed. Zhengsong Lou et al. [43] has synthesized submicron size MgFe<sub>2</sub>O<sub>4</sub> particles of different shapes such as sphere and flakes using different salt to reactants mass ratio at 900°C in MSS. Kimura et al. [44] has prepared NiFe<sub>2</sub>O<sub>4</sub> particles using NiO, Fe<sub>2</sub>O<sub>3</sub> in Li<sub>2</sub>SO<sub>4</sub>-Na<sub>2</sub>SO<sub>4</sub> molten salt. It has been observed that reactants with large size difference and density difference are not suitable for MSS because sedimentation of large and heavy particles causes inhomogeneous mixing. Yoshihiro et al. [45] have been prepared acicular NiFe<sub>2</sub>O<sub>4</sub> and NiZn ferrite from acicular Fe<sub>2</sub>O<sub>3</sub>, NiO, and ZnO in presence of molten chlorides and sulphates of alkali metals. Plausible mechanisms for formation of other morphology ferrite particles have been explained.

Magnetic field assisted compaction is used to orient the magnetic domains and magnetic particles during preparation of green compact before sintering process. Researchers have tried different Magnetic field assisted compaction techniques such as magnetic field assisted gel

casting [47-48], applying constant magnetic field during compaction [49-54] in hydraulic magnetic field press. Textured barium hexa ferrite has been produced by Magnetic field assisted gel casting using barium hexaferrite powder prepared by seeded matrix template and templated grain growth technique [47]. Dramatic change in peak intensity ratios (I<sub>110</sub>:I<sub>008</sub>) has been observed for x-ray diffraction pattern of barium hexaferrite prepared in magnetic field assisted gel casting compare to the barium hexaferrite prepared without magnetic field assisted gel casting. In X-ray diffraction pattern of barium hexaferrite, the ratio of the integrated intensities I<sub>110</sub>:I<sub>008</sub> has been changed from 3:1 to 1:40 for the magnetically-aligned barium hexaferrite compare to the barium hexaferrite prepared without magnetic field assisted gel casting. Oriented polycrystalline Cobalt ferrite with [001] texture has been synthesized by magnetic field assisted gel casting [48]. Significant difference in intensities of X-ray diffraction peaks have been observed for cobalt ferrite prepared with and without magnetic field assisted gel casting. Substantial improvements in magnetostriction and strain sensitivity have been observed for CFO and Zr-substituted CFO synthesized by magnetic field assisted gel casting and magnetic field assisted compaction through hydraulic magnetic field press respectively [48,51]. Prominent enhancement in intensity of the (002) peak has been observed in the XRD pattern of SmCo<sub>5</sub> sintered pellet synthesized by magnetic field assisted compaction. The intensity ratio of (002) to (111) peaks has been enhanced from 0.063 to 24.9 for Bragg reflections of SmCo<sub>5</sub> magnets prepared by magnetic field assisted compaction [56]. Multiferroic properties of BiFeO<sub>3</sub> have been improved by in situ magnetic field assisted compaction [50]. In the magnetic field pressed BiFeO<sub>3</sub> pellets, a significant increase in the intensity of (300), (208) and (113) planes have been observed when compared to the BiFeO<sub>3</sub> processed without magnetic field. This observed increase in intensity of the Xrd peaks indicates that there is a texture formation in the magnetic field pressed BiFeO<sub>3</sub> pellets [50].

#### 2.3 OBJECTIVE OF THE WORK

Even though TGG is a well-established technique for preparing oriented ceramics, preparation of CFO by TGG is not available in the open literature. Similarly, not many reports are available on oriented CFO by magnetic field assisted compaction by hydraulic magnetic field press.

Based on above observations, objectives of the present work are,

1) To investigate magnetic and magnetoelastic properties of oriented CoFe<sub>2</sub>O<sub>4</sub> prepared by magnetic field assisted compaction (MAC) technique.

2) To investigate magnetic and magnetoelastic properties of oriented CoFe<sub>2</sub>O<sub>4</sub> prepared by template grain growth (TGG) method.

#### **References:**

- 1. Joule, J. P. Sturgeon's Ann. Electr., 8 (1842) 219.
- 2. M. R. J. Gibbs, Modern Trends in Magnetostriction Study and Application; Kluwer Academic: Dordrecht, The Netherlands, 2001.
- 3. G. Engdhal, Handbook of Giant Magnetostrictive Materials; Academic Press: San Diego, 2000.
- 4. Y. Chen, 1. E. Snyder, C. R. Schwichtenberg, K. W. Dennis, R. W. McCallum, and D. C. Jiles, Paper HF-09, 43'd Annual Conference on Magnetism and Magnetic Materials, Nov. 1998.
- 5. D. C. Jiles, J. Phys. D: Appl. Phys. 28 (1995) 1537-1546.
- Y. Chen, J. E. Snyder, K. W. Dennis, R. W. McCallum, D.C. Jiles, J. Appl. Phys., 87 (2000) 5798.
- 7. R. W. McCallum, K. W. Dennis, D. C. Jiles, J. E. Snyder, Y. H. Chen, Low Temp. Phys., 27 (2001) 266.
- 8. J. A. Paulsen, A. P. Ring, C. C. H. Lo, J. E. Snyder, D. C. Jiles, J.Appl. Phys., 97 (2005) 044502
- 9. S. J. Lee, C. C. H. Lo, P. N. Matlage, S. H. Song, Y. Melikhov, J. E. Snyder, D. C. Jiles, J. Appl. Phys. 102 (2007) 073910.
- 10. I. C. Nlebedim, Y. Melikhov, J. E. Snyder, N. Ranvah, A. J. Moses, D. C. Jiles, J. Appl. Phys., 109 (2011) 07A908.
- 11. Somaiah N., Jayaraman T. V., Joy P. A., Das D. J. Magn. Magn. Mater. 324 (2012) 2286.
- 12. J. Q. Wang, J. H. Li, C. Yuan, X. Q. Bao, X. X. Gao, Rare Met. 37 (2018) 421–426
- 13. S. D. Bhame, P. A. Joy, Sens. Actuators, A, 137 (2007) 256.
- 14. K. K. Mohaideen, P. A. Joy, Appl. Phys. Lett., 101 (2012) 072405.
- 15. Z.H. Zhou, J.M. Xue, J. Wang, H.S.O. Chan, T. Yu, Z.X. Shen, J. Appl. Phys. 91 (2002) 6015.
- 16. L.A. Garcia-Cerda, V.A. Torres-Garcia, J.A. Matutes-Aquino, J.A.Matutes-Aquino, J. Alloy Compd. 369 (2004) 148.
- 17. F.X. Cheng, Z.Y. Peng, C.S. Liao, Z.G. Xu, Solid State Commun. 107 (1998) 471.

18. J. Gwak, A. Ayral, V. Rouessac, L. Cot, J. C. Grenier, J. H. Choy, Microporous Mesoporous Mater. 63 (2003) 177.

- 19. S. S. Hayrapetyan, H. G. Khachatryan, Microporous Mesoporous Mater. 72 (2004) 105.
- 20. T. Pannaparayil, S. Komarneni, K. Marande, M. Zadarko, J. Appl. Phys. 67 (1990) 5509.
- 21. G. B. Ji, S. L. Tang, S. K. Ren, F. M. Zhang, J. Cryst. Growth 270 (2004) 156.
- 22. S. F. Yan, W. Ling, E. L. Zhou, J. Cryst. Growth 273 (2004) 226.
- 23. Z. X. Yue, J. H. Shan, X. W. Qi, Mater. Sci. Eng. B99 (2003) 217.
- 24. S. Arul Antory, K.S. Nagaraja, O.M. Sreedharan, J. Nucl. Mater. 295 (2001)189.
- 25. X. W. Qi, J. Zhou, Z. X. Yue, Z. L. Gui, L. T. Li, Ceram. Int. 29 (2003) 347.
- 26. C. H. Yan, Z. G. Xu, F. X. Cheng, Z. M. Wang, L. D. Sun, C. S. Liao, J. T. Jia, Solid State Commun. 111 (1999) 287.
- 27. B. H. Liu, J. Ding, Appl. Phys. Lett. 88 (2006), 042506-1.
- 28. J. Schafer, W. Sigmung, S. Roy, F. Aldinger, J. Mater. Res. 12 (1997) 2518.
- 29. R. D. Purohit, S. Saha, A. K. Tyagi, J. Nucl. Mater. 288 (2001) 7.
- 30. K. Watari, B. Brahmaroutu, G. L. Messing, S. T. McKinstry, J. Mater. Res. 15 (2000) 4.
- 31. Y. Mao, S. Banerjee, S. S. Wong, J. Am. Chem. Soc. 125 (2003) 15718-15719.
- 32. K. Huang, T. Huang, W. Hsieh, Inorg. Chem. 48 (2009) 9180–9184.
- 33. X. Xing, C. Zhang, L. Qiao, G. Liu, J. Am. Ceram. Soc. 89 (2006) 1150–1152.
- 34. Z. Cai, X. Xing, R. Yu, G. Liu, O. Xing, J. Alloy Compd. 420 (2006) 273–277.
- 35. Z. Cai, X. Xing, R. Yu, X. Sun, G. Liu, Inorg. Chem. 46 (2007) 7423-7427.
- 36. Q. Ji, P. Xue, H. Wu, Z. Pei, X. Zhu, Nanoscale Res. Let 14 (2019) 62
- 37. L. Zhao, F. Gao, C. Zhang, M. Zhao, C. Tian, J. Cryst. Growth 276 (2005) 446–452
- 38. Z. Yang, L. Wei, Y. Chang, B. Liu, J. Mater. Sci 42 (2007) 3627–3631
- 39. D. Arney, B. Porter, B. Greve, P. A. Maggard, J. Photochem. Photobiol. A: Chemistry 199 (2008) 230–235.
- 40. L. Li, J. Deng, J. Chen, X. Sun, R. Yu, G. Liu, X. Xing, Chem. Mater. 21 (2009) 1207–1213
- 41. S. L. Darshane, R. G. Deshmukh, S. S. Suryavanshi, I. S. Mulla, J. Am. Ceram. Soc., 91 (2008) 2724–2726.
- 42. G. Ji, X. Lin, Y. Sun, S. A. A. Trimizi, H. Sub, Y. Du, Cryst. Eng. Comm, 13 (2011) 6451
- 43. Z. Lou, M. He, R. Wang, W. Qin, D. Zhao, C. Chen, Inorg. Chem. 53 (2014) 2053–2057.
- 44. T. Kimura, T. Takahashi, T. Yamaguchi, J. Mate. Sci. 15 (1980) 1491-1497.

- 45. T. Kimura, T. Takahashi, T. Yamaguchi, J. Mate. Sci. 21 (1986) 2876 2880.
- 46. C. H. Han, Y. Hong, K. Kim, Solid State Ion. 159 (2003) 241–247
- 47. D. B. Hovis, K.T. Faber, Scripta Mater. 44 (2001) 2525–2529
- 48. J. Wang, X. Gao, C. Yuan, J. Li, X. Bao, J. Magn. Magn. Mater. 401 (2016) 662–666
- 49. A. Srinivas, T. Karthik, R. Gopalan, V. Chandrasekaran, Mater. Sci. Eng. B. 172 (2010) 289–293
- 50. T. Karthik, A. Srinivas, V. Kamaraj, V. Chandrasekeran, Ceram. Inter. 38 (2012) 1093–1098
- 51. M. V. Reddy, A. Lisfi, S. Pokharel, D. Das, Sci. Rep. 7 (2017) 7935
- 52. N. Ouar, F. E. Schoenstein, S. Mercone, S. Farhat, B. Villeroy, B. Leridon, N. Jouini, J.
- Appl. Phy. 114 (2013) 163907
- 53. N. P. Kumar, K. A. Chary, B. Sumana, K. S. Rao, M. B. Suresh, M. M. Raja, A. Srinivas,
- Mater. Res. Express 6 (2019) 086112
- 54. C. Rong, V. V. Nguyen, J. P. Liu, J. Appl. Phys. **107** (2010) 09A717
- 55. D. T. Zhang, R. C. Zhu, M. Yue, W. Q. Liu, Rare Met. 39 (2020) 1295–1299.

# **CHAPTER 3**

# **EXPERIMENTAL PROCEDURE**

# **Chapter 3**

# **Experimental Procedure**

In this chapter details of synthesis and various experimental techniques carried out in this work are reported in detail.

#### 3.1 MATERIALS

Coblat (II)nitrate hexahydrate (Sigma Aldrich, 98%,), iron (III) nitrate nonahydrate (Sigma Aldrich,  $\geq$  98%, ACS), glycine (Merck,  $\geq$ 99%), iron (III) oxide (Sigma Aldrich,  $\geq$ 99%,), cobalt (II,III)oxide (Alfa Aesar,  $\geq$ 99%), NaCl (SRL,  $\geq$ 99.9%), KCl (SRL,  $\geq$ 99.5%), poly vinyl alcohol (Loba Chemie, MW=1,15,000) have been used in synthesis and compaction of CFO in different methods.

#### 3.2. METHODS

CoFe<sub>2</sub>O<sub>4</sub> has been synthesized by autocombustion synthesis route (G/N=0.09 and 0.5), solid state synthesis route and molten salt synthesis methods. Nanocrystalline CFO obtained from autocombustion (G/N=0.5) method has been calcined at 800°C to obtain phase pure CFO. Phase pure CFO obtained from autocombustion (G/N=0.5) and solid state synthesis routes have been used for magnetic field assisted compaction. CFO templates have been prepared in Molten salt synthesis using pre-synthesized CFO nanoparticles obtained in autocombustion method (G/N=0.09) and 1:1 molar ratio of KCl+NaCl salt mixture. The obtained CFO templates have been used for templated grain growth synthesis.

#### 3.2.1 Preparation of CFO by auto-combustion method:

Pure cobalt-ferrites with nominal compositions CoFe<sub>2</sub>O<sub>4</sub> has been synthesized by auto-combustion technique [1-2]. Co(NO<sub>3</sub>)<sub>2</sub>.6H<sub>2</sub>O and Fe(NO<sub>3</sub>)<sub>3</sub>.9H<sub>2</sub>O and glycine have been used as precursors. Here, glycine acts as fuel and nitrates acts as oxidizers. According to the principle of propellant chemistry, for stoichiometric redox reaction between fuel and an oxidizer, the ratio of the net oxidizing valency of the metal nitrate to net reducing valency of the fuel should be unity. According to this stoichiometric relation for cobalt ferrite the glycine to nitrate ratio (G/N ratio) is 0.38. CFO powder has been synthesized using two different G/N ratios such as 0.09 and 0.5.

To prepare 10gm of CoFe<sub>2</sub>O<sub>4</sub> compositions required amount of nitrates and glycine have been weighed and taken into beaker.50-100ml of water added to these precursors and continuous stirring was done to obtain homogeneous aqueous solution and the temperature was maintained at 80°c. In order to obtain a homogeneous solution, magnetic stirring has been performed throughout the dehydration process. A viscous gel has been formed when the water got completely evaporated. Auto-ignition of this viscous gel is initiated by increasing the temperature to 200°C. The ignition process has accompanied by the evolution of large volume of gases along with cobalt ferrite powder in the form of black ash. Fig.3.1. shows the flow chart of synthesis of cobalt ferrite. This cobalt ferrite powder has been characterized by XRD, TEM and VSM for structural, morphological and magnetic properties respectively.

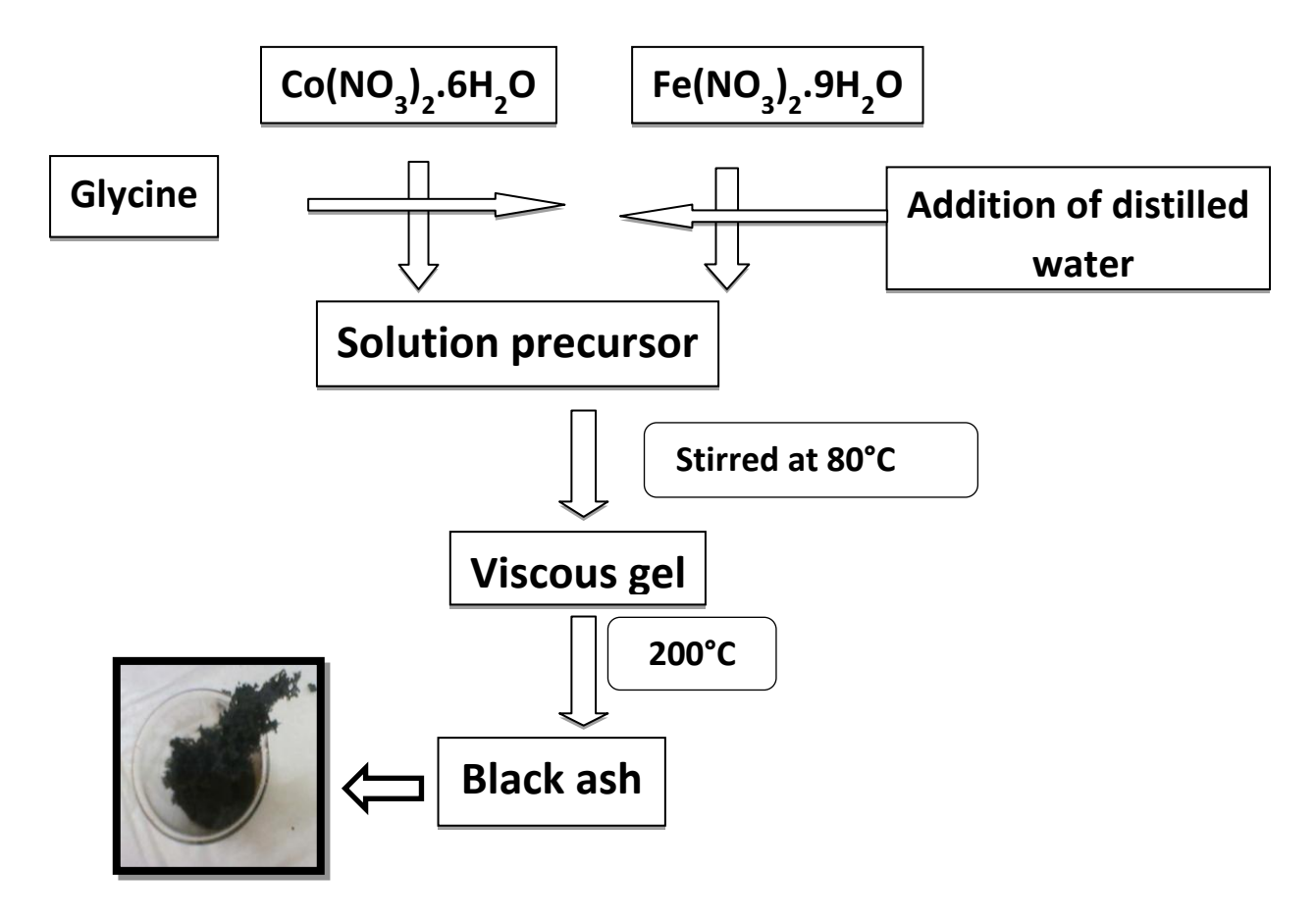


Figure 3.1 Synthesis of CFO by autocombustion method

#### 3.2.2 Preparation of CFO by solid state method

CFO has been synthesized by conventional solid state method [3-5]. The precursors used in the synthesis are Co<sub>3</sub>O<sub>4</sub> and Fe<sub>2</sub>O<sub>3</sub>. Stoicheometric amount of Co<sub>3</sub>O<sub>4</sub> and Fe<sub>2</sub>O<sub>3</sub> have been milled at 300rpm for 3h using ZrO<sub>2</sub> grinding media. The crushed powder has been double calcined at 1000°C, 12h to obtain phase pure CFO. This CFO powder has been characterized by XRD for structural properties.

#### 3.2.3 Magnetic field assisted compaction (MAC)

Magnetic field press has been used to carry magnetic field assisted compaction. CFO synthesized by autocombustion and solid state technique have been used in magnetic field assisted compaction (MAC). In autocombustion technique CFO was prepared by using glycine to nitrate ratio of 0.5. As synthesized CFO is calcined at 800°C, 3h to get phase purity. This phase pure calcined CFO (AC-CFO) and phase pure CFO synthesized from solid state method has been used for magnetic field assisted compaction. Magnetic field assisted compaction is carried out in two ways depending on the direction of applied magnetic field to the direction of applied pressure during compaction such as parallel magnetic field assisted compaction and perpendicular magnetic field assisted compaction.

#### 3.2.3.1 Parallel magnetic field assisted compaction

Phase pure CFO obtained in autocombustion (G/N=0.5) and solid state method have been mixed with 1wt% of PVA, which acts as a binder. Powder along with the binder has been thoroughly mixed and subsequently granulated to yield spherical granules. These spherical granules have been used for parallel magnetic field assisted compaction. In parallel magnetic field assisted compaction, magnetic field is applied simultaneously in the direction of applied pressure during compaction. Parallel MAC of CFO spherical granules synthesized by autocombustion and solid state routes have been done at different magnetic fields such as 0T, 0.5T, 1T and 1.5T. These green compacts were sintered at 1350°C, 12h. The sintering protocol used in sintering has been shown fig, 3.2. Structural, morphological, magnetic and magnetoelastic properties of sintered compacts were studied by XRD, SEM, PQMS and magnetostriction setup respectively.

#### 3.2.3.2 Perpendicular magnetic field assisted compaction

Phase pure CFO obtained in autocombustion (G/N=0.5) and solid state method have been mixed with 1wt% of PVA, which acts as a binder. Powder along with the binder has been thoroughly mixed and subsequently granulated to yield spherical granules. These spherical granules have been used for perpendicular magnetic field assisted compaction. In perpendicular magnetic field assisted

compaction, magnetic field is applied simultaneously perpendicular to the direction of applied pressure during compaction. Perpendicular MAC of CFO synthesized by autocombustion (AC-CFO) and solid state (SS-CFO) routes were done at different magnetic fields such as 0T, 0.5T, 1T, 1.5T and 2T. These green compacts were sintered at 1350°C, 12h. Structural, morphological, magnetic and magnetoelastic properties of sintered compacts were studied by XRD, SEM, PQMS and magnetostriction setup respectively.

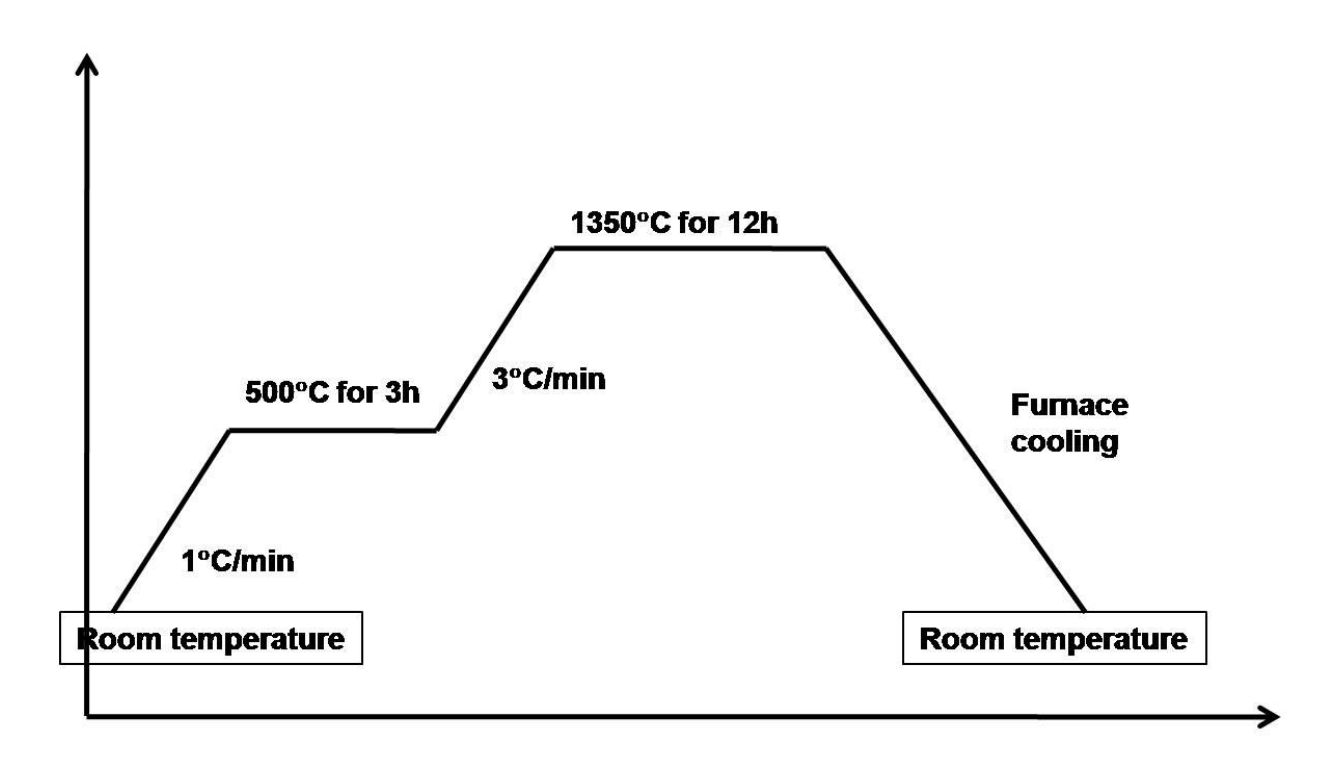


Figure 3.2 Sintering protocol used for sintering of CFO at 1350°C for 12h.

#### 3.2.4 Molten salt synthesis of CFO

In MSS technique, CFO templates have been prepared by using pre-synthesized CFO nanoparticles obtained in autocombustion (G/N=0.09) technique and salt mixture [6]. The salt mixture consists 1:1 molar ratio of KCl and NaCl. CFO nanoparticles and Salt mixture with varied salt to CFO powder mass ratios (1:1, 3:1, and 5:1) have been mixed in a mortar using pestle for one hour in the presence of small amount of isopropanol to attain homogeneous reactant mixture. The mixed powders have been dried at 60°C, and transferred into alumina crucibles, then placed in a muffle furnace. This reactant mixture has been heated in furnace at different temperatures (700°C, 800°C, 900°C and 1000°C), different time intervals (4h, 6h and

12h) and different salt to powder mass ratios (1:1, 3:1, and 5:1). The obtained powder mixture is treated with hot water to remove salts from the powder mixture and dried.

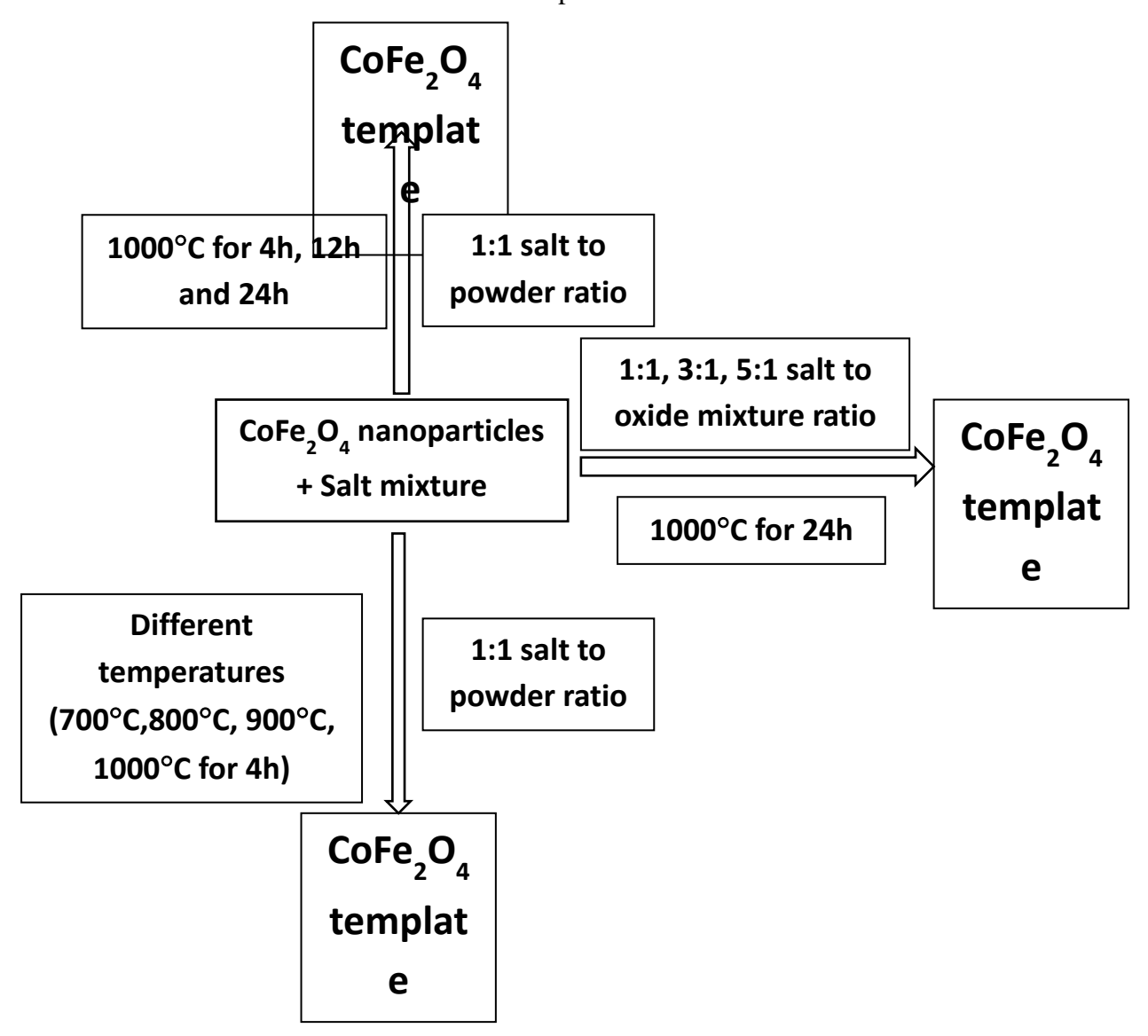


Figure 3.3 flow chart for synthesis of CFO templates in various conditions

These CFO templates have been characterized for XRD, FESEM and VSM for structural, morphological and magnetic properties respectively.

These CFO template powders have been mixed with 1wt% of PVA, which acts as a binder. Powder along with the binder has been thoroughly mixed and subsequently granulated to yield spherical granules. These spherical granules have been pressed into pellets in hydraulic press. These pellets have been sintered at 1350°C, 12h. Structural, morphological, magnetic and

magnetoelastic properties of sintered compacts have been studied by XRD, SEM, VSM and magnetostriction setup respectively.

#### **References:**

- 1. S. D. Bhame, P. A. Joy, Sens. Actuators, A, 137 (2007) 257.
- 2. S. H. Xiao, W. F. Jiang, L. Y. Li, X. J. Li, Mater. Chem. Phys. 106 (2007) 82–87.
- 3. J. A. Paulsen, A. P. Ring, C. C. H. Lo, J. E. Snyder, D. C. Jiles, J.Appl. Phys., 97 (2005) 044502.
- 4. I. C. Nlebedim, N. Ranvah, P. I. Williams, Y. Melikhov, J. E. Snyder, A. J. Moses, D. C. Jiles, J. Magn. Magn. Mater. 322 (2010) 1929–1933.
- 5. I. C. Nlebedim, J. E. Snyder, A. J. Moses, D. C. Jiles, J. Magn. Magn. Mater. 322 (2010) 3938 3942.
- 6. G. Ji, X. Lin, Y. Sun, S. A. A. Trimizi, H. Sub, Y. Du, Cryst. Eng. Comm, 13 (2011) 6451.

# **CHAPTER 4**

# **RESULTS & DISCUSSIONS**

## **Chapter 4**

## **Results & Discussions**

Chapter 4 is divided into two sections, 4.1 and 4.2. Section 4.1 describes magnetic and magnetoelastic properties of textured CoFe<sub>2</sub>O<sub>4</sub> prepared by magnetic field assisted compaction (MAC). Section 4.1 is again divided into four subsections. Subsection 4.1.1 describes magnetic and magnetoelastic properties of CoFe<sub>2</sub>O<sub>4</sub> prepared by autocombustion followed by parallel MAC. Subsection 4.1.2 describes magnetic and magnetoelastic properties of CoFe<sub>2</sub>O<sub>4</sub> prepared by solid state technique followed by parallel MAC. Sub section 4.1.3 describes magnetic and magnetoelastic properties of CoFe<sub>2</sub>O<sub>4</sub> prepared by autocombustion followed by perpendicular MAC. Subsection 4.1.4 describes magnetic and magnetoelastic properties of CoFe<sub>2</sub>O<sub>4</sub> prepared by solid state technique followed by perpendicular MAC. Section 4.2 describes the Investigation of magnetic and magnetoelastic properties of CoFe<sub>2</sub>O<sub>4</sub> prepared by template grain growth (TGG) technique. Section 4.2 is again subdivided into two subsections, 4.2.1 and 4.2.2. Subsection 4.2.1 describes structural, morphological and magnetic properties of CFO template only synthesized by molten salt synthesis method and Subsection 4.2.2 describes magnetic and magnetoelastic properties of textured CoFe<sub>2</sub>O<sub>4</sub> prepared by template grain growth (TGG) technique.

#### SECTION 4.1 MAGNETIC FIELD ASSISTED COMPACTION OF CFO

# 4.1.1. Investigation of magnetic and magnetoelastic properties of CoFe<sub>2</sub>O<sub>4</sub> prepared by auto-combustion followed by parallel MAC

This section deals with preparation of nano crystalline CFO by auto-combustion method using glycine as fuel and investigation of the effect of parallel magnetic assisted compaction (MAC) on the structural, morphological, and magnetic properties of CFO. The fuel to nitrate ratio was maintained as 0.5. As synthesized CFO powder was calcined at 800°C to obtain CFO with pure phase. Further, phase pure CFO was pressed into pellets using parallel MAC at different magnetic fields (0T, 0.5T, 1T and 1.5T). These pellets were sintered at 1350°C for 12h. Applied Magnetic field direction in the sample is called oriented direction. Structural, morphological, magnetic and magnetoelastic

properties of sintered compacts (referred to as AC-CFO) were studied by XRD, SEM, PQMS and magnetostriction setup techniques respectively.

#### 4.1.1.1 Characterization of CFO powder

#### 4.1.1.1 Structural properties

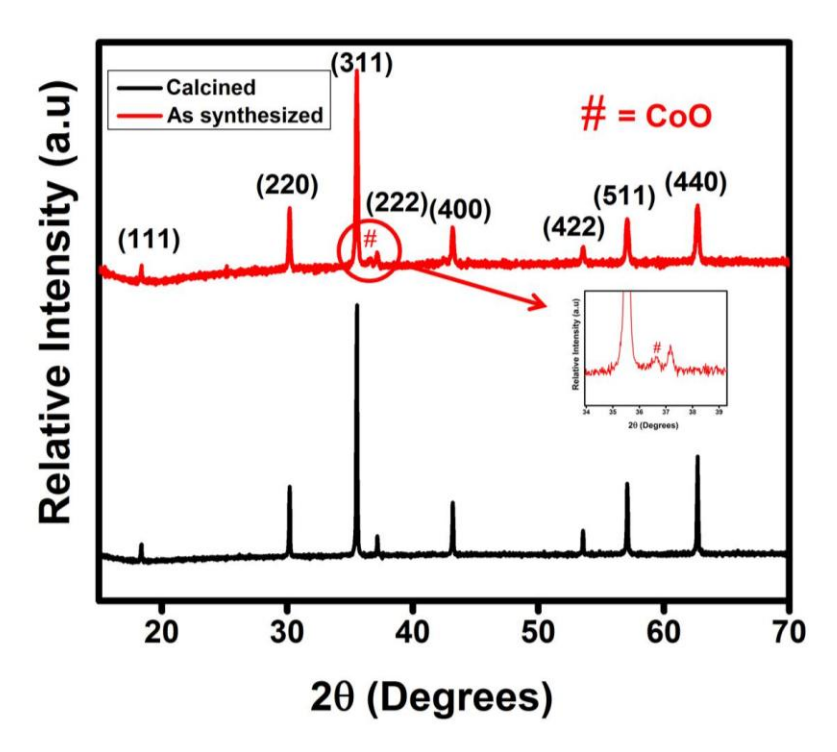


Figure 4.1.1.1 Powder X-ray Diffraction (XRD) pattern of as synthesized and calcined (800°C for 3 hrs) CFO powder. The impurity phase of CoO (marked as # in the peak profile) in the as synthesized powder is shown in the inset of the figure.

XRD pattern of as-synthesized and calcined CFO powder samples are shown in figure 4.1.1.1. Powder diffraction pattern of as-synthesized powder revealed CFO phase (matches with JCPDF file no. 22-1086) along with CoO impurity phase. Average crystallite size was calculated using Sherrer formula,  $D=0.9\lambda/\beta Cos\theta$ , where D is the average crystallite size,  $\beta$  is full width at half maximum of peaks corrected for instrumental broadening, and  $\theta$  is the Bragg's angle. The estimated average crystallite size of the as synthesized CFO powder was ~ 40 nm. Metal oxide impurity which was formed during combustion reaction was successfully removed by calcination of the as synthesized powder at 800°C for 3hrs. The powder diffraction pattern of the calcined powder showed CFO phase (JCPDF file no. 22-1086) without any impurity and the estimated average crystallite size was ~ 85nm.

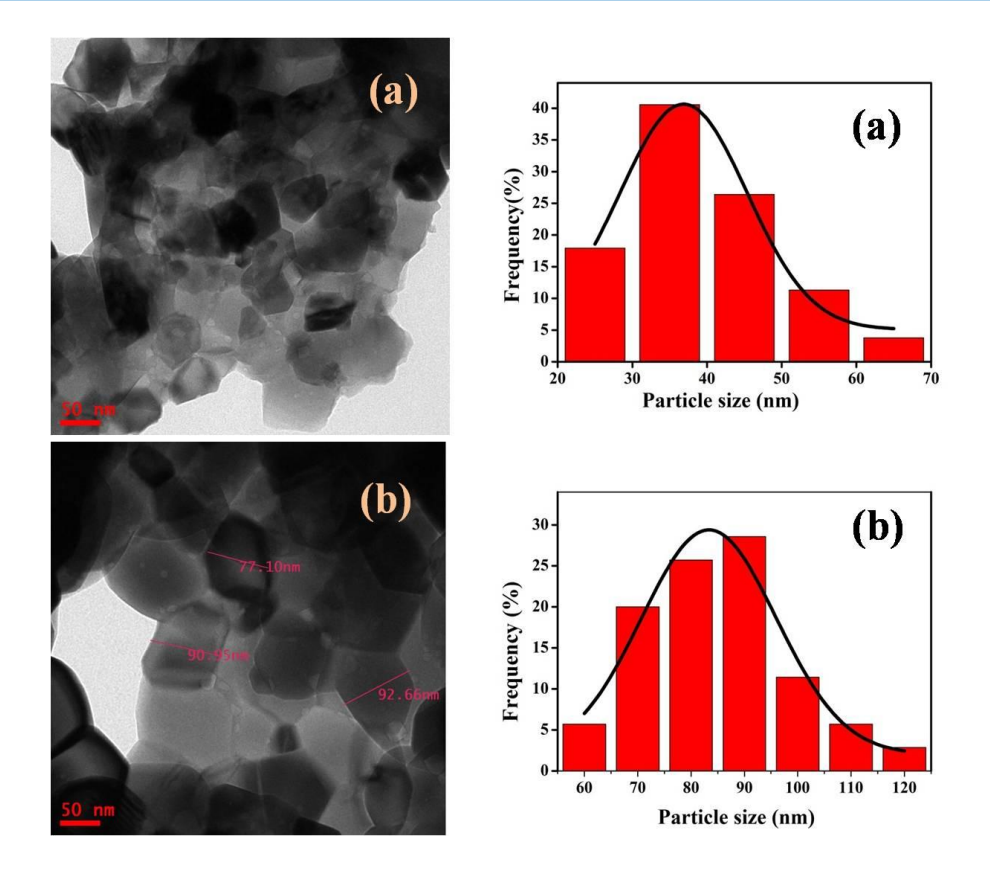


Figure 4.1.1.2 TEM images of the powder particle sizes and their distribution of a) as-synthesized and b) Calcined (800°C for 3 h) CFO powder

TEM micro images of the as-synthesized (a) and calcined (800°C for 3 h) CFO powder (b) was shown in figure 2. The average particle sizes of ~36 nm and ~83 nm were measured for the as prepared and calcined CFO powder respectively. The particle size distribution graph revealed that as-synthesized powder consists of particle size ranging from 20 to 60 nm, while the calcined powder consists of particle size ranging from 60 to 120 nm. This particle sizes were in good agreement with the crystallite sizes calculated from the XRD data. From TEM images it has been observed that both the as synthesized and calcined powder particles were agglomerated and having distorted spherical particle morphology. The increased particle size of the calcined CFO powder was due to the enhanced diffusion of the constituent ions at high calcination temperature [1].

#### 4.1.1.2. Magnetic properties

Figure 4.1.1.3 depicts the M-H curve of calcined CFO sample at 800 C for 3 hrs. High remanence and coercive field characteristics are essential to keep the orientation state of the

magnetic dipole/domain intact before sintering. The maximum magnetization of 68 Am $^2$ /kg at an applied field of ~1200 kA/m has been obtained which agrees well with the reported value in the literature for CFO [2]. This saturation magnetization value is high enough to provide magnetostatic torque during the field assisted compaction process [3]. The obtained values of remanent magnetization and coercive field of CFO are about 31A.m $^2$ /kg and 90 kA/m, respectively. A remanence ratio ( $M_r/M_s$ , here  $M_{max}$  has been taken as  $M_s$  at the maximum applied field) of 0.46 indicated the randomly oriented distribution of equiaxial CFO particles with cubic magneto crystalline anisotropy [3].

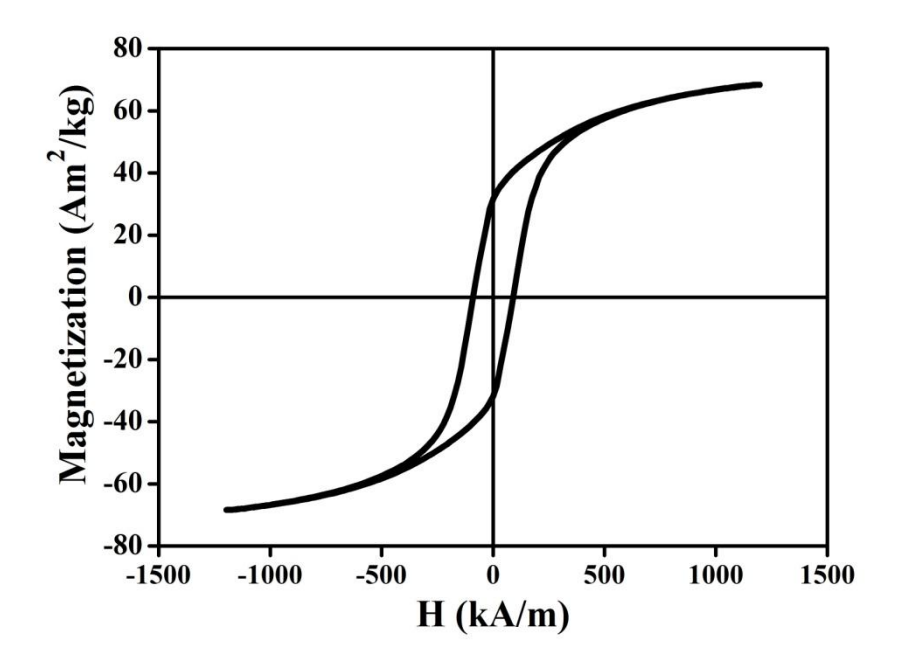


Figure 4.1.1.3 Room temperature magnetization (M-H) curve of CFO powder calcined at  $800^{\circ}$ C for 3h

#### 4.1.1.2 Characterization of sintered AC-CFO pellets compacted under magnetic field

#### 4.1.1.2.1 Structural properties

XRD pattern of CFO pellets compacted in parallel MAC at different magnetic fields such as 0T, 0.5T, 1T and 1.5T are shown in figure 4.1.1.4, which resulted in pure cubic spinel phase (JCPDF file no. 22-1086). No preferential orientation of the XRD peaks were observed in the pattern of pellets obtained by magnetic field assisted compaction as compared to the normal pressing, suggesting possible absence of any crystallographic texture in the sample. Lattice parameter of the samples pressed in parallel MAC at the different magnetic fields was calculated from XRD

using nelson relay extrapolation plots and values are summarized in table 4.1.1.1. No significant variation in lattice parameter was observed for the samples compacted at different magnetic fields.

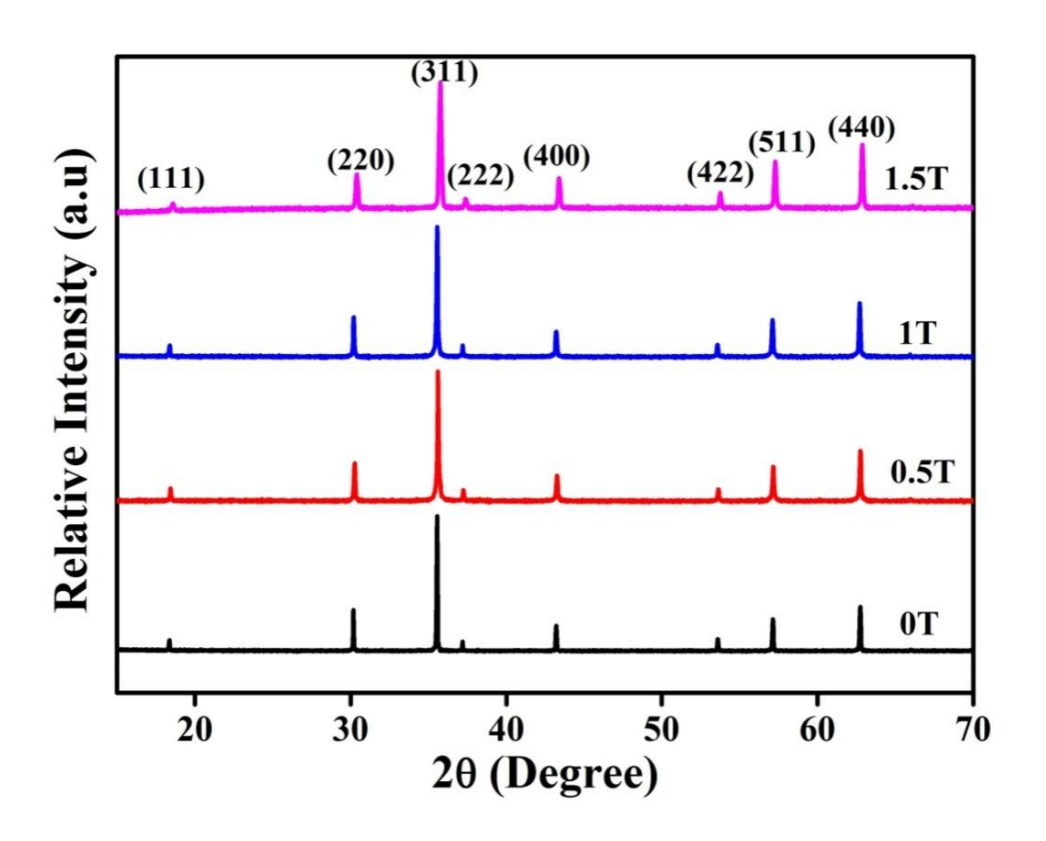


Figure 4.1.1.4 XRD of sintered AC-CFO Pellets compacted in parallel MAC at different magnetic fields

Table.4.1.1.1 lattice parameter values of sintered AC-CFO Pellets compacted in parallel MAC at different magnetic fields

S.No	Sample name	Lattice parameter (A°)		
1	0Т	8.37		
2	0.5T	8.37		
3	1T	8.37		
4	1.5T	8.37		

#### 4.1.1.2.2 Microstructural analysis

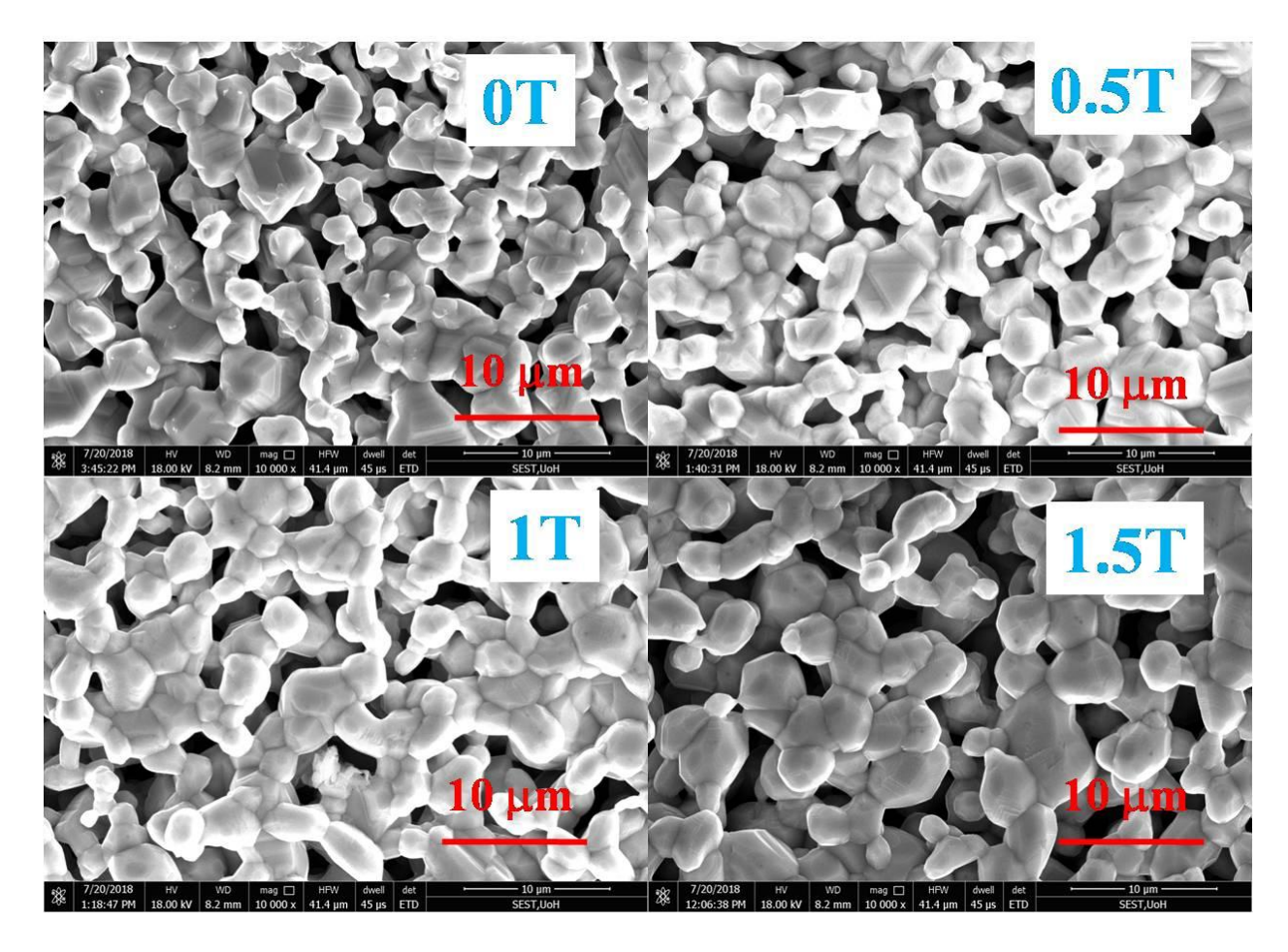


Figure 4.1.1.5 SEM micrographs of sintered AC-CFO Pellets compacted in parallel MAC at different magnetic fields

Figure 4.1.1.5shows the SEM micrographs of sintered AC-CFO pellets pressed under parallel MAC at different magnetic fields (0T, 0.5T, 1T, 1.5T). From SEM micrographs of all AC-CFO pellets, it is observed that porosity is present and complete densification of pellets has not taken place during sintering. Sintered density is calculated from Archimedes method following ASTM standard (C373-88) and it is found to be ~85% of the theoretical density for all AC-CFO pellets, which is similar to the percent of theoretical density reported for CFO pellets synthesized by auto-combustion method [2]. The estimated average grain size lies between 2 and 4 μm for all AC-CFO pellets pressed under different magnetic fields. No visible difference in grain size is observed for AC-CFO pellets compacted at different magnetic fields. Therefore, almost negligible effect of magnetic field assisted compaction on microstructure, density and grain size

has been observed. It is exactly similar to reported literature, where grain size is not affected by field assisted compaction for CFO sample [3].

#### 4.1.1.2.3. Magnetic properties

Applied stress and magnetic field dominate the magnetic crystalline energy in controlling the magnetization direction in domains [4]. Magnetic strain energy ( $E_{\sigma}$ ) created because of applied stress during compaction in CFO try to orient the domains parallel to stress axis whereas applied magnetic field orient the domains in the direction of applied field in CFO green compact during magnetic field assisted compaction. Since, sintering temperature (1350°C) of CFO is greater than its Curie temperature (520°C) spin orientation may get randomized but due to strong lattice orbit coupling the resultant magnetization vectors orient along the direction of initial stable magnetization direction after cooling [5].

Parallel and perpendicular magnetic hysteresis loops for AC-CFO samples compacted in parallel MAC at different magnetic fields were measured in PQMS by applying magnetic field parallel and perpendicular to oriented direction of the sample. Parallel and perpendicular magnetic hysteresis loops of AC-CFO samples compacted in parallel MAC at different magnetic fields are shown in figure 4.1.1.6. Saturation magnetization values of 83emu/g and 85emu/g were observed in parallel and perpendicular hysteresis loops respectively for AC-CFO sample compacted without magnetic field (0T). These saturation magnetization values are in good agreement with the reported values of saturation magnetization of CFO [6]. It has been reported that magnetic moment of cobalt ferrite depends on cation distribution in the octahedral (Oh) and tetrahedral (Td) sites of CFO lattice. Structure of CFO can be written as  $[Co_{1-i}^{+2}Fe_i^{+3}]_{Td}[Co_i^{+2}Fe_{2-i}^{+3}]_{Oh}O_4$ . Magnetic moment ( $\mu$ ) of CFO is expressed as (7-4i)  $\mu_B$  where "i" is the inversion factor or degree of inversion, which is dependent on the processing history (mainly heat treatment conditions) of the sample. If all the  $Co^{+2}$  ions are in the octahedral environment, i = 1 (results in purely inverse spinel structure) and if all the  $Co^{+2}$  ions are in the tetrahedral sites, i = 0 (results in purely normal spinel structure). For purely inverse spinel structure of CFO (i = 1), magnetic moment is close to 70emu/g. Depending on the "i" value saturation magnetization of CFO keeps changing. As "i" value decreases saturation magnetization increases. Saturation magnetizations of 81 - 87 emu/g were found for CFO with variation in the inversion factor (i) in between 0.90 -0.84 [6].

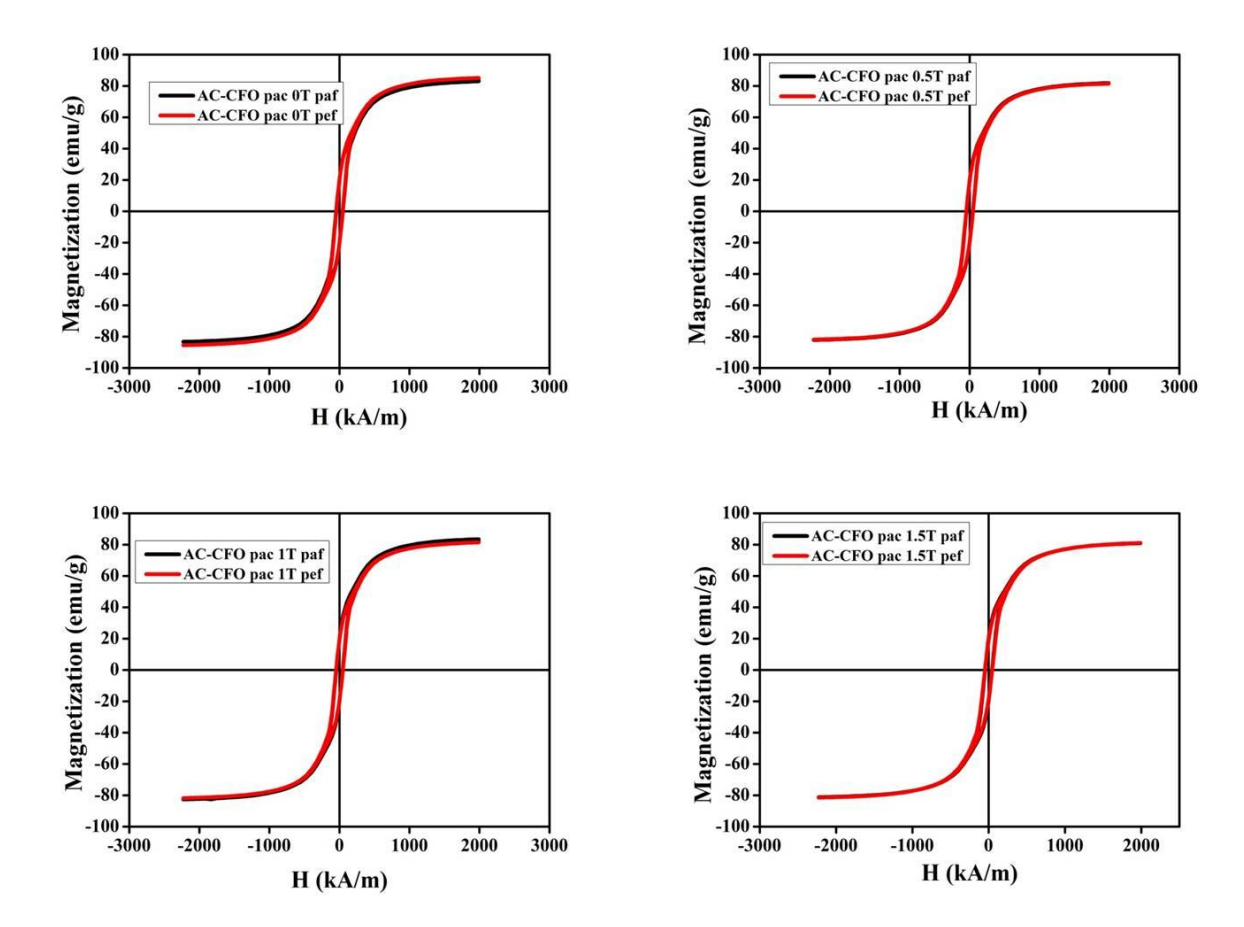


Figure 4.1.1.6 M–H curve of sintered AC–CFO Pellets compacted in parallel MAC at different magnetic fields

Magnetic properties obtained from parallel and perpendicular hysteresis loops of AC-CFO samples compacted in parallel MAC at different magnetic fields are summarized in table 4.1.1.2. Marginal variation in saturation magnetization (81 emu/g to 83 emu/g), remanence (19 emu/g to 20 emu/g), and coercivity (45 kA/m to 47 kA/m) values have been observed in parallel magnetic hysteresis loops of AC-CFO pellets compacted in parallel MAC as a function of the different applied magnetic fields. Similarly, a small variation in saturation magnetization (81 emu/g to 85 emu/g), remanence (19 emu/g to 20 emu/g), and coercivity (45 kA/m to 48 kA/m) values have been observed in perpendicular magnetic hysteresis loops of AC-CFO pellets compacted in parallel MAC as a function of the different applied magnetic fields.

Table 4.1.1.2 Magnetic properties of sintered AC-CFO Pellets compacted in parallel MAC at different magnetic fields

Sl.No.	Sample	Par M <sub>S</sub> (emu/g)	Par M <sub>r</sub> (emu/g)	Par H <sub>C</sub> (kA/m)	Per M <sub>S</sub> (emu/g)	Per M <sub>r</sub> (emu/g)	Per H <sub>C</sub> (kA/m)
1	OT	83	20	47.5	85	20	45.1
2	0.5T	82	19	46.8	82	19	47.0
3	1T	83	19	46.2	81	19	47.9
4	1.5T	81	19	46.0	81	19	47.5

#### **4.1.1.2.4.** Magnetoelastic properties

Magnetostriction was measured on AC-CFO pellets obtained by the magnetic field assisted compaction at the different fields and the data is plotted in figure 4.1.1.7. Strain gauge was mounted on the flattened surface of the pellets along the oriented direction of the sample pellet. Parallel magnetostriction ( $\lambda_{\parallel}$ ) has been measured along the oriented direction while perpendicular magnetostriction ( $\lambda_{\perp}$ ) has been measured perpendicular to oriented direction of sample pellets. In AC-CFO pellets compacted in parallel MAC applied magnetic field direction during compaction is oriented direction. Significant improvement in magnetostriction and strain derivative has been observed in sintered pellets compacted at 1.5 Tesla magnetic field compared to the sample compacted without magnetic field. For 0T samples, maximum parallel magnetostriction ( $\lambda_{\parallel}$ ) and maximum perpendicular magnetostriction ( $\lambda_{\perp}$ ) have been observed to be ~139 ppm and ~49 ppm, respectively, which are in good agreement with the reported values of CFO in the literature [7]. Maximum parallel magnetostriction ( $\lambda_{\parallel}$ ) of ~185 ppm and maximum perpendicular magnetostriction ( $\lambda_{\perp}$ ) of ~69ppm has been observed for samples prepared at 1.5T. Nearly 40% improvement has been observed in parallel magnetostriction of 1.5T sample compared to 0T sample.

Variation of magnetostriction of sintered AC–CFO samples with the applied magnetic field during parallel MAC has been plotted in figure 4.1.1.8. It is clear from the plot that the increase in magnetostriction has been observed with an increase in the applied magnetic field during parallel MAC. Maximum increase in magnetostriction ( $\lambda_{\parallel}$ ) has been observed for the sample prepared at 0.5T compare to the sample without magnetic field. However, a further increase in the applied

magnetic field to 1T and 1.5T resulted in a relatively less increase in magnetostriction compare to the sample prepared at 0.5T.

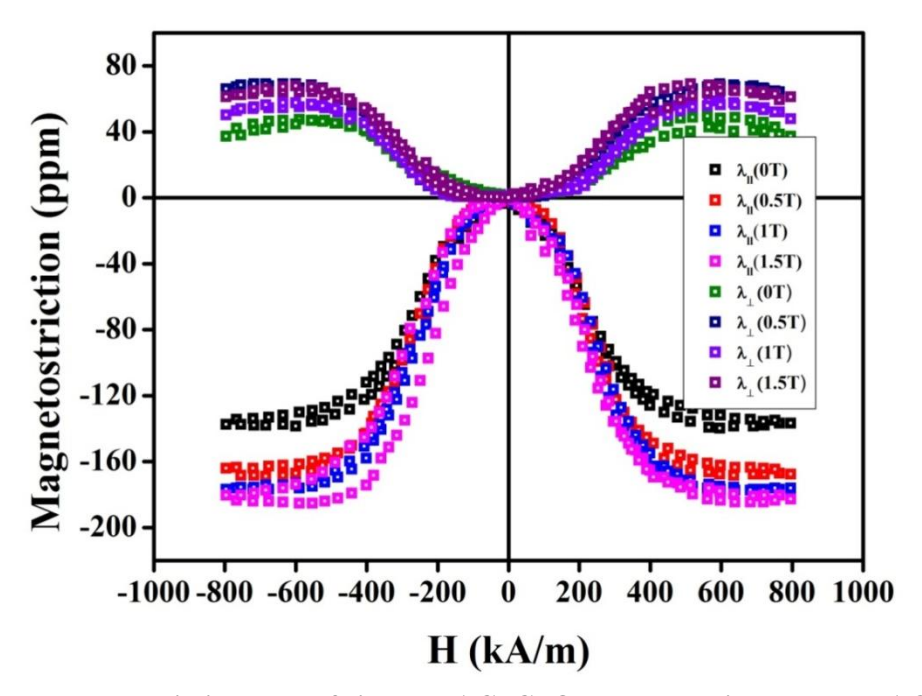


Figure 4.1.1.7 Magnetostriction data of sintered AC-CFO compacted in parallel MAC at different magnetic fields

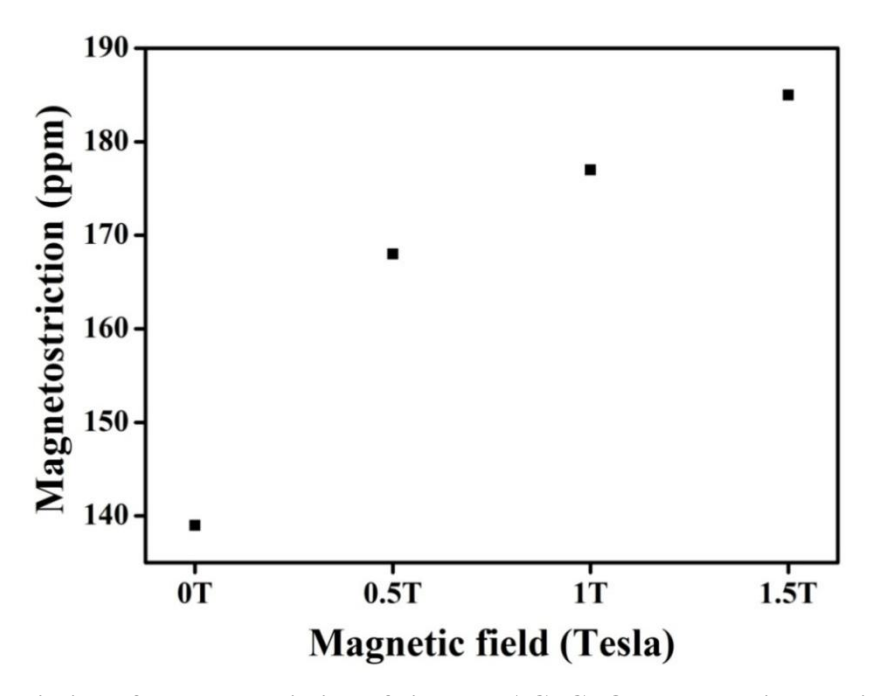


Figure 4.1.1.8. Variation of magnetostriction of sintered AC-CFO samples with applied magnetic field during parallel MAC.

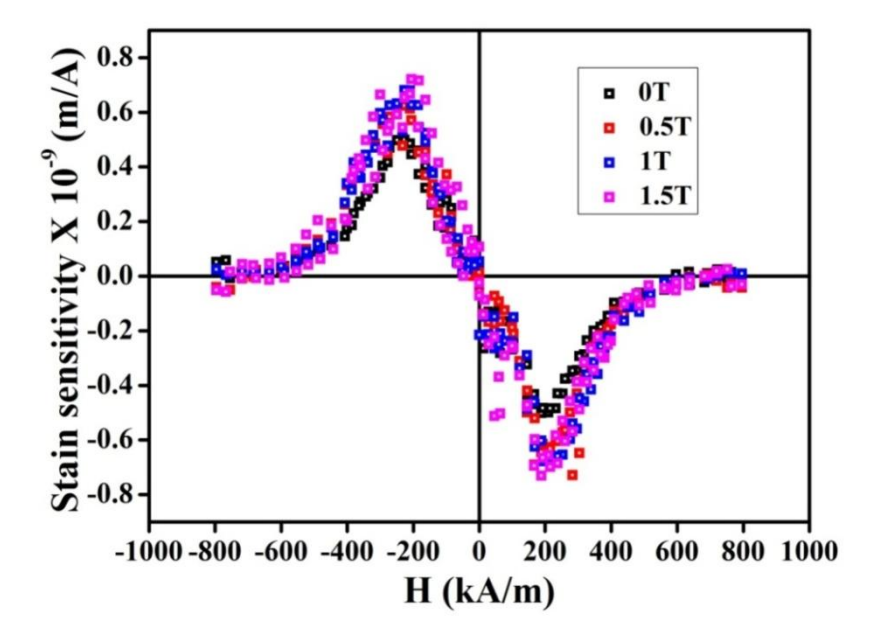


Figure 4.1.1.9 Strain sensitivity data of sintered AC-CFO compacted in parallel MAC at different magnetic fields

Maximum strain sensitivity (d $\lambda$ /dH)  $_{max}$  of  $0.5 \times 10^{-9}$  m/A and  $0.7 \times 10^{-9}$  m/A have been observed for AC-CFO samples compacted at 0T and 1.5T samples, respectively. Nearly 40% improvement in strain derivative has been achieved in 1.5T sample compared to sample prepared without magnetic field.

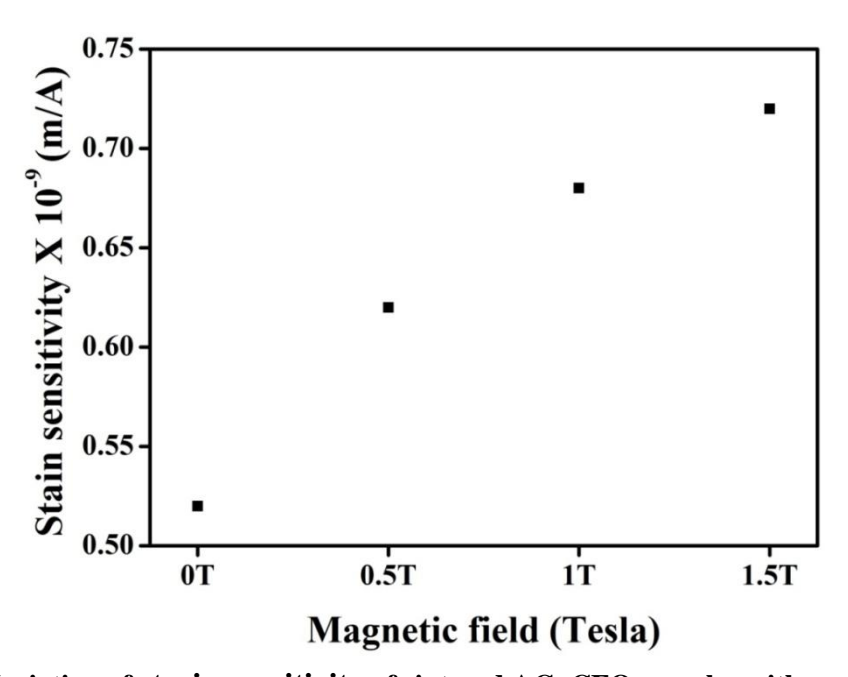


Figure 4.1.1.10 Variation of strain sensitivity of sintered AC-CFO samples with applied magnetic field during parallel MAC

The maximum strain sensitivity observed in MP sample is greater than that observed in polycrystalline CFO (prepared from 3nm powder) after magnetic annealing [8]. In parallel MAC, maximum magnetostriction and strain derivative have been observed in the direction of oriented axis direction [3-5]. But for magnetic annealed sample, high strain derivative and magnetostriction have been observed in perpendicular to the oriented direction, where the direction in which the magnetic field was applied during magnetic annealing [9]. 90° domain wall motion followed by domain rotation is responsible for the observed magnetostriction in the CFO. In parallel MAC, more 90°domains are created compared to the sample prepared without magnetic field. As the magnetic field increased in parallel MAC, magnetostriction is improved up to 1.5T. A sharp increase in magnetostriction suggests that more number of 90° domains are created in 1.5T sample compare to the sample prepared without the applied magnetic field. But, the number of domains decreased with the increased magnetic field during compaction at 1T and 1.5T.

#### 4.1.1.3 Conclusions

Phase pure cobalt ferrite nanoparticles have been synthesized in auto-combustion synthesis. Particle size of 36 nm and 83 nm has been observed for as synthesized and calcined CFO particles. No visible difference in grain size has observed for AC-CFO pellets compacted at different magnetic fields. A small variation in magnetic properties has been observed for AC-CFO pellets compacted at different magnetic fields. Nearly 40% improvement has been observed in parallel magnetostriction of 1.5T sample compared to 0T sample. Increase in number of 90° domains with increasing applied magnetic field during compaction is reason for the improved magnetostriction and strain sensitivity with applied magnetic field during field assisted compaction.

# 4.1.2. Investigation of magnetic and magnetoelastic properties of CoFe<sub>2</sub>O<sub>4</sub> prepared by solid state technique followed by parallel MAC

This section deals with preparation of CFO powder by solid state method and investigation of the effect of parallel magnetic assisted compaction (MAC) on the structural, morphological, and magnetic properties of the prepared CFO. The synthesized powder pressed into pellets and sintered at 1350°C for 12h.Structural, morphological, magnetic and magnetoelastic properties of sintered compacts (referred to as AC-CFO) were studied by XRD, SEM, PQMS and magnetostriction setup techniques respectively.

#### 4.1.2.1 Characterization of CFO powder

#### **4.1.2.1.1** Structural properties

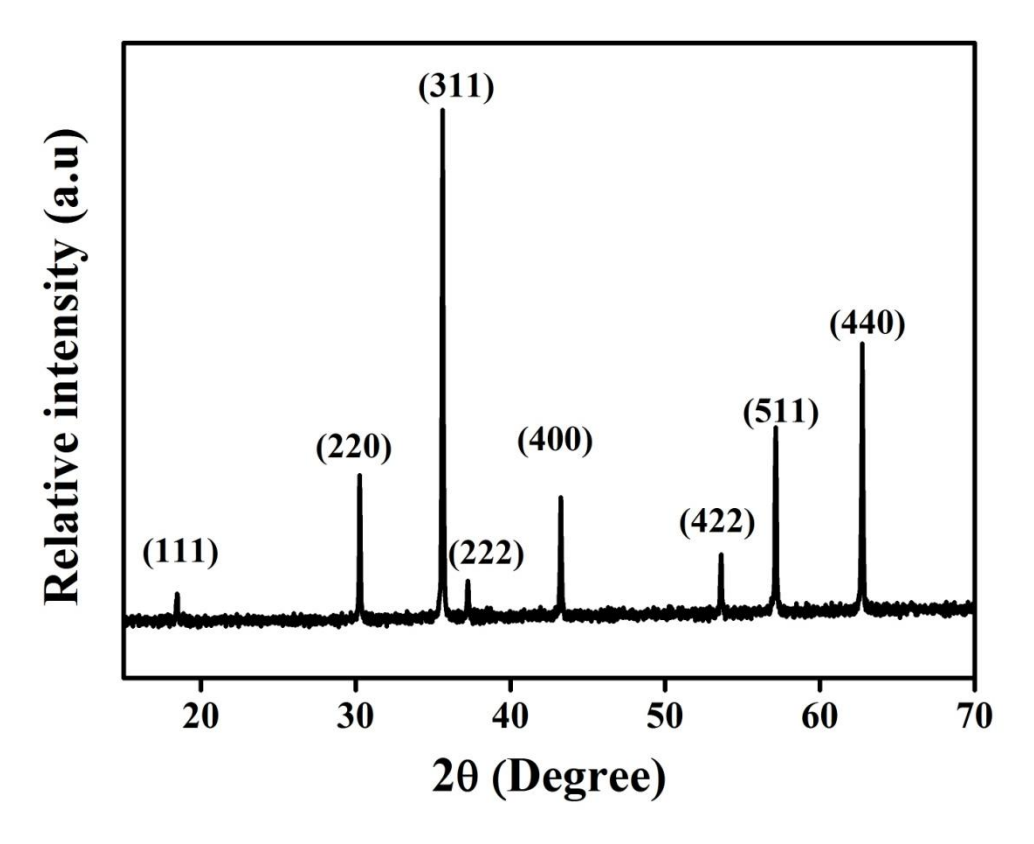


Figure 4.1.2.1 Powder X-ray Diffraction (XRD) pattern of CFO powder double calcined at 1000°C, 12h

X-ray diffraction pattern of calcined CFO powder synthesized by solid state method is shown in fig 4.1.2.1. Powder diffraction of calcined CFO revealed cubic spinel phase(matches with JCPDF file no. 22-1086). SEM micrographs of calcined CFO and particle size distribution have been

shown in 4.1.2.2. The average particle size of 0.27 µm is measured from SEM micrograph. The particle size distribution plot revealed that CFO powder particles consist of particle size ranging from 150 nm to 400 nm. From SEM images it has been observed that calcined CFO powder particles were agglomerated and having distorted spherical particle morphology.

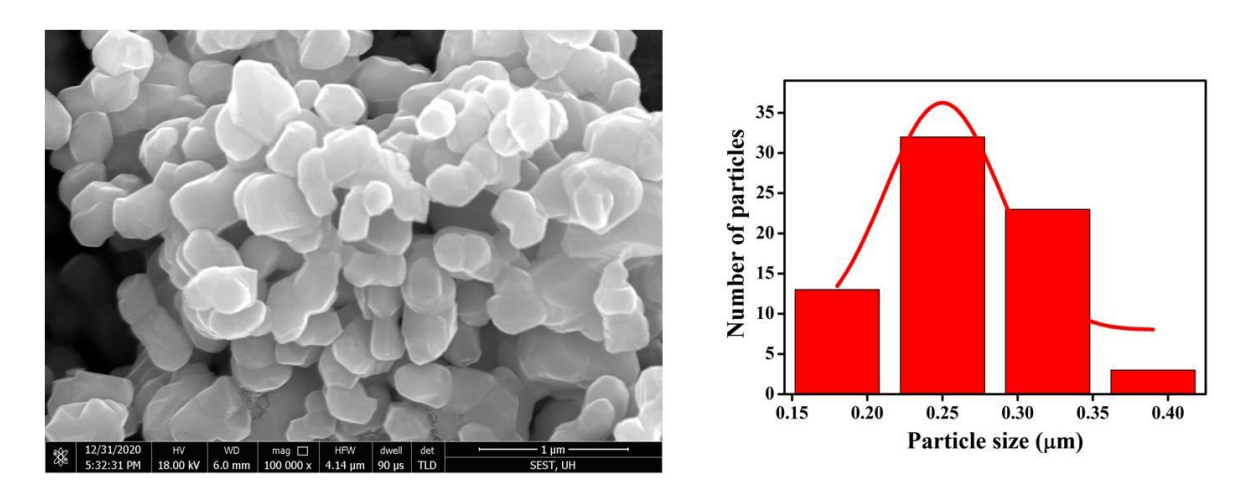


Figure 4.1.2.2 SEM micrograph and particle size distribution of CFO powder double calcined at  $1000^{\circ}$ C, 12h

#### 4.1.2.1.2 Magnetic properties

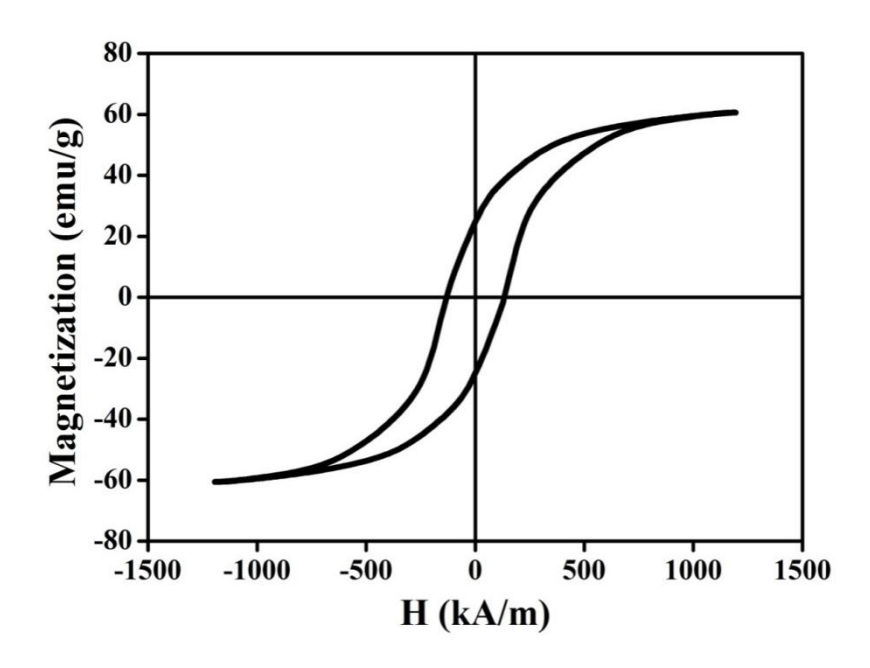


Figure 4.1.2.3Room temperature magnetization (M-H) curve of CFO powder double calcined at 1000°C, 12h

Figure 4.1.2.3 depicts the M-H curve of double calcined CFO powder at  $1000^{\circ}$  C for 12 h. The maximum magnetization of 60.6 emu/g at an applied field of ~1200 kA/m has been obtained which agrees well with the reported value in the literature for CFO. The obtained values of remanent magnetization and coercive field of CFO are about 24.7 emu/g and 131 kA/m, respectively. A remanence ratio ( $M_r/M_s$ , here  $M_{max}$  has been taken as  $M_s$  at the maximum applied field) of 0.4 indicated the randomly oriented distribution of equiaxial CFO particles with cubic magneto crystalline anisotropy.

## 4.1.2.2. Characterization of sintered SS-CFO pellets compacted under magnetic field

#### 4.1.2.2.1 Phase analysis

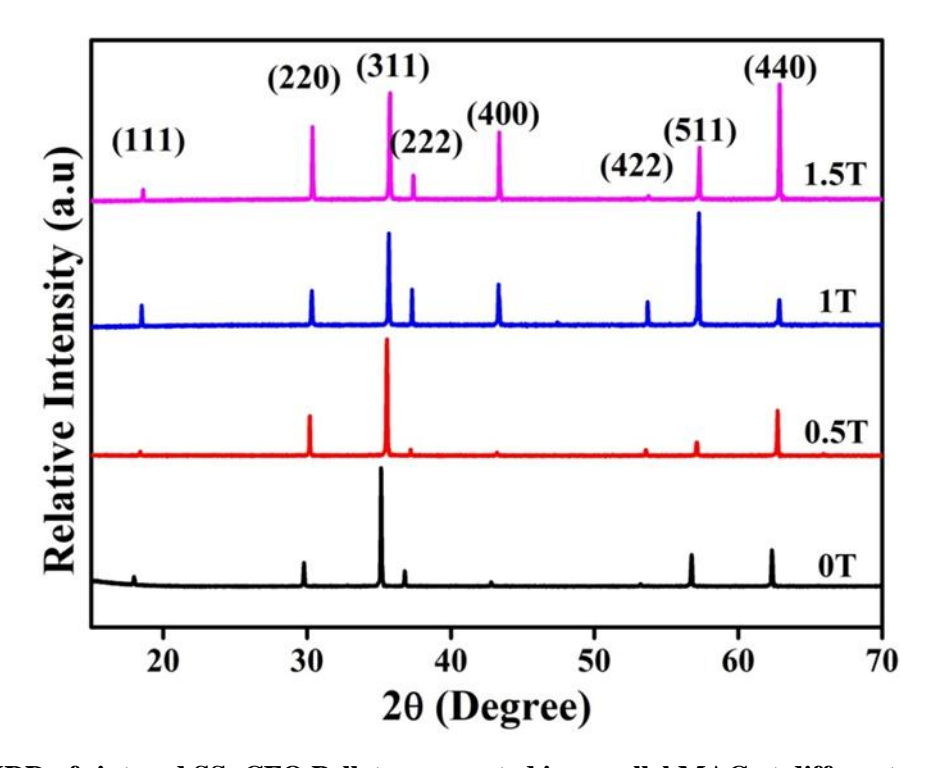


Figure 4.1.2.4 XRD of sintered SS-CFO Pellets compacted in parallel MAC at different magnetic fields

XRD pattern of CFO pellets compacted in parallel MAC at different magnetic fields such as 0T, 0.5T, 1T and 1.5T are shown in figure 4.1.2.4, which resulted in pure cubic spinel phase (JCPDF file no. 22-1086). Preferential orientation of the XRD peaks has been observed in the pattern of 1T and 1.5T pellets obtained by magnetic field assisted compaction as compared to the pellet prepared by normal pressing. Highest intensity has been observed for (511) and (440) peaks for

the pellets compacted at 1T and 1.5T respectively, whereas (311) is the highest intensity peak for the isotropic CFO pellet. Texture coefficient of 2.2 has been observed for (511) peak for the pellet compacted at 1T. Texture coefficient of 1.65 has been observed for (411) peak for the pellet compacted at 1.5T. Lattice parameter of the samples has been calculated from XRD. No variation in lattice parameter has been observed for the samples compacted at different magnetic fields. The lattice parameter values of samples compacted at different magnetic fields has been shown in table 4.1.2.1.

Table.4.1.2.1 lattice parameter values of sintered SS-CFO Pellets compacted in parallel MAC at different magnetic fields

S.No	Sample name	Lattice parameter (A°)		
1	0T	8.38		
2	0.5T	8.38		
3	1T	8.38		
4	1.5T	8.38		

#### 4.1.2.2.2 Microstructural analysis

Figure 4.1.2.5shows the SEM micrographs of sintered SS-CFO pellets pressed under parallel MAC at different magnetic fields (0T, 0.5T, 1T, 1.5T). From SEM micrographs of all SS-CFO pellets, it is observed that porosity is not present and complete densification of pellets has taken place during sintering. Sintered density is calculated from Archimedes method following ASTM standard (C373-88) and it is found to be ~95% of the theoretical density for all SS-CFO pellets, which is similar to the percent of theoretical density reported for CFO pellets synthesized by ceramic method [10]. Exaggerated grain growth has been observed for all SS-CFO pellets pressed in parallel MAC under different magnetic fields. Very large grains and small grains in between the large grains have been observed in microstructure of all SS-CFO pellets pressed in parallel MAC. Therefore, almost negligible effect of magnetic field on microstructure, density and grain size has been observed for pellets pressed under magnetic field. It is exactly similar to reported literature, where grain size is not affected by field assisted compaction for CFO sample [3].

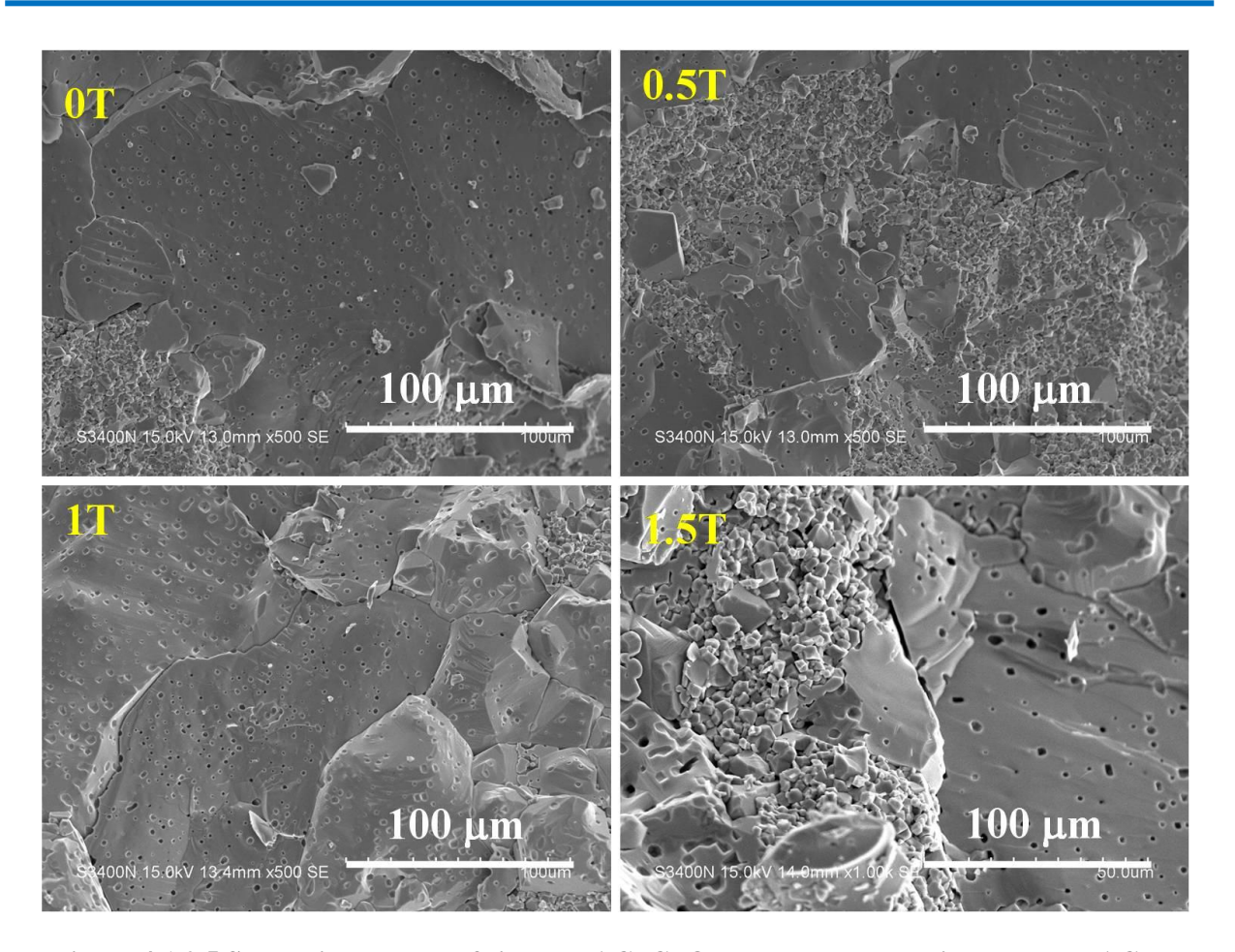


Figure 4.1.2.5 SEM micrographs of sintered AC-CFO Pellets compacted in parallel MAC at different magnetic fields

#### 4.1.2.2.3. Magnetic properties

Applied stress and magnetic field dominates the magnetic crystalline energy in controlling the magnetization direction in domains [4]. Magnetic strain energy ( $E_{\sigma}$ ) created because of applied stress during compaction in CFO try to orient the domains parallel to stress axis where as applied magnetic field orient the domains in the direction of applied field in CFO green compact during magnetic field assisted compaction. Since, sintering temperature (1350°C) of CFO is greater than its Curie temperature (520°C) spin orientation may get randomized but due to strong lattice orbit coupling the resultant magnetization vectors orient along the direction of initial stable magnetization direction after cooling [5].

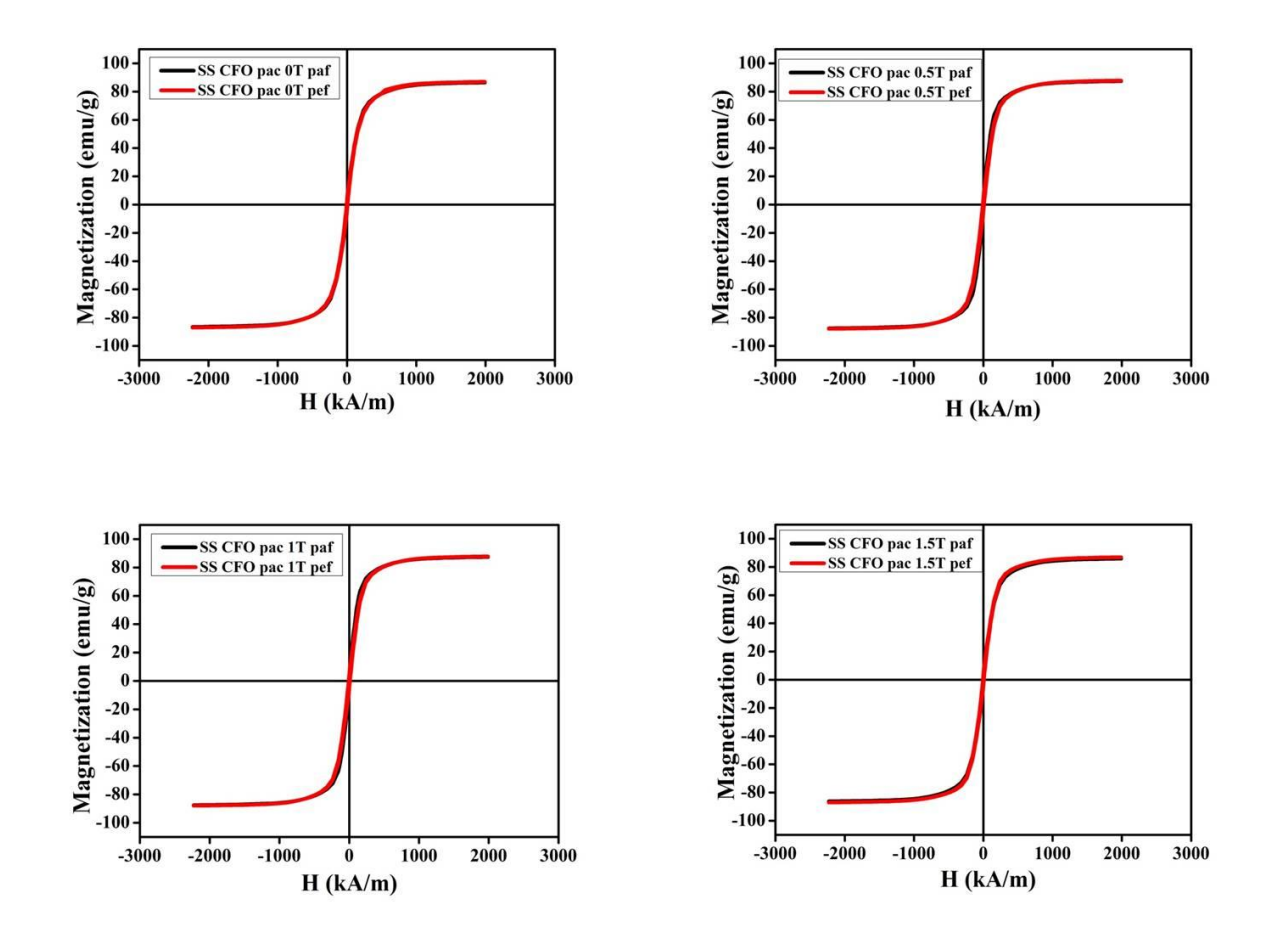


Figure 4.1.2.6 M–H curve of sintered AC–CFO Pellets compacted in parallel MAC at different magnetic fields

Table 4.1.2.2 Magnetic properties of sintered SS-CFO Pellets compacted in parallel MAC at different magnetic fields

Sl.No.	Sample	Par M <sub>S</sub> (emu/g)	Par M <sub>r</sub> (emu/g)	Par H <sub>C</sub> (kA/m)	Per M <sub>S</sub> (emu/g)	Per M <sub>r</sub> (emu/g)	Per H <sub>C</sub> (kA/m)
1	OT	86	3	6.2	87	2	5.4
2	0.5T	87	4	7.3	87	4	8.8
3	1T	85	3	7.8	86	3	6.6
4	1.5T	86	3	6.9	86	3	6.2

Parallel and perpendicular magnetic hysteresis loops for SS-CFO samples compacted in parallel MAC at different magnetic fields were measured in PQMS by applying magnetic field parallel and perpendicular to oriented direction of the sample. Parallel and perpendicular magnetic hysteresis loops of SS-CFO samples compacted in parallel MAC at different magnetic fields are

shown in figure 4.1.2.6. Saturation magnetization values of 86 emu/g and 87 emu/g were observed in parallel and perpendicular hysteresis loops respectively for SS-CFO sample compacted without magnetic field (0T). These saturation magnetization values are in good agreement with the reported values of saturation magnetization of CFO [6].

Magnetic properties obtained from parallel and perpendicular hysteresis loops of SS-CFO samples compacted in parallel MAC at different magnetic fields are summarized in table 4.1.2.2. Marginal variation in saturation magnetization (85 emu/g to 87 emu/g), remanence (3 emu/g to 4 emu/g), and coercivity (6.2 kA/m to 7.8 kA/m) values have been observed in parallel magnetic hysteresis loops of SS-CFO pellets compacted in parallel MAC as a function of the different applied magnetic fields. Similarly, a small variation in saturation magnetization (86 emu/g to 87 emu/g), remanence (2 emu/g to 4 emu/g), and coercivity (5.4 kA/m to 8.8 kA/m) values have been observed in perpendicular magnetic hysteresis loops of AC-CFO pellets compacted in parallel MAC as a function of the different applied magnetic fields.

#### 4.1.2.2.4. Magnetoelastic properties

Magnetostriction was measured on SS-CFO pellets obtained by the magnetic field assisted compaction at the different fields and the data is plotted in figure 4.1.2.7 Strain gauge was mounted on the flattened surface of the pellets along the oriented direction of the sample. Parallel magnetostriction (λ<sub>||</sub>) has been measured along the oriented direction while perpendicular magnetostriction ( $\lambda_1$ ) has been measured perpendicular to oriented direction of the sample pellets. In SS-CFO pellets compacted in parallel MAC applied magnetic field direction during compaction is oriented direction. Significant improvement in magnetostriction and strain derivative has been observed for sintered pellets compacted at 1.5 Tesla magnetic field compared to the sample compacted without magnetic field (OT). For OT samples, maximum parallel magnetostriction ( $\lambda_{\parallel}$ ) has been observed to be ~110 ppm, which is in good agreement with the reported values of CFO in the literature [11]. Variation of magnetostriction of sintered SS-CFO samples with the applied magnetic field during parallel MAC has been plotted in figure 4.1.2.8. It is clear from the plot that there is a linear increase in magnetostriction with increase in the applied magnetic field up to 1.5T during parallel MAC. Maximum parallel magnetostriction ( $\lambda_{\parallel}$ ) of 207ppm has been observed for the sample prepared at 1.5T. Nearly 90% improvement has been observed in parallel magnetostriction of 1.5T sample compared to 0T sample.

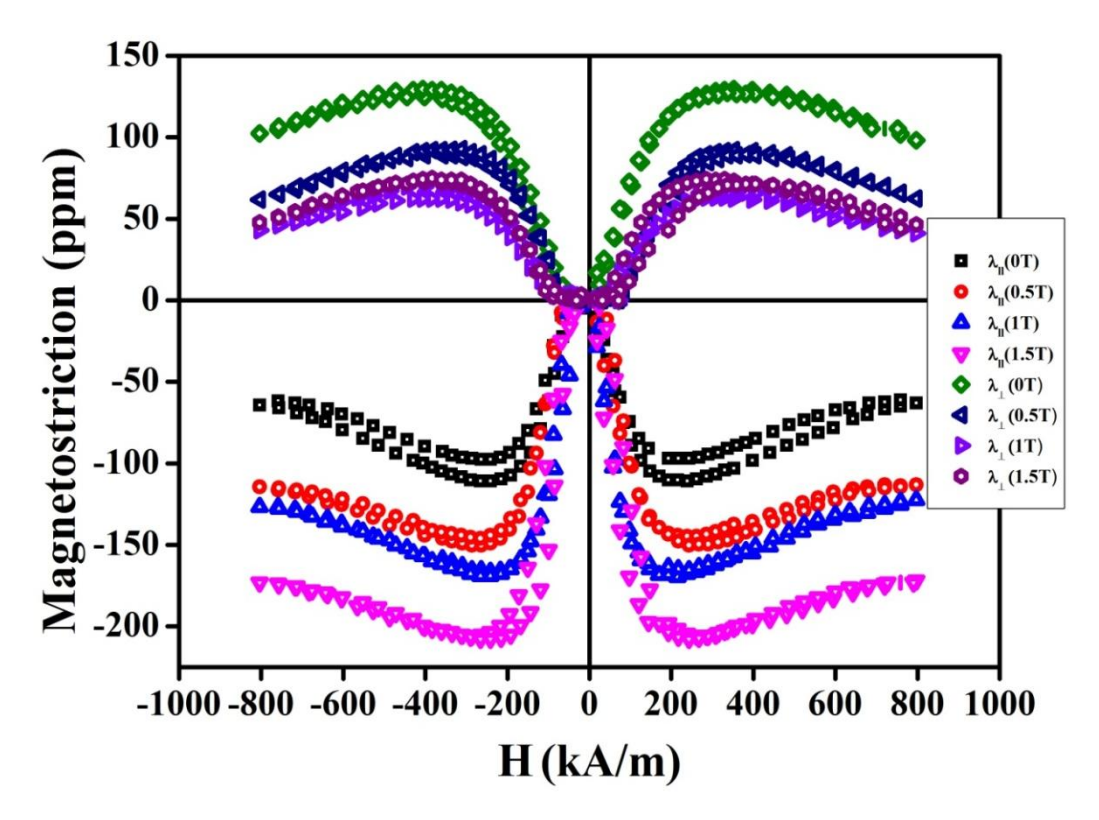


Figure 4.1.2.7 Magnetostriction data of sintered SS-CFO compacted in parallel MAC at different magnetic fields

Strain sensitivity has been calculated from parallel magnetostriction data of AC-CFO pellets prepared in parallel MAC and data is shown in figure 4.1.2.9. Strain sensitivity of  $0.5 \times 10^{-9}$  m/A has been observed for the sample prepared without magnetic field, which is in good agreement with strain sensitivity of CFO [8]. As shown in figure 4.1.2.109, a continuous increase in strain sensitivity has been observed for AC-CFO pellets compacted in parallel MAC with an increase in magnetic field during compaction.

Maximum strain sensitivity ( $d\lambda/dH$ )  $_{max}$  of  $0.5 \times 10^{-9}$  m/A and  $0.7 \times 10^{-9}$  m/A have been observed for AC-CFO samples compacted at 0T and 1.5T samples, respectively. Nearly 40% improvement in strain derivative has been achieved in 1.5T sample compared to sample prepared without magnetic field. The maximum strain sensitivity observed in MP sample is greater than that observed in polycrystalline CFO (prepared from 3nm powder) after magnetic annealing [8].In parallel MAC, maximum magnetostriction and strain derivative have been observed in the direction of oriented axis direction [3, 5]. But for magnetic annealed sample, high strain derivative and magnetostriction have been observed in perpendicular to the oriented direction,

where the direction in which the magnetic field was applied during magnetic annealing [9]. 90° domain wall motion followed by domain rotation is responsible for the observed magnetostriction in the CFO. In parallel MAC, more 90°domains are created compared to the sample prepared without magnetic field. As the magnetic field increased in parallel MAC, magnetostriction is improved up to 1.5T. A sharp increase in magnetostriction suggests that more number of domains is created in 1.5T sample compare to the sample prepared without magnetic field. But, increase in domains has been decreased with increased magnetic field during compaction at 1T and 1.5T.

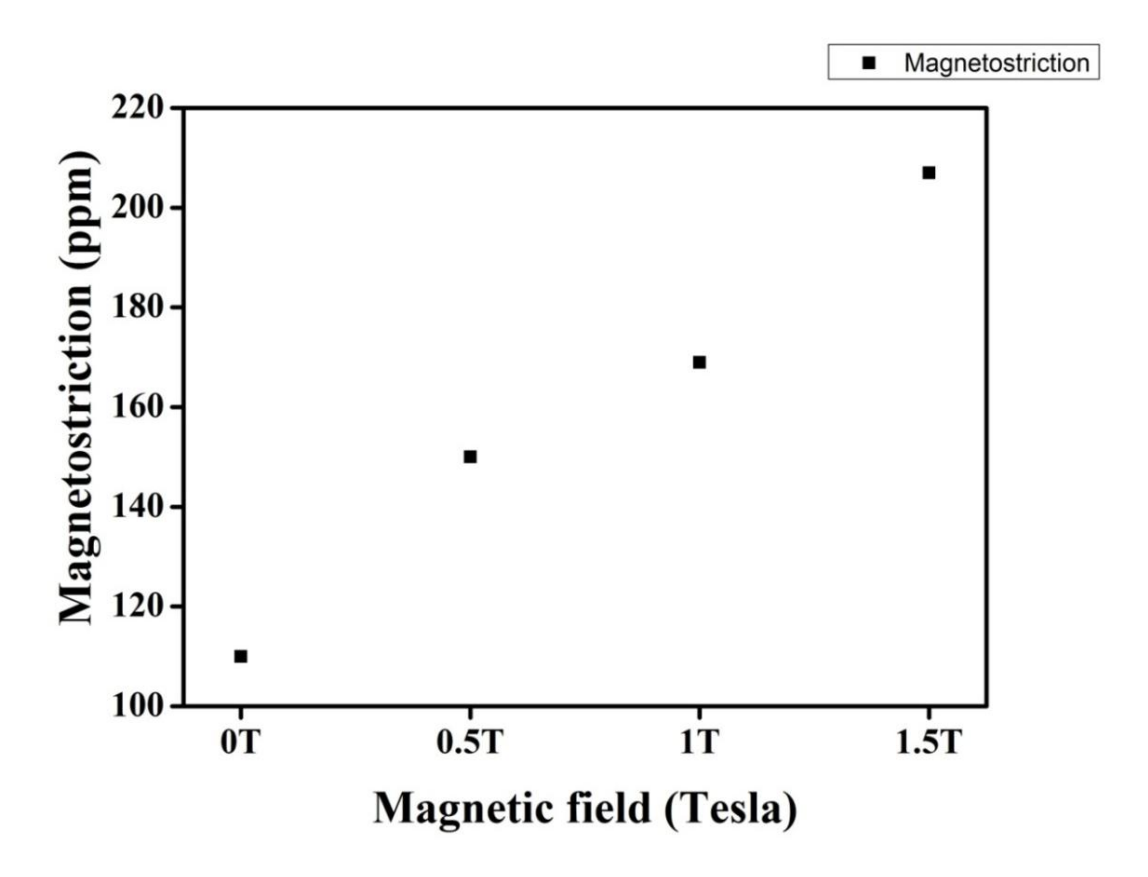


Figure 4.1.2.8 Variation of magnetostriction of sintered SS-CFO samples with applied magnetic field during parallel MAC.

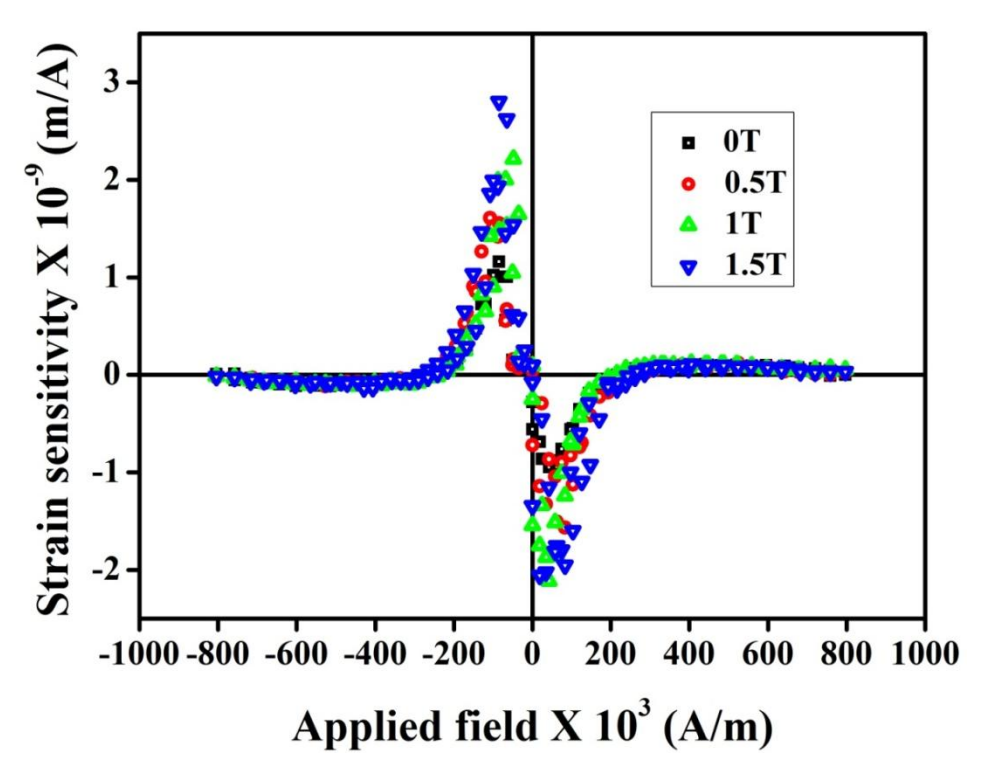


Figure 4.1.2.9 Strain sensitivity data of sintered AC-CFO compacted in parallel MAC at different magnetic fields

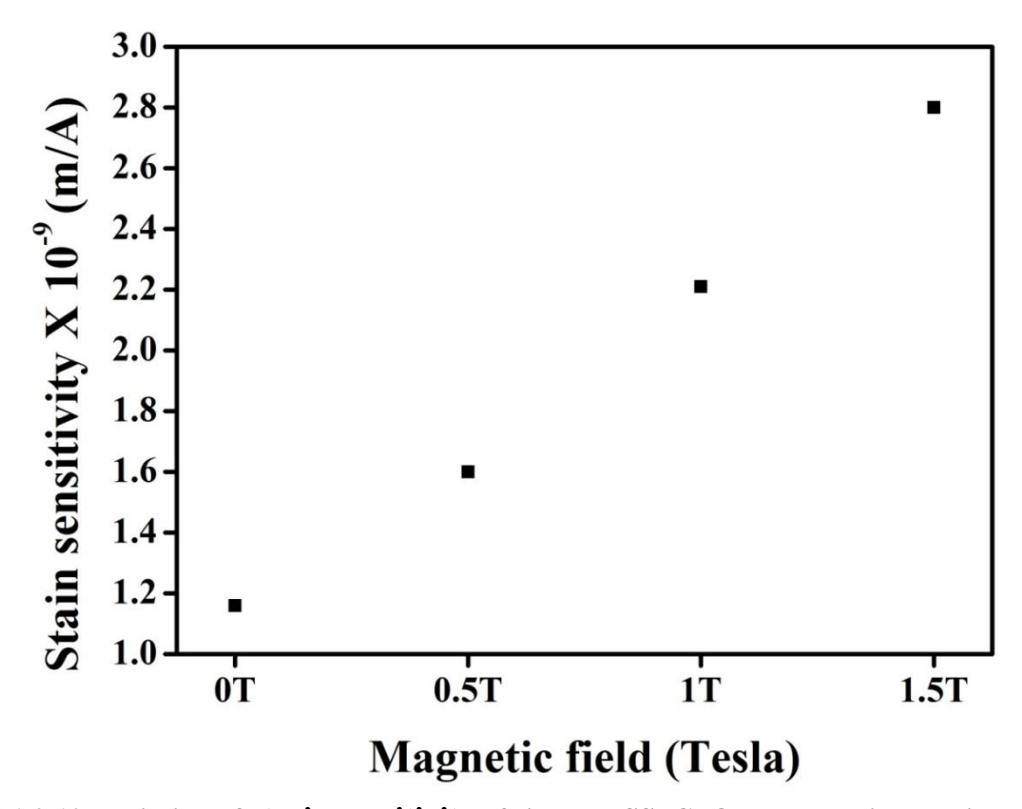


Figure 4.1.2.10 Variation of strain sensitivity of sintered SS-CFO samples with applied magnetic field during parallel MAC

#### 4.1.2.3 Conclusions

Phase pure cobalt ferrite nanoparticles have been synthesized in solid state synthesis. CFO powder particles consist of particle size ranging from 150 nm to 400 nm has been observed in FESEM. Grains with exaggerate grain growth mixed with small grains have been observed for all AC-CFO pellets compacted at different magnetic fields. A small variation in magnetic properties has been observed for AC-CFO pellets compacted at different magnetic fields. Nearly 90% improvement in magnetostriction and 40% improvement in strain sensitivity have been observed in parallel magnetostriction of 1.5T sample compared to 0T sample. Increase in number of 90° domains with increasing applied magnetic field during compaction is reason for the improved magnetostriction and strain sensitivity with applied magnetic field during field assisted compaction.

## 4.1.3. Investigation of magnetic and magnetoelastic properties of CoFe<sub>2</sub>O<sub>4</sub> prepared by autocombustion followed by perpendicular MAC

This section deals with preparation of nano crystalline CFO by auto-combustion method using glycine as fuel and investigation of the effect perpendicular magnetic assisted compaction (MAC) on the structural, morphological, and magnetic properties of CFO. The fuel to nitrate ratio was maintained as 0.5. As synthesized CFO powder was calcined at 800°C to obtain CFO with pure phase. Further, phase pure CFO was pressed into pellets using parallel MAC at different magnetic fields (0T, 0.5T, 1T, 1.5T and2T). These pellets were sintered at 1350°C for 12h. Applied Magnetic field direction in the sample is called oriented direction. Structural, morphological, magnetic and magnetoelastic properties of sintered compacts (referred to as AC-CFO) were studied by XRD, SEM, PQMS and magnetostriction setup techniques respectively.

Synthesis and characterization of nanocrystalline CFO powder prepared by autocombustion synthesis was discussed in chapter 4.1.1.

### 4.1.3.1 Characterization of sintered AC-CFO pellets compacted under perpendicular magnetic field

#### **4.1.3.1.1 Phase analysis**

XRD pattern of CFO pellets compacted in perpendicular MAC at different magnetic fields such as 0T, 0.5T, 1T, 1.5T and 2T are shown in figure 4.1.3.1, which resulted in pure cubic spinel phase (JCPDF file no. 22-1086). No preferential orientations of the XRD peaks were observed in the pattern of pellets suggesting possible absence of any crystallographic texture in the sample. Lattice parameter of the samples was calculated from XRD. No variation in lattice parameter has been observed for the samples compacted at different magnetic fields. The lattice parameter values of samples compacted at different magnetic fields was calculated from XRD using nelson relay extrapolation plots and values are summarized in table 4.1.3.1are summarized in table 4.1.3.1.

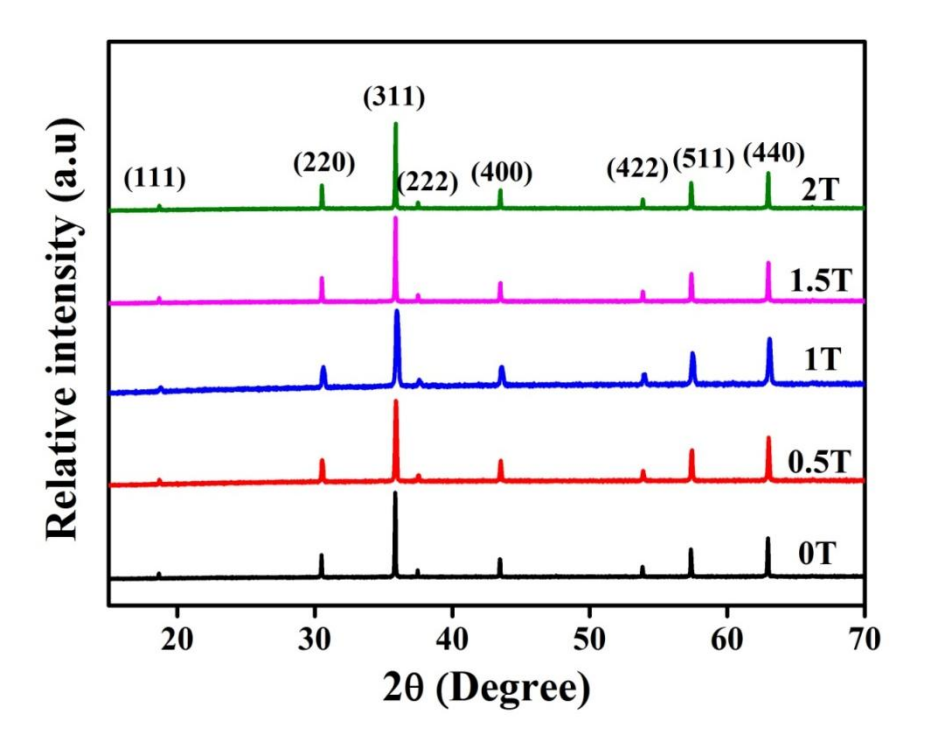


Figure 4.1.3.1 XRD of sintered AC-CFO Pellets compacted in perpendicular MAC at different magnetic fields

Table.4.1.3.1 lattice parameter values of sintered AC-CFO Pellets compacted in perpendicular MAC at different magnetic fields

S.No	Sample name	Lattice parameter (A°)
1	OT	8.37
2	0.5T	8.37
3	1T	8.37
4	1.5T	8.37
5	2T	8.37

#### 4.1.3.1.2 Microstructural analysis

Figure 4.1.3.2shows the SEM micrographs of sintered AC-CFO pellets are pressed under perpendicular MAC at different magnetic fields (0T, 0.5T, 1T, 1.5T and 2T). From SEM micrographs of all AC-CFO pellets, it is observed that porosity is present and complete densification of pellets has not taken place during sintering. Sintered density is calculated from Archimedes method following ASTM standard (C373-88) and it is found to be ~85% of the theoretical density for all AC-CFO pellets, which is similar to the percent of theoretical density

reported for CFO pellets synthesized by autocombustion method [2]. The average grain size of 2-4 µm is estimated for all AC-CFO pellets pressed under different magnetic fields. No visible difference in grain size is observed for AC-CFO pellets compacted at different magnetic fields. Therefore, almost negligible effect of magnetic field assisted compaction on microstructure, density and grain size has been observed for pellets pressed under magnetic field. It is exactly similar to reported literature, where grain size is not affected by field assisted compaction for CFO sample [3].

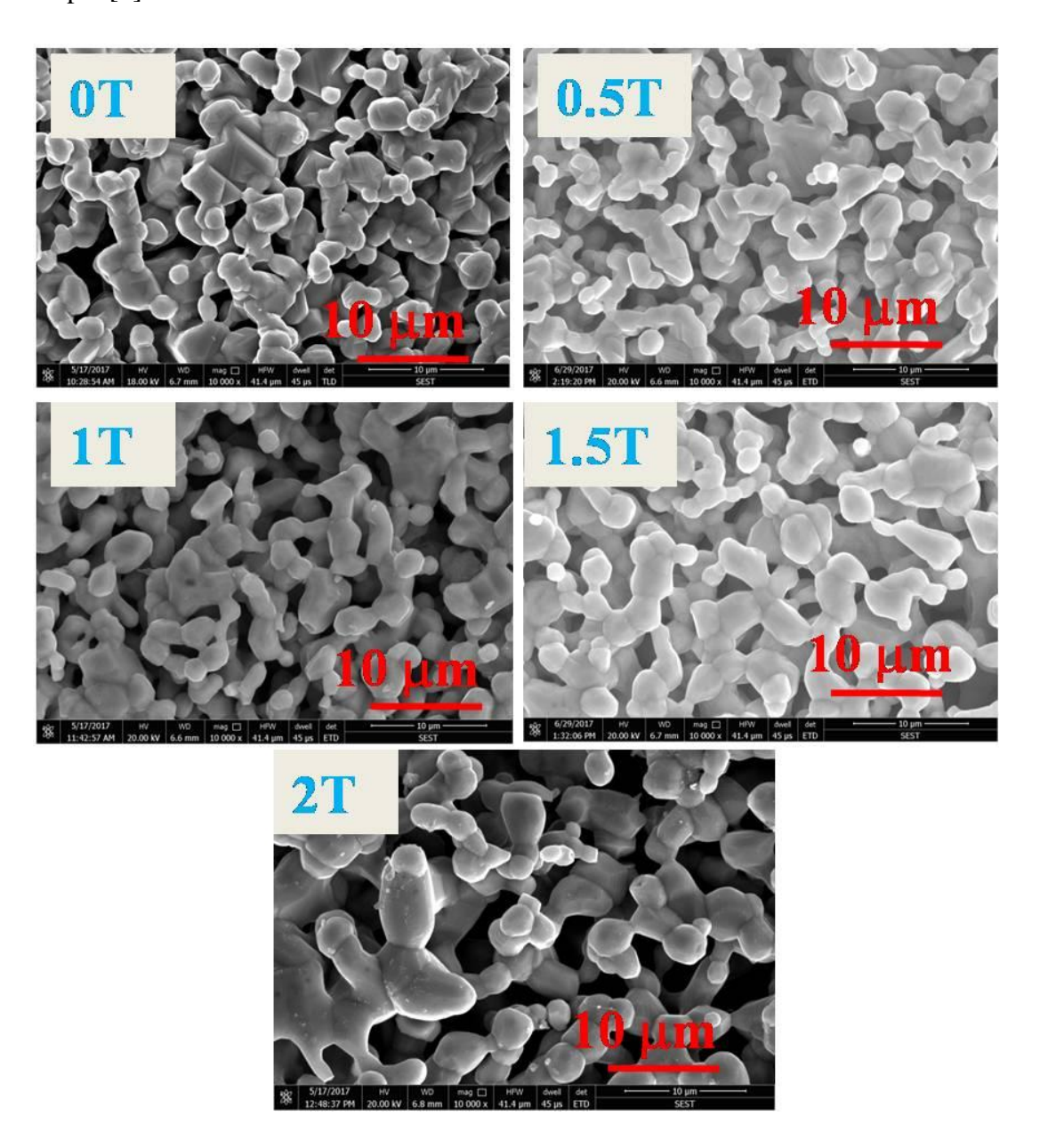


Figure 4.1.3.2 SEM micrographs of sintered AC-CFO Pellets compacted in perpendicular MAC at different magnetic fields

#### **4.1.3.1.3** Magnetic properties

Parallel and perpendicular magnetic hysteresis loops for AC-CFO samples compacted in perpendicular MAC at different magnetic fields were measured in PQMS by applying magnetic field parallel and perpendicular to oriented direction of the sample. Parallel and perpendicular magnetic hysteresis loops of AC-CFO samples compacted in perpendicular MAC at different magnetic fields are shown in figure 4.1.3.3. Saturation magnetization values of 85 emu/g and 83 emu/g were observed in parallel and perpendicular hysteresis loops respectively for AC-CFO sample compacted without magnetic field (0T). These saturation magnetization values were in good agreement with the reported values of saturation magnetization of CFO [6].

Table 4.1.3.2 Magnetic properties of sintered AC-CFO Pellets compacted in perpendicular MAC at different magnetic fields

Sl.No.	Sample	Par M <sub>S</sub> (emu/g)	Par M <sub>r</sub> (emu/g)	Par H <sub>C</sub> (kA/m)	Per M <sub>S</sub> (emu/g)	Per M <sub>r</sub> (emu/g)	Per H <sub>C</sub> (kA/m)
1	OT	85	20	41.5	83	20	43.2
2	0.5T	81	20	43.9	80	21	43.7
3	1T	81	19	43.1	81	19	43.7
4	1.5T	81	20	42.9	80	20	42.9
5	2T	83	19	42.9	82	20	42.7

Magnetic properties obtained from parallel and perpendicular hysteresis loops of AC-CFO samples compacted in perpendicular MAC at different magnetic fields are summarized in table 4.1.3.2. Marginal variation in saturation magnetization (81emu/g to 85 emu/g), remanence (19emu/g to 20 emu/g), and coercivity (41.5 kA/m to 43.9 kA/m) values have been observed in parallel magnetic hysteresis loops of AC-CFO pellets compacted in perpendicular MAC at different magnetic fields.

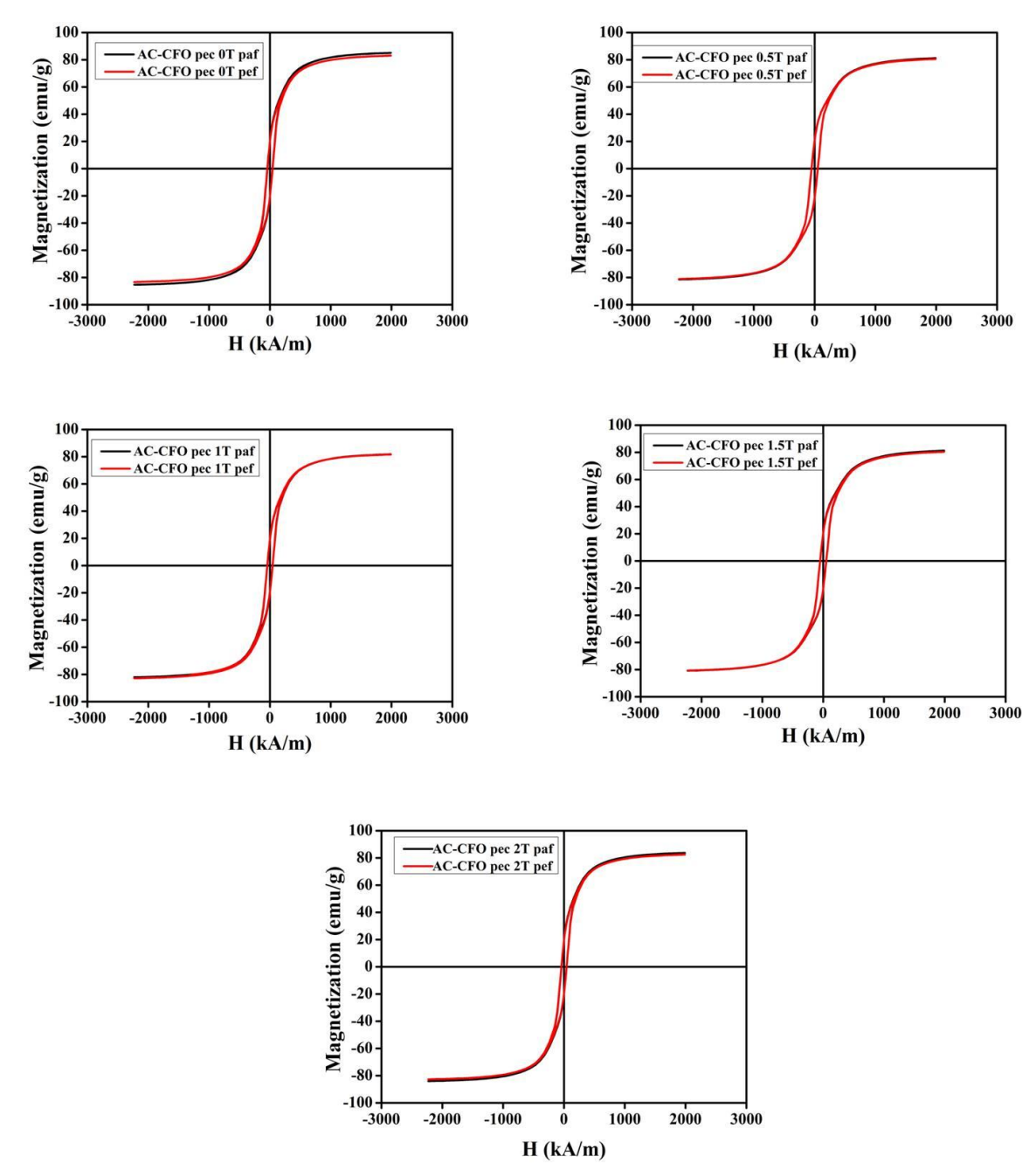


Figure 4.1.3.3 M–H curve of sintered AC–CFO Pellets compacted in perpendicular MAC at different magnetic fields

Similarly, a small variation in saturation magnetization (80 emu/g to 83 emu/g), remanence (19emu/g to 21 emu/g), and coercivity (42.7 kA/m to 43.7 kA/m) values have been observed in perpendicular magnetic hysteresis loops of AC-CFO pellets compacted in perpendicular MAC at different magnetic fields.

#### 4.1.3.1.4. Magnetoelastic properties

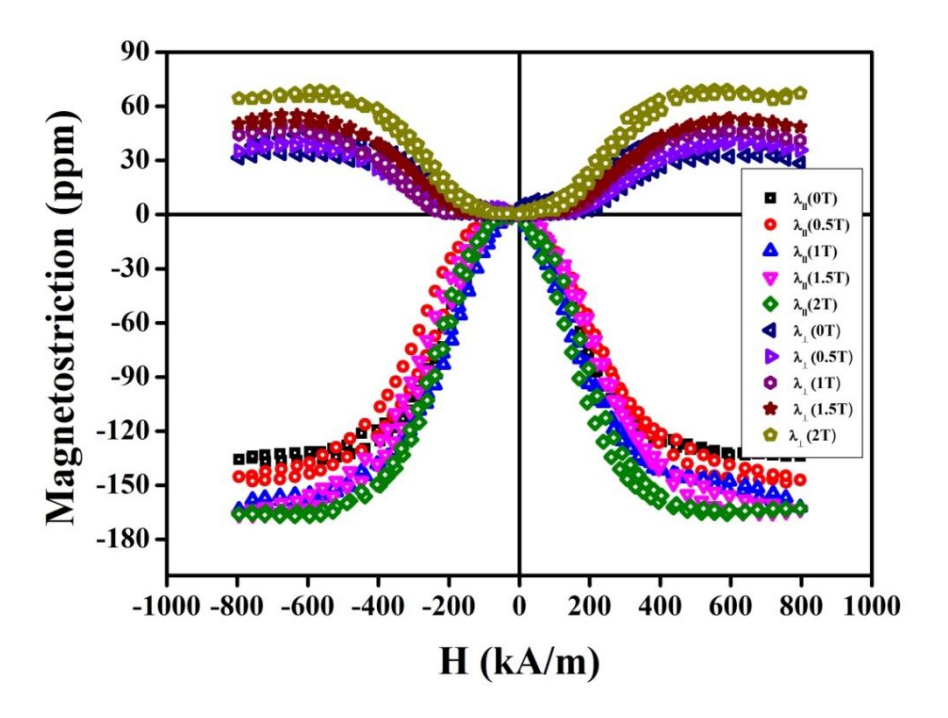


Figure 4.1.3.4 Magnetostriction data of sintered AC-CFO compacted in parallel MAC at different magnetic fields

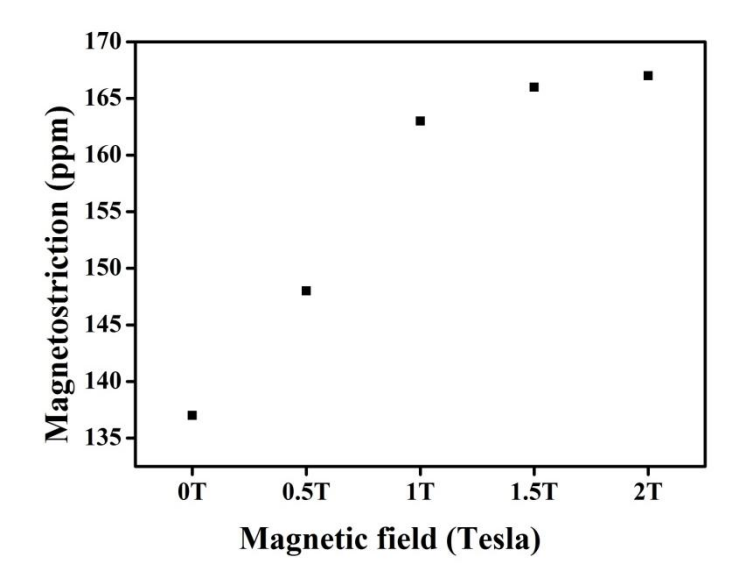


Figure 4.1.3.5 Variation of magnetostriction of sintered AC-CFO samples with applied magnetic field during perpendicular MAC.

Magnetostriction has been measured on AC-CFO pellets obtained by the magnetic field assisted compaction at the different fields and the data is plotted in figure 4.1.3.4. Strain gauge

was mounted on the flattened surface of the pellets along the oriented direction of the sample. Parallel magnetostriction  $(\lambda_{\parallel})$  has been measured along the oriented direction and perpendicular magnetostriction  $(\lambda_{\perp})$  has been measured perpendicular to the oriented direction of sample pellets. In AC-CFO pellets compacted in perpendicular MAC applied magnetic field direction during compaction is oriented direction. Significant improvement in magnetostriction and strain derivative has been observed in sintered pellets compacted at 2 Tesla magnetic field compared to the sample compacted without magnetic field. For 0T samples, maximum parallel magnetostriction  $(\lambda_{\parallel})$  and maximum perpendicular magnetostriction  $(\lambda_{\perp})$  have been observed to be ~137 ppm and ~39 ppm, respectively, which are in good agreement with the reported values of CFO in the literature [1]. Maximum parallel magnetostriction  $(\lambda_{\parallel})$  of ~167 ppm and maximum perpendicular magnetostriction  $(\lambda_{\perp})$  of ~69ppm have been observed for samples prepared at 2T. Nearly 22% improvement has been observed in parallel magnetostriction of 0T sample compared to 2T sample.

Variation of magnetostriction of sintered AC–CFO samples with applied magnetic field during parallel MAC has been plotted in figure 4.1.3. It is clear from the plot that the increase in magnetostriction has been observed with an increase in the applied magnetic field up to 2T magnetic field during perpendicular MAC. Large increase in magnetostriction ( $\lambda_{\parallel}$ ) has been observed for samples prepared up to 1T and increase in magnetostriction has been decreased with increase in magnetic field during compaction. Maximum magnetostriction of 167 ppm has been observed for sample prepared at 2T field.

Strain sensitivity has been calculated from parallel magnetostriction data of AC-CFO pellets prepared in perpendicular MAC and data is shown in figure 4.1.3.4. Strain sensitivity of  $\sim 0.5 \times 10^{-9}$  m/A has been observed for the sample prepared without magnetic field, which is in good agreement with strain sensitivity of CFO [5]. Variation of strain sensitivity of sintered AC-CFO samples with applied magnetic field during perpendicular MACis shown in figure 4.1.3.6. a continuous increase in strain sensitivity has been observed for AC-CFO pellets compacted in parallel MAC with increase in magnetic field during compaction. Maximum strain sensitivity  $(d\lambda/dH)_{max}$  of  $\sim 0.5 \times 10^{-9}$  m/A and  $\sim 0.7 \times 10^{-9}$  m/A have been observed for AC-CFO samples compacted at 0T and 2T samples, respectively. Nearly 40% improvement in strain derivative has been achieved in 2T sample compared to sample prepared without magnetic field.

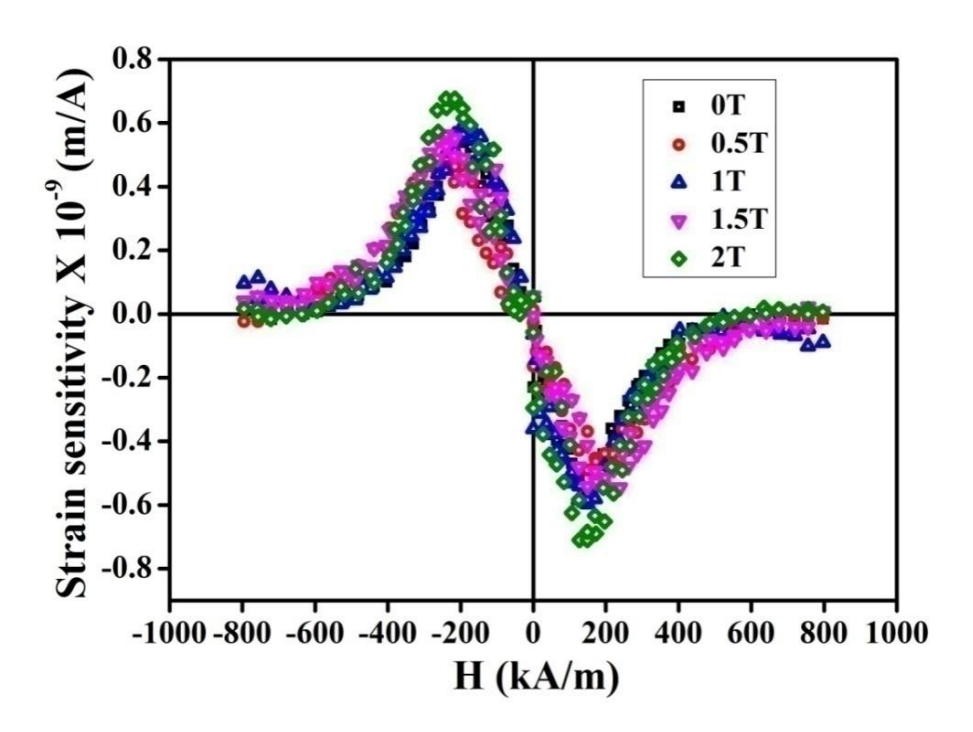


Figure 4.1.3.6 Strain sensitivity data of sintered AC-CFO compacted in parallel MAC at different magnetic fields

In perpendicular MAC, maximum magnetostriction and strain derivative have been observed in the direction of oriented axis direction [3, 5]. But for magnetic annealed sample, high strain derivative and magnetostriction have been observed in perpendicular to the oriented direction, where the direction in which magnetic field was applied during magnetic annealing [9]. 90° domain wall motion followed by domain rotation is responsible for the observed magnetostriction in the CFO. In perpendicular MAC, more 90° domains are created compared to the sample prepared without magnetic field. As the magnetic field increased in perpendicular MAC, magnetostriction and strain sensitivity is improved up to 2T. A sharp increase in magnetostriction suggests that more number of 90° domains have been created during magnetic field assisted compaction.

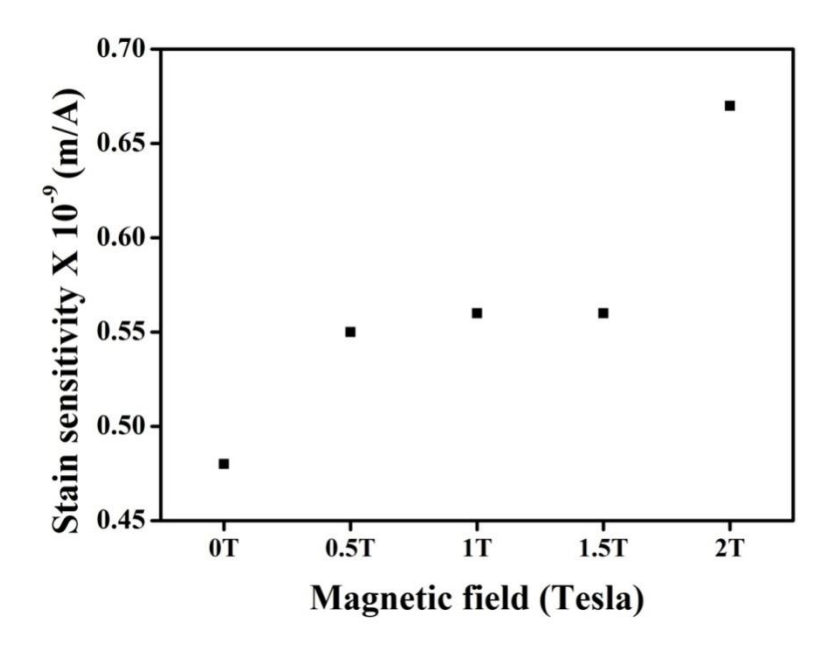


Figure 4.1.3.7 Variation of strain sensitivity of sintered AC-CFO samples with applied magnetic field during perpendicular MAC.

#### 4.1.3.2 Conclusions

Phase pure AC-CFO pellets have been prepared in perpendicular MAC. No visible difference in grain size has observed for AC-CFO pellets compacted at different magnetic fields. A small variation in magnetic properties has been observed for AC-CFO pellets compacted at different magnetic fields. Nearly 22% improvement in magnetostriction and 40% improvement in strain sensitivity have been observed in parallel magnetostriction of 2T sample compared to 0T sample. Increase in number of 90° domains with increasing applied magnetic field during compaction is reason for the improved magnetostriction and strain sensitivity with applied magnetic field during field assisted compaction.

# 4.1.4. Investigation of magnetic and magnetoelastic properties of CoFe<sub>2</sub>O<sub>4</sub> prepared by solid state technique followed by perpendicular MAC.

This section deals with preparation of CFO by solid state method followed by perpendicular MAC of SS-CFO powder at different magnetic fields (0T, 0.5T, 1T, 1.5T and 2T). These compacts were sintered at 1350°C for 12h and investigated the effect of perpendicular MAC on the structural, morphological, magnetic and magnetoelastic properties of CFO using XRD, SEM, PQMS and magnetostriction setup techniques respectively.

#### 4.1.4.1 Characterization of sintered AC-CFO pellets compacted under magnetic field

Synthesis and characterization of CFO prepared by solid state synthesis has been discussed in section 4.1.2.

#### **4.1.4.1.1 Phase analysis**

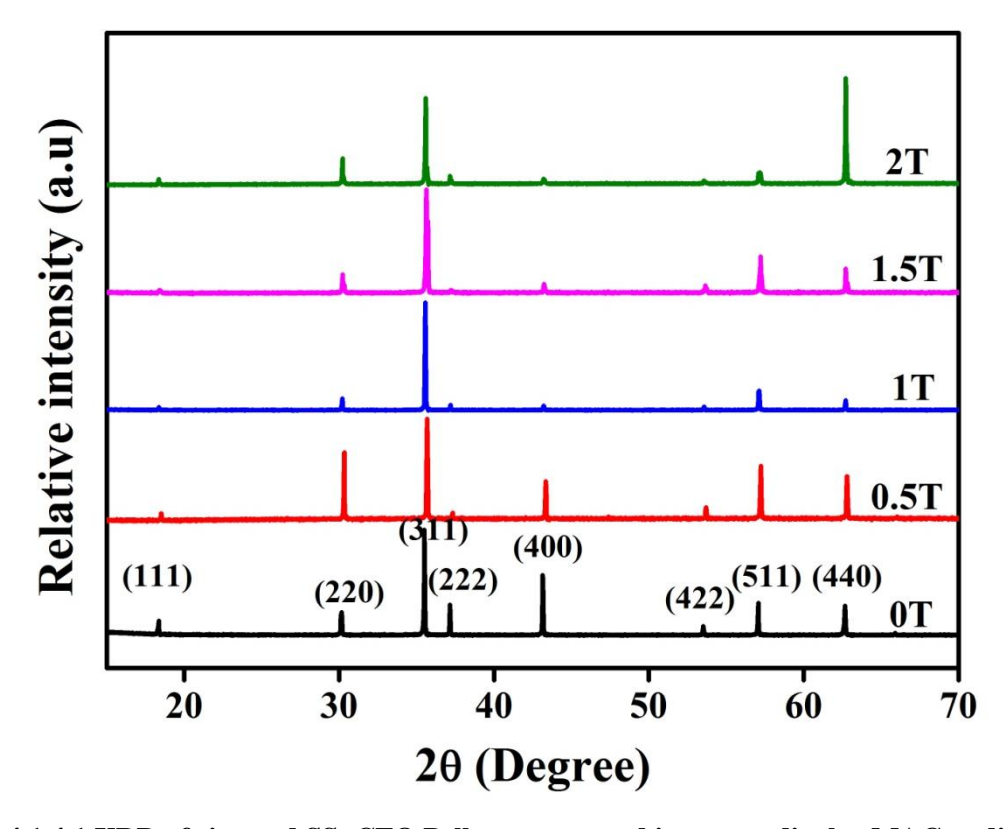


Figure 4.1.4.1 XRD of sintered SS-CFO Pellets compacted in perpendicular MAC at different magnetic fields

XRD pattern of CFO pellets compacted in perpendicular MAC at different magnetic fields such as 0T, 0.5T, 1T, 1.5T and 2T are shown in figure 4.1.4.1, which resulted in pure cubic spinel

phase (JCPDF file no. 22-1086). Preferential orientation of the XRD peaks has been observed for the pellet compacted at 2T magnetic field. Highest intensity has been observed for (440) peak for the pellet compacted at 2T whereas (311) is the highest intensity peak for the isotropic CFO pellet. Texture coefficient of 2.2 has been observed for (440) peak for the pellet compacted at 2T. Lattice parameter of the samples has been calculated from XRD. No variation in lattice parameter has been observed for the samples compacted at different magnetic fields. The lattice parameter values of samples compacted at different magnetic fields was shown in table 4.1.4.1.

Table.4.1.4.1 lattice parameter values of sintered SS-CFO Pellets compacted in perpendicular MAC at different magnetic fields

S.No	Sample name	Lattice parameter (A°)
1	0T	8.37
2	0.5T	8.37
3	1T	8.37
4	1.5T	8.37
5	2T	8.37

#### 4.1.4.1.2 Microstructural analysis

Figure 4.1.4.2shows the SEM micrographs of sintered SS-CFO pellets pressed under perpendicular MAC at different magnetic fields (0T, 0.5T, 1T, 1.5T and 2T). From SEM micrographs of all SS-CFO pellets, it is observed that porosity is not present and complete densification of pellets has taken place during sintering. Sintered density is calculated from Archimedes method following ASTM standard (C373-88) and it is found to be ~95% of the theoretical density for all SS-CFO pellets, which is similar to the percent of theoretical density reported for CFO pellets synthesized by ceramic method [10]. Exaggerated grain growth has been observed for all SS-CFO pellets pressed in perpendicular MAC under different magnetic fields. Very small grains in between the large grains have been observed in microstructure of all SS-CFO pellets pressed in perpendicular MAC. Therefore, almost negligible effect of magnetic field on microstructure and density has been observed for pellets pressed under magnetic field. It is exactly similar to reported literature, where microstructure is not affected by field assisted compaction for CFO sample [3].

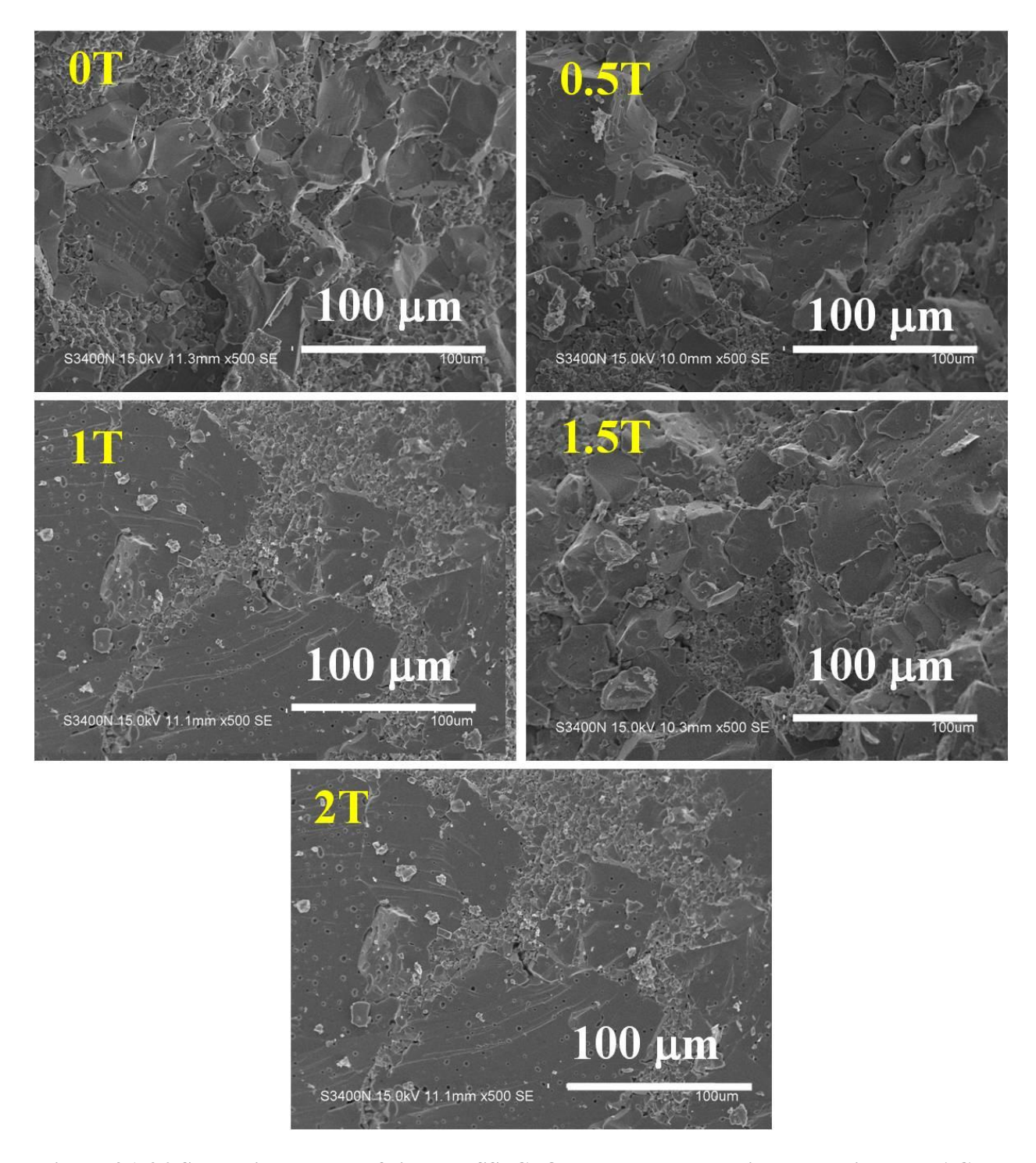


Figure 4.1.4.2 SEM micrographs of sintered SS-CFO Pellets compacted in perpendicular MAC at different magnetic fields

#### 4.1.4.1.3 Magnetic properties

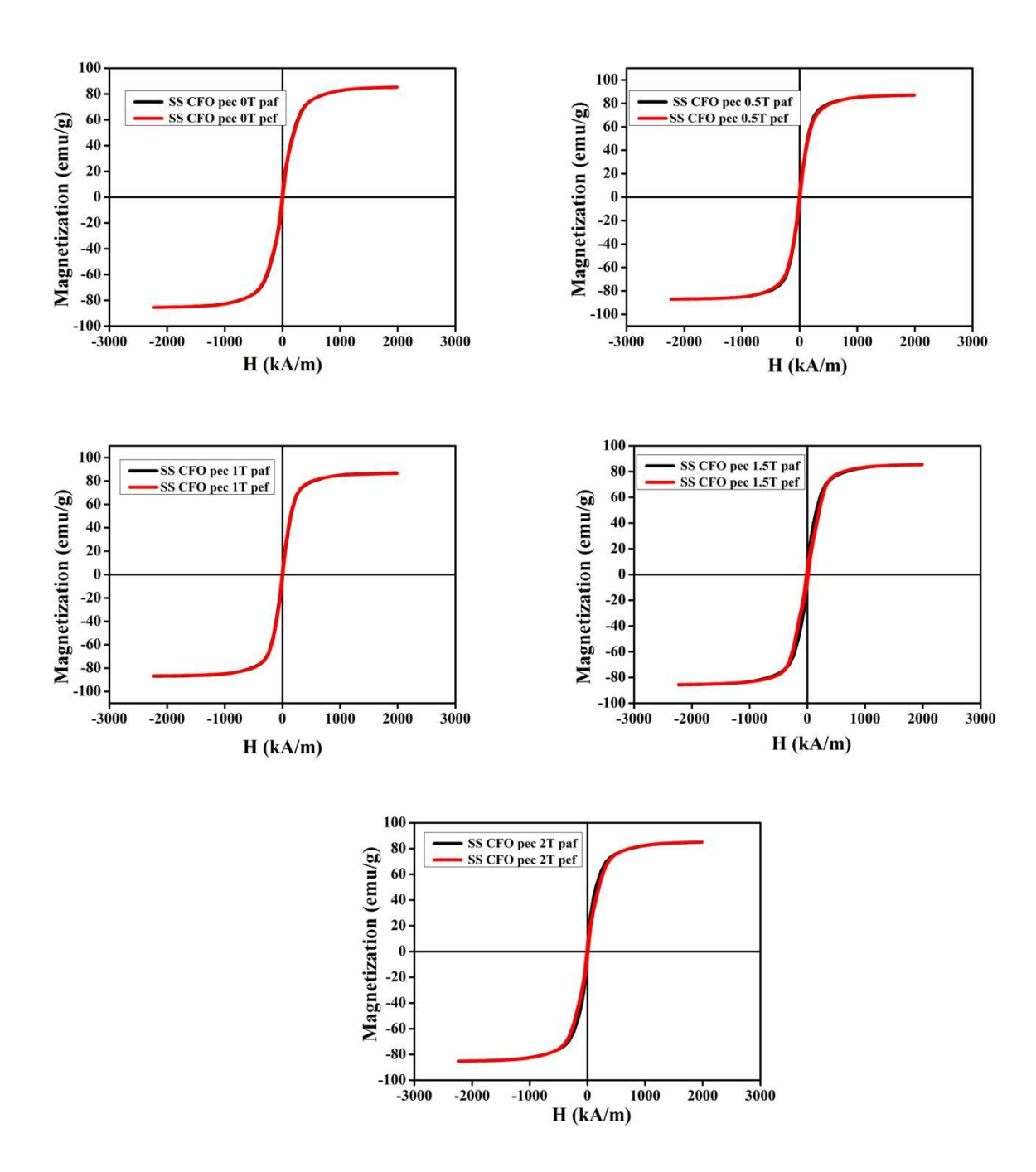


Figure 4.1.4.3 SEM micrographs of sintered SS-CFO Pellets compacted in perpendicular MAC at different magnetic fields

Applied stress and magnetic field dominates the magnetic crystalline energy in controlling the magnetization direction in domains [4]. Magnetic strain energy ( $E_{\sigma}$ ) created because of applied stress during compaction in CFO try to orient the domains parallel to stress axis where as applied

magnetic field orient the domains in the direction of applied field in CFO green compact during magnetic field assisted compaction. Since, sintering temperature (1350°C) of CFO is greater than its Curie temperature (520°C) spin orientation may get randomized but due to strong lattice orbit coupling the resultant magnetization vectors orient along the direction of initial stable magnetization direction after cooling [5].

Table 4.1.4.2 Magnetic properties of sintered SS-CFO Pellets compacted in perpendicular MAC at different magnetic fields

Sl.No.	Sample	Par M <sub>S</sub> (emu/g)	Par M <sub>r</sub> (emu/g)	Par H <sub>C</sub> (kA/m)	Per M <sub>S</sub> (emu/g)	Per M <sub>r</sub> (emu/g)	Per H <sub>C</sub> (kA/m)
1	OT	85	4	8	85	4	8.3
2	0.5T	86	4	7.8	87	3	6.8
3	1T	86	3	6.7	86	3	5.9
4	1.5T	85	4	11.7	85	4	15.7
5	2T	85	5	8.1	85	5	10.5

Parallel and perpendicular magnetic hysteresis loops for SS-CFO samples compacted in perpendicular MAC at different magnetic fields were measured in PQMS by applying magnetic field parallel and perpendicular to oriented direction of the sample. Parallel and perpendicular magnetic hysteresis loops of SS-CFO samples compacted in perpendicular MAC at different magnetic fields were shown in figure 4.1.4.3. Saturation magnetization values of 85 emu/g and 85 emu/g were observed in parallel and perpendicular hysteresis loops for SS-CFO sample compacted without magnetic field (0T). These saturation magnetization values were in good agreement with the reported values of saturation magnetization of CFO [5]. Magnetic properties obtained from parallel and perpendicular hysteresis loops of SS-CFO samples compacted in perpendicular MAC at different magnetic fields are summarized in table 4.1.4.2. Marginal variation in saturation magnetization (85 emu/g to 86 emu/g), remanence (3 emu/g to 5 emu/g), and coercivity (6.7 kA/m to 11.7 kA/m) have been observed in parallel magnetic fields. Similarly, a small variation in saturation magnetization (85 emu/g to 87 emu/g), remanence (3 emu/g to 5 emu/g), and coercivity (5.9 kA/m to 15.7 kA/m) have been observed in perpendicular magnetic

hysteresis loops of SS-CFO pellets compacted in perpendicular MAC at different magnetic fields.

#### **4.1.4.1.4.** Magnetoelastic properties

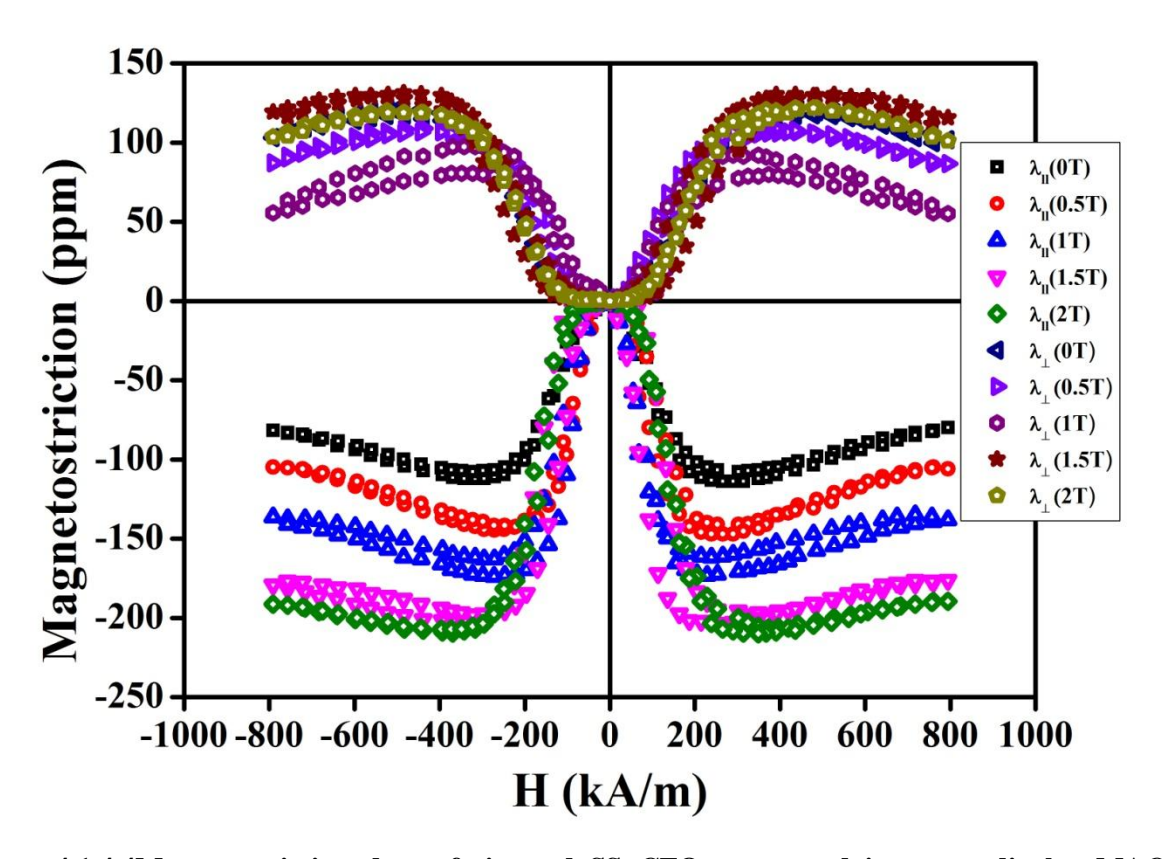


Figure 4.1.4.4Magnetostriction data of sintered SS-CFO compacted in perpendicular MAC at different magnetic fields

Magnetostriction was measured on SS-CFO samples and the data is shown in figure 4.1.4.4. Strain gauges have been mounted on the flattened surface of the pellets along the oriented direction of the sample. For samples parallel magnetostriction ( $\lambda_{\parallel}$ ) has been measured along the oriented direction of pellet and perpendicular magnetostriction ( $\lambda_{\perp}$ ) has been measured perpendicular to oriented direction. In SS-CFO pellets compacted in perpendicular MAC applied magnetic field direction during compaction is oriented direction. Significant improvement in magnetostriction and strain derivative has been observed for sintered pellets compacted under perpendicular magnetic field compared to the sample compacted without magnetic field (0T). For 0T samples, maximum parallel magnetostriction ( $\lambda_{\parallel}$ ) has been observed to be ~113 ppm,

which is in good agreement with the reported values of CFO in the literature [8]. Variation of magnetostriction of sintered SS–CFO samples with applied magnetic field during perpendicular MAC has been shown in figure 4.1.4.5. Linear increase in magnetostriction has been observed with increase in applied magnetic field up to 2T during parallel MAC. Maximum parallel magnetostriction ( $\lambda_{\parallel}$ ) of 209 ppm have been observed for samples prepared at 2T. Nearly 85% improvement has been observed in parallel magnetostriction of 2T sample compared to 0T sample.

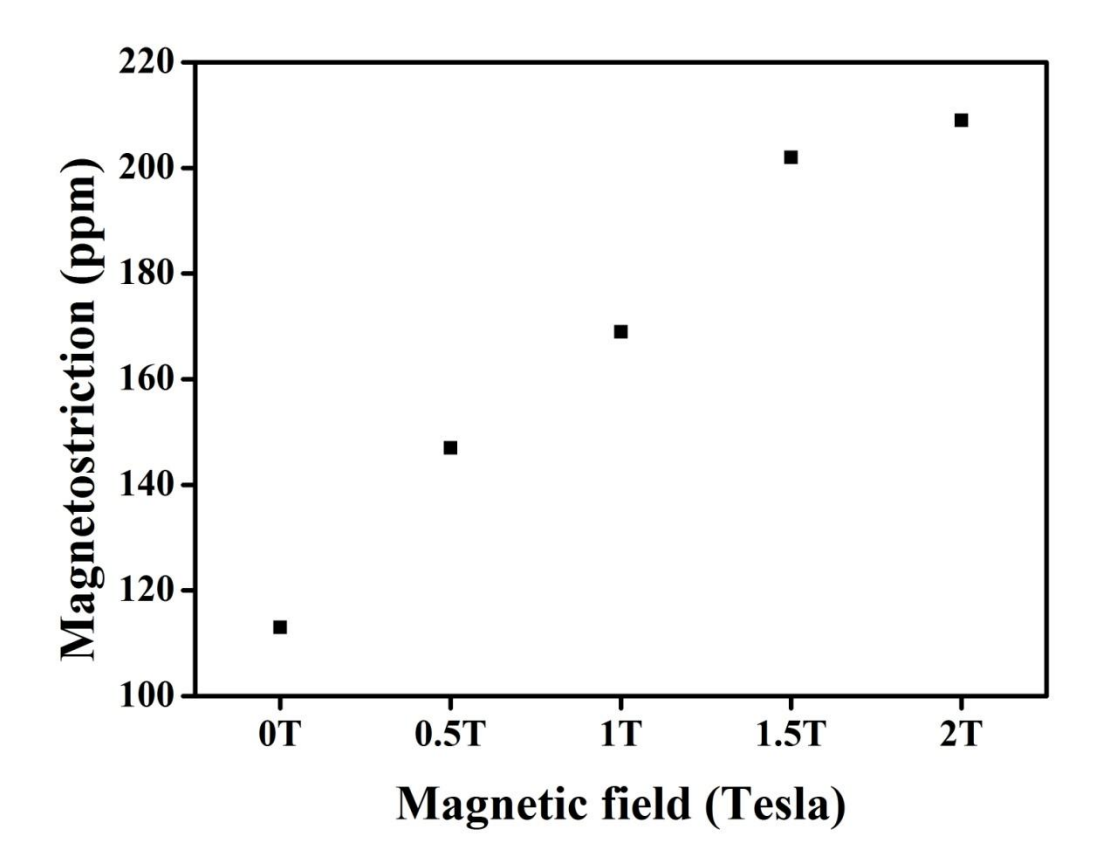


Figure 4.1.4.5 Variation of magnetostriction of sintered SS-CFO samples with applied magnetic field during perpendicular MAC.

Strain sensitivity has been calculated from parallel magnetostriction data of SS-CFO pellets prepared in perpendicular MAC and data is shown in figure 4.1.4.6. Strain sensitivity of  $0.8 \times 10^{-9}$  m/A has been observed for the sample prepared without magnetic field, which is in good agreement with strain sensitivity of CFO [7]. As shown in figure 4.1.4.7, Continuous increase in strain sensitivity has been observed for SS-CFO pellets compacted in perpendicular MAC with

increase in magnetic field during compaction. Maximum strain sensitivity  $(d\lambda/dH)_{max}$  of  $0.8 \times 10^{-9}$  m/A and  $2.5 \times 10^{-9}$  m/A have been observed for SS-CFO samples compacted at 0T and 2T samples, respectively. Nearly 185% improvement in strain derivative has been achieved in 2T sample compared to sample prepared without magnetic field.

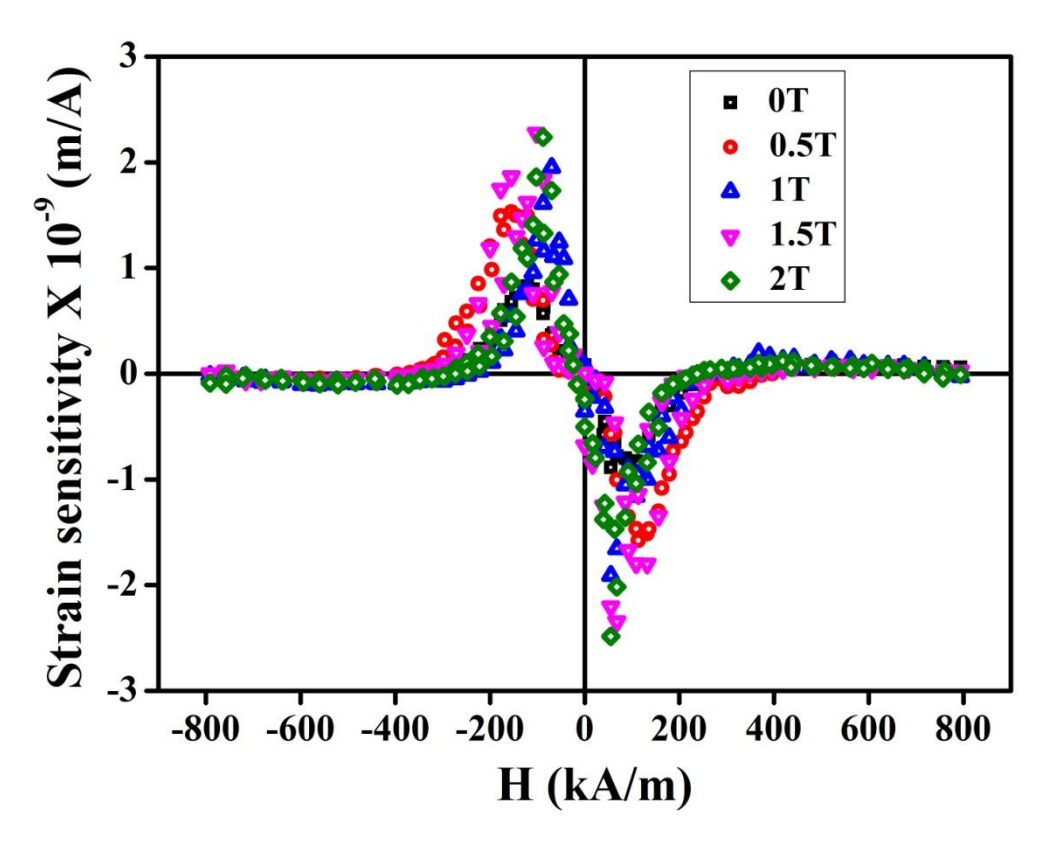


Figure 4.1.4.6 Strain sensitivity data of sintered SS-CFO compacted in perpendicular MAC at different magnetic fields

In perpendicular MAC, maximum magnetostriction and strain derivative have been observed in the direction of oriented axis direction [2, 4]. But for magnetic annealed sample, high strain derivative and magnetostriction have been observed in perpendicular to the oriented direction, where the direction in which magnetic field was applied during magnetic annealing [8]. 90° domain wall motion followed by domain rotation is responsible for the observed magnetostriction in the CFO. In perpendicular MAC, more 90°domains are created compare to the sample prepared without magnetic field. As the magnetic field increased in parallel MAC, magnetostriction is improved up to 2T. A linear increase in magnetostriction suggests that linear increase in the number of domains with increase in magnetic field during perpendicular MAC.

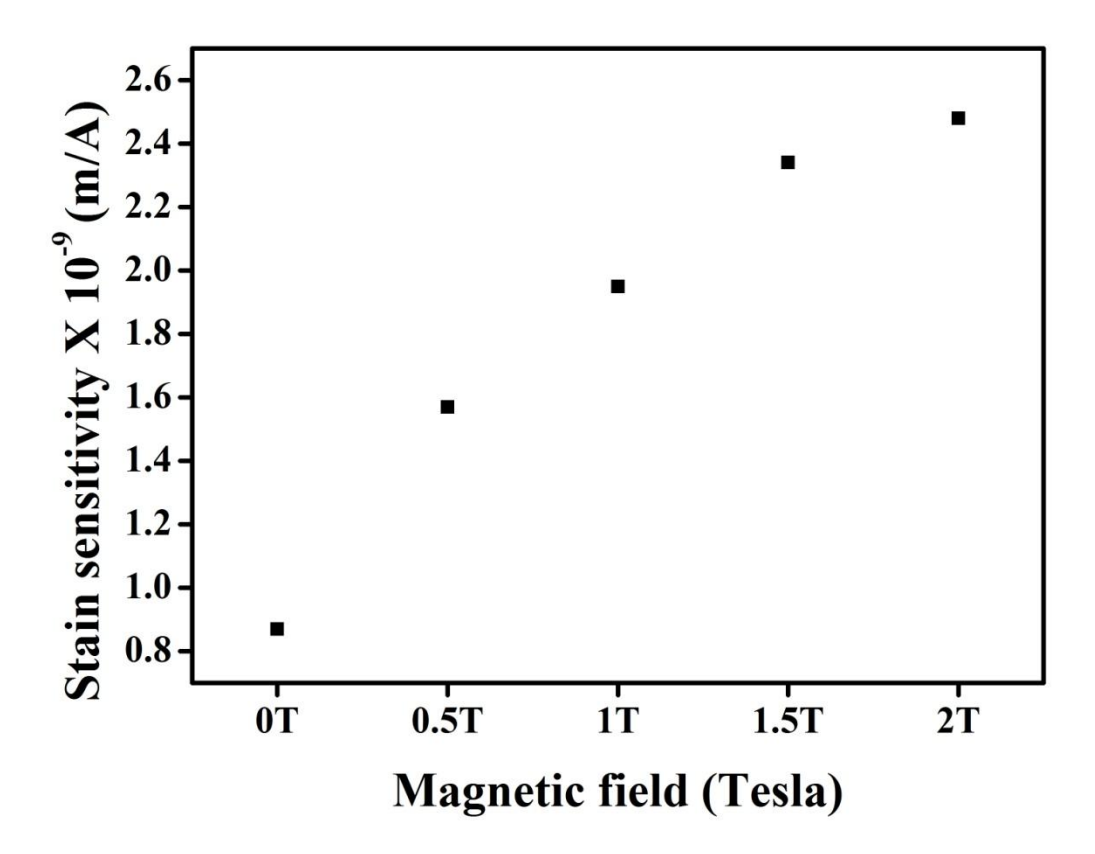


Figure 4.1.4.7 Variation of strain sensitivity of sintered SS-CFO samples with applied magnetic field during perpendicular MAC

#### 4.1.4.2 Conclusions

Phase pure SS-CFO pellets have been prepared in perpendicular MAC. No visible difference in grain size has observed for SS-CFO pellets compacted at different magnetic fields. A small variation in magnetic properties has been observed for SS-CFO pellets compacted at different magnetic fields. Nearly 85% improvement in magnetostriction and 185% improvement in strain sensitivity have been observed in parallel magnetostriction of 2T sample compared to 0T sample. Increase in number of 90° domains with increasing applied magnetic field during compaction is reason for the improved magnetostriction and strain sensitivity with applied magnetic field during field assisted compaction.

#### SECTION 4.2 TEMPLATE GRAIN GROWTH OF CFO

## 4.2.1 Investigation of structural, morphological and magnetic properties of CFO template synthesized by molten salt synthesis

This section deals with molten salt synthesis of CFO templates using CFO nanoparticles and salt mixture (1:1 molar ratio of KCl and NaCl) at different temperatures (700°C, 800°C, 900°C, and 1000°C for 4h), different dwell time (4h, 12h, 24h), and different salt to powder ratios (1:1, 3:1, and 5:1). Followed by the sample preparation, we studied the effect of different temperature and duration on the structural, morphological and magnetic properties of the CFO templates using XRD, FESEM and VSM techniques respectively.

#### 4.2.1.1 Characterization of CFO nanoparticles used for molten salt synthesis

#### 4.2.1.1.1 Structural properties of CFO nanoparticles

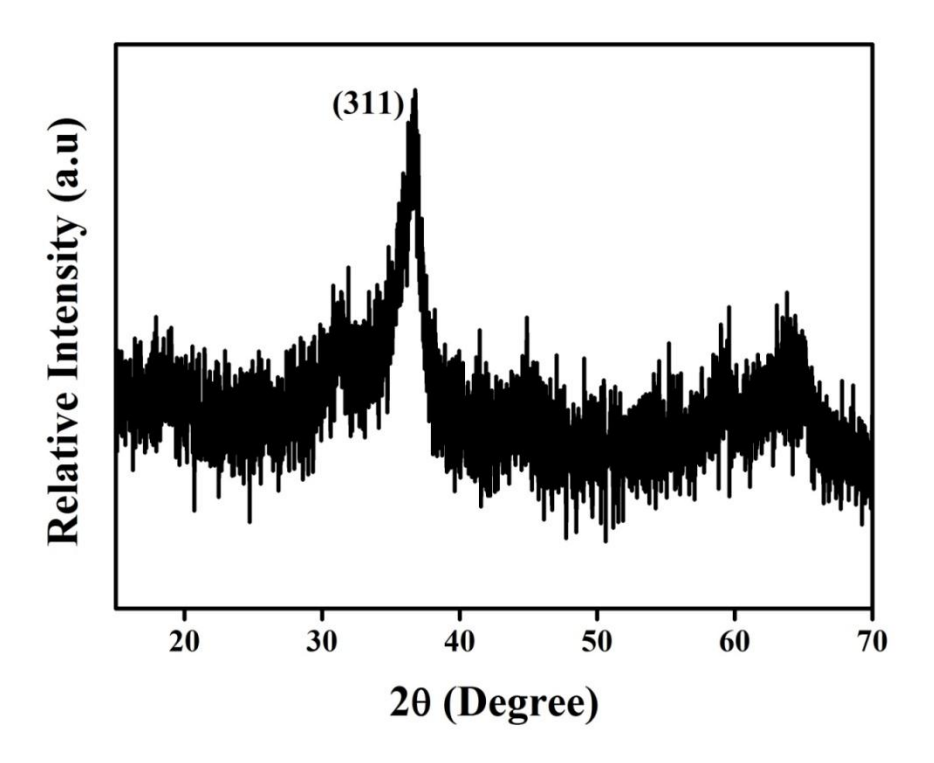


Figure 4.2.1.1 XRD pattern of CFO particles

Figure 4.2.1.1 shows the XRD pattern of CFO nanoparticles prepared by auto-combustion method. Intense broad peak has been observed around  $2\Theta$ = 35 in the XRD pattern and it matches with (311) peak of pure cubic spinel phase. The observed peak broadening could be attributed to small particles size of CFO particles. The average crystallite size of CFO nanoparticles was calculated using sherrer's equation and it is found to be 6 nm. TEM images of CFO nanoparticles and its particles distribution are shown in figure 4.2.1.2. The average particle size from the TEM analysis was found to be 8 nm which is correlated with the crystallite sizes calculated from the XRD analysis.

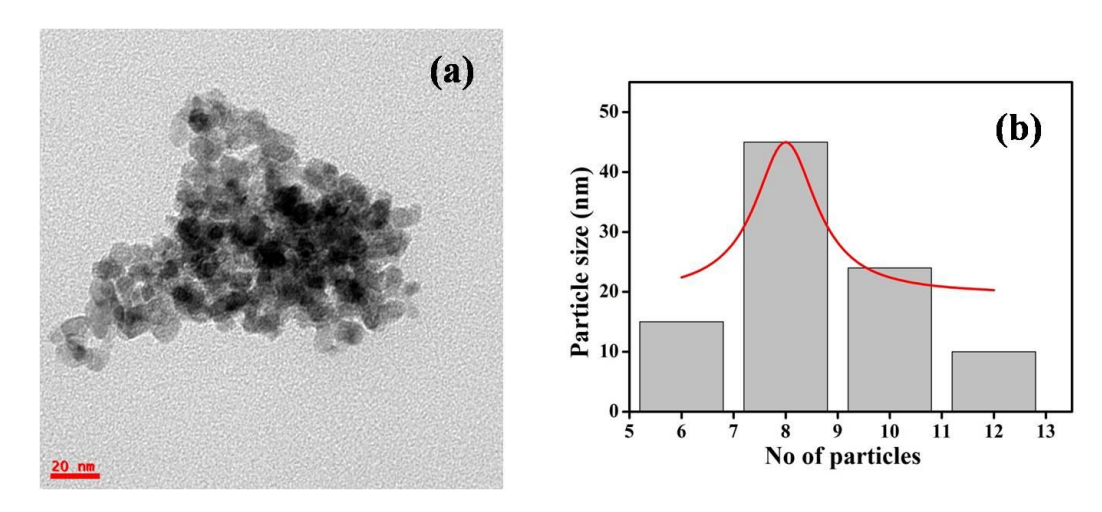


Figure 4.2.1.2 (a) TEM image of CFO particle and (b) size distribution of CFO nanoparticles.

#### 4.2.1.1.2 Magnetic properties of CFO nanoparticles

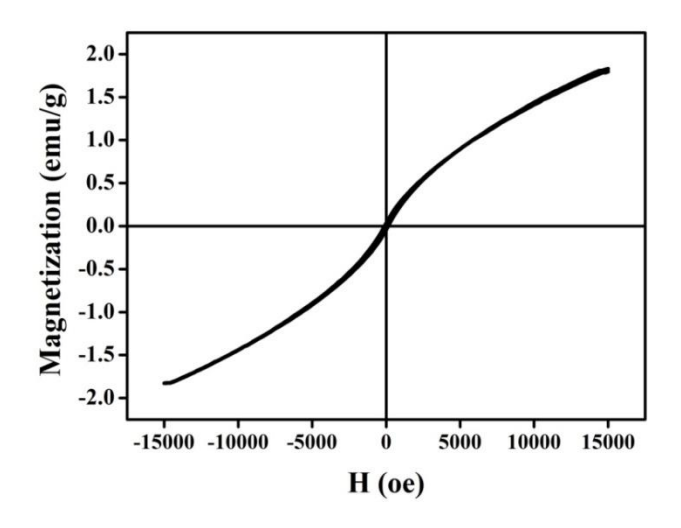


Figure 4.2.1.3 Room temperature magnetization (M-H) curve of CFO nanoparticles

Room temperature magnetization curve of CFO nanoparticles synthesized by auto-combustion method is shown in figure 4.2.1.3. It is clearly observed from magnetic hysteresis loop that CFO nanoparticles exhibited superparamagnetic behavior. This is exactly similar to the literature where superparamagnetic nature observed by CFO nanoparticles having 5nm particle size [1].

#### 4.2.1.2 Characterization of CFO particles prepared in molten salt synthesis

#### 4.2.1.2.1 Structural properties of CFO particles prepared at different temperatures

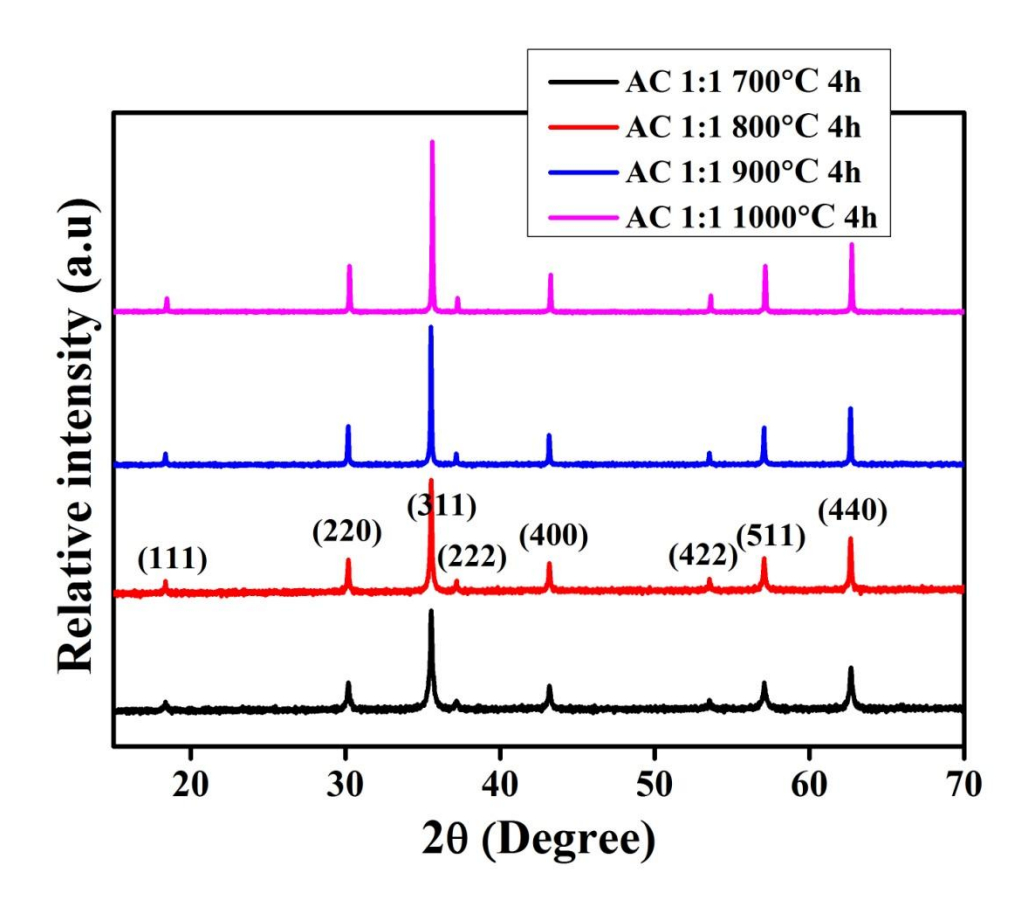


Figure 4.2.1.4 XRD pattern of CFO powder prepared at different temperatures (700°C, 800°C, 900°C and 1000°C for 4h) with 1:1 salt to powder mass ratio.

XRD patterns of CFO powders synthesized at different temperatures (700°C, 800°C, 900°C and 1000°C for 4h) with 1:1 salt to powder mass ratio are shown in figure 4.2.1.4. All the samples are crystallized in pure cubic spinel phase (JCPDF file no. 22-1086) with Fm-3m space group. Lattice parameter and crystallite size have been calculated using Nelson relay extrapolation plot from XRD and sherrer's formula respectively. The Crystallite size and lattice parameter values

of CFO synthesized at different temperatures are summarized in table 4.2.1.1. The crystallite size has been increased from 45nm to 113nm with increase in temperature from 700°C to 1000°C respectively. There is no change in lattice parameter as a function of different temperatures.

Table 4.2.1.1 crystallite size and lattice parameters of CFO powder prepared at different temperatures (700°C, 800°C, 900°C and 1000°C for 4h) with 1:1 salt to powder mass ratio

Sl. No	Sample	Crystallite size (nm)	Lattice parameter (Å)
1	700°C, 4h	45	8.38
2	800°C, 4h	72	8.38
3	900°C, 4h	108	8.38
4	1000°C, 4h	113	8.38

#### 4.2.1.2.2 Microstructural properties of CFO particles prepared at different temperatures

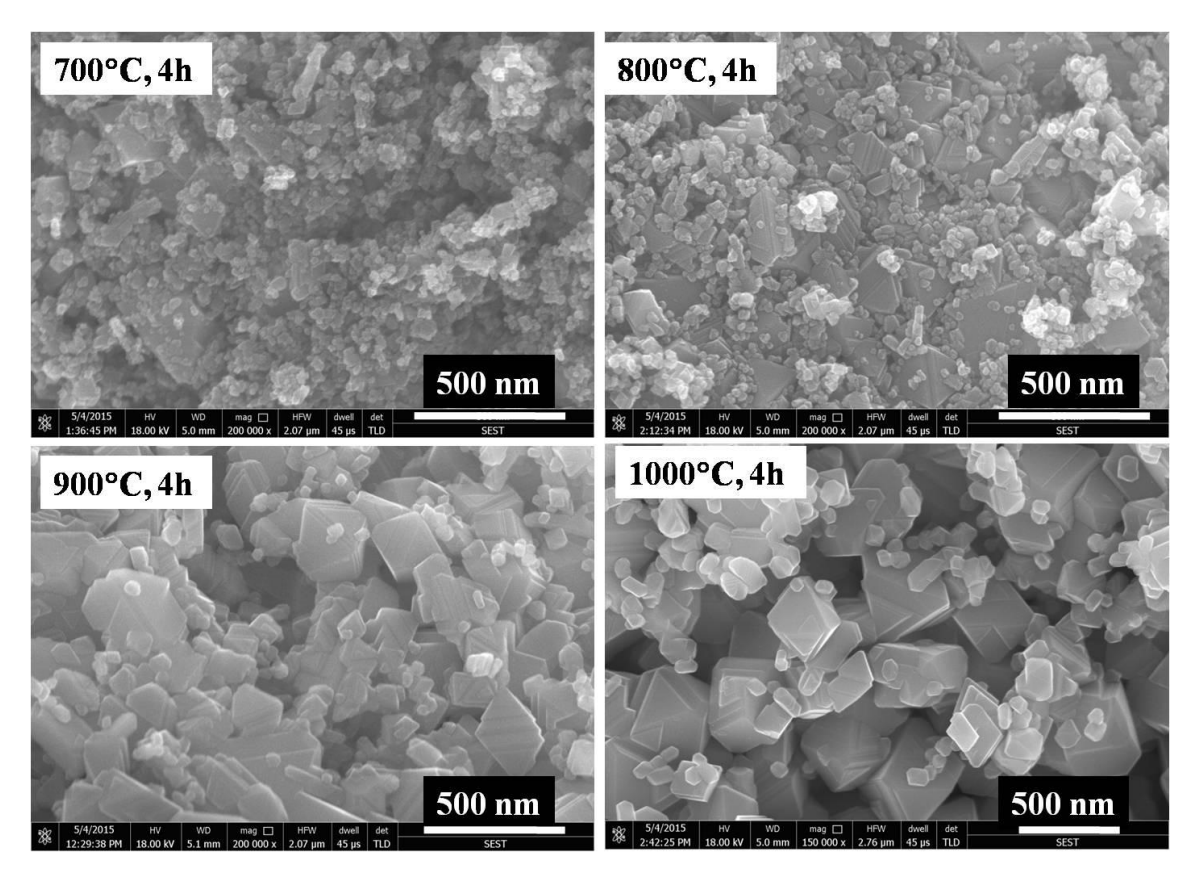


Figure 4.2.1.5 SEM micrographs of CFO powder prepared at different temperatures (700°C, 800°C, 900°C and 1000°C for 4h) with 1:1 salt to powder mass ratio.

Figure 4.2.1.5 shows SEM micrographs of CFO powder prepared at different temperatures, it has been observed that particle size of CFO particles have been increased with increase in temperature (700°C to 1000°C for 4h). All samples exhibit micro images composed of two different groups of particle size, one with smaller size and another group with larger particle size. Average particle sizes of larger particles and smaller particles at different temperatures are summarized in table 4.2.1.2. Average particle size of small particles has been increased from 20 nm to 90 nm with increase in temperature from 700°C, 4h to 1000°C, 4h respectively. On the other hand, average particle size of larger particles has been increased from 110 nm to 335 nm with increase in temperature from 700°C, 4h to 1000°C, 4h respectively. Larger particles are having triangular and octahedral shapes whereas smaller particles are having distorted spherical shape. The Number of particles with triangular and octahedral shapes has been increased with an increase in temperature.

Table 4.2.1.2 Average particle size of bigger particles and smaller particles calculated from SEM micrographs of CFO powder prepared at different temperatures (700°C, 800°C, 900°C and 1000°C for 4h) with 1:1 salt to powder mass ratio

Sl. No	Sample	Average particle size of	Average particle size of
		larger particles (nm)	smaller particles (nm)
1	AC-1:1-700°C, 4h	110	20
2	AC-1:1-800°C, 4h	145	30
3	AC-1:1-900°C, 4h	205	43
4	AC-1:1-1000°C, 4h	335	90

#### 4.2.1.2.3 Magnetic properties of CFO particles prepared at different temperatures

Room temperature M-H curves of CFO particles prepared at different temperatures are shown in figure 4.2.1.6. Table 4.2.1.3 summarized the magnetic properties. It has been observed that saturation magnetization ( $M_s$ ) values of CFO particles have been increased from 59 emu/g to 67 emu/g with increase in temperature from 700°C to 1000°C respectively. Remanence magnetization ( $M_r$ ) has been increased with temperature up to 800°C and then decreased with increase in temperature up to 1000°C. Coercivity of CFO particles has been decreased from 76 kA/m to 63 kA/m with increase in temperature from 700°C to 1000°C, respectively.

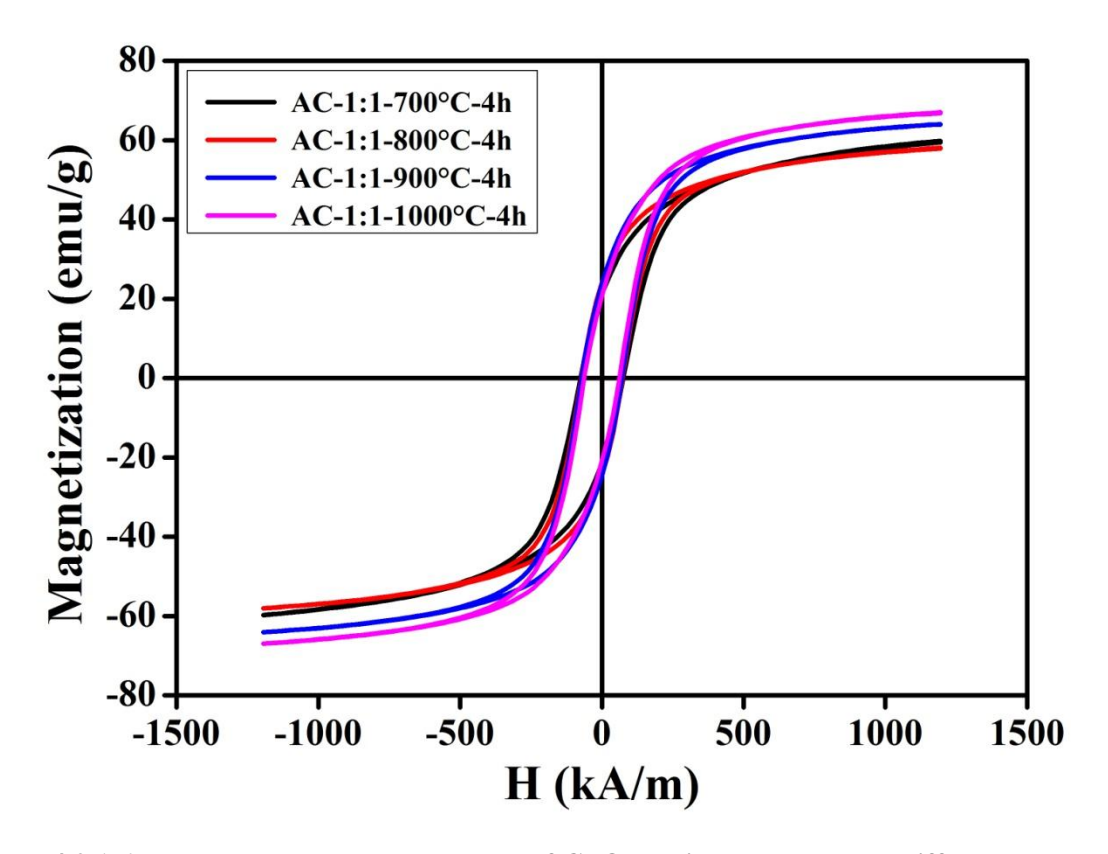


Figure 4.2.1.6 Room temperature M-H curve of CFO particles prepared at different temperatures (700°C, 800°C, 900°C and 1000°C for 4h) with 1:1 salt to powder mass ratio.

Table 4.2.1.3 magnetic properties of CFO particles prepared at different temperatures (700°C, 800°C, 900°C and 1000°C for 4h) with 1:1 salt to powder mass ratio.

Sl. No	Sample	M <sub>s</sub> (emu/g)	M <sub>r</sub> (emu/g)	$H_c$ (kA/m)
1	AC-1:1-700°C, 4h	59	21.2	76
2	AC-1:1-800°C, 4h	60	24.1	73
3	AC-1:1-900°C, 4h	64	23.8	71
4	AC-1:1-1000°C, 4h	67	21.8	63

#### 4.2.1.2.4 Structural properties of CFO prepared at different dwell time

XRD pattern of CFO powders synthesized at 1000°Cwith 1:1 salt to powder ratio with different dwell time (4h, 12h and 24h), are shown in figure 4.2.1.4. The XRD patterns revealed that all the samples are crystallized in pure cubic spinel phase (JCPDS file no. 22-1086) with Fm-3m space group. Lattice parameter of the samples was calculated from XRD using Nelson relay

extrapolation plot and it is found to be 8.38Å. No change in lattice parameter has been observed as a function of dwelling time (4h, 12h, and 24h). Crystallite size has been calculated from sherrer's formula [2]. The Crystallite size and lattice parameter values of CFO synthesized at different temperatures are summarized in table 4.2.1.4. The crystallite size has been marginally increased from 113nm to 120nm with increase in dwell time from 4h to 24h respectively.

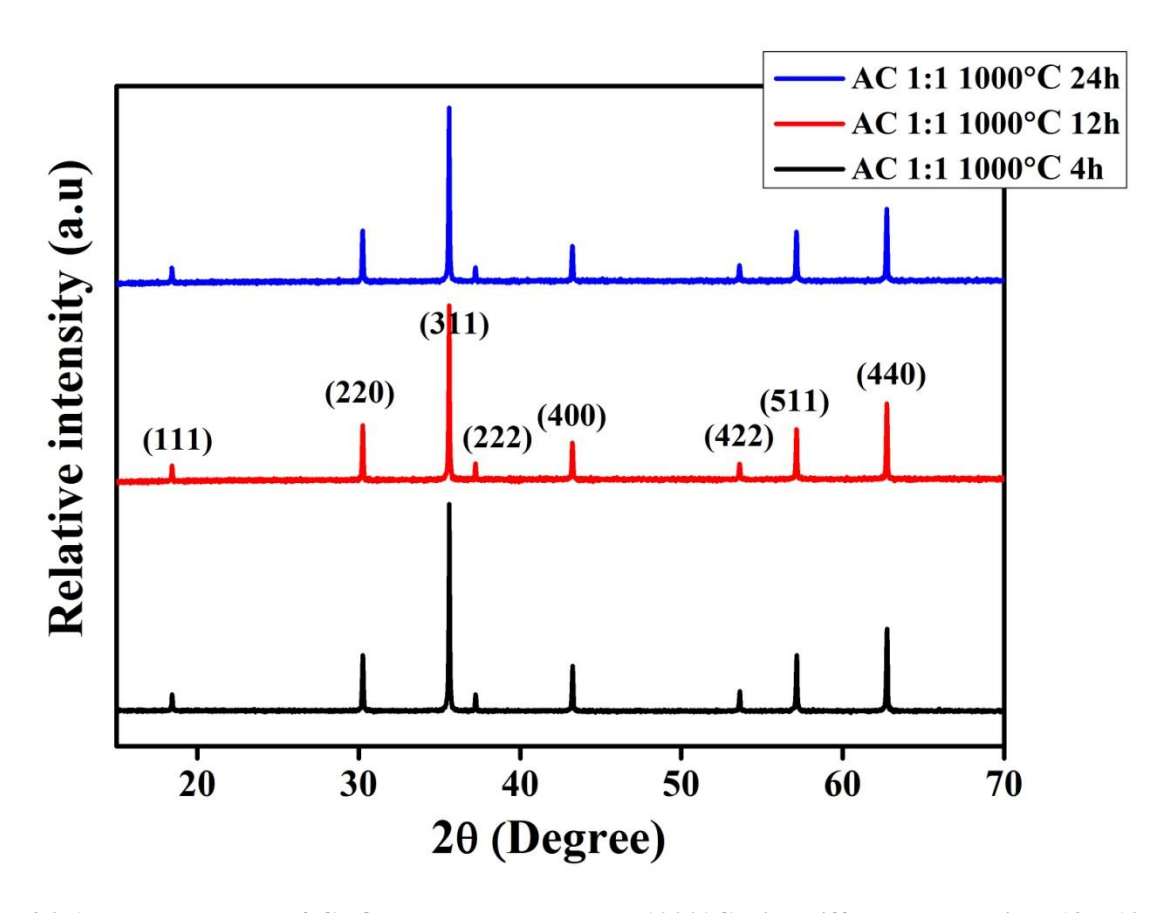


Figure 4.2.1.7 XRD pattern of CFO powder prepared at 1000°C with different dwell time (4h, 12h, 24h) and 1:1 salt to powder mass ratio.

Table 4.2.1.4 crystallite size and lattice parameters of CFO particles prepared at 1000 °C with different dwell time (4h, 12h, and 24h) and 1:1 salt to powder mass ratio.

Sl. No	Sample	Crystallite size (nm)	Lattice parameter (A°)
1	AC-1:1-1000°C-4h	113	8.38
2	AC-1:1-1000°C-12h	116	8.38
3	AC-1:1-1000°C-24h	120	8.38

#### 4.2.1.2.5 Microstructural properties of CFO prepared at different dwell time

SEM micrographs of CFO powder prepared at 1000°C with different dwell time are shown in figure 4.2.1.8. It has been observed that particle size of CFO particles have been increased with increase in dwell time (4h, 12h, and 24h). All samples exhibit micro images of two groups of particles, one group with smaller size and another group with larger size. Average particle sizes of larger particles and smaller particles at different dwell time are summarized in table 4.2.1.5. Average particle size of small particles has been increased from 90 nm to 100 nm with increase in dwell time from 4h to 12h respectively at 1000°C. On the other hand, average particle size of larger particles has been increased from 335 nm to 565 nm with increase in dwell time from 4h to 24h respectively at 1000°C. larger particles are having triangular and octahedral shapes where as the smaller particles are having distorted spherical shape. Numbers of particles with triangular and octahedral shapes has been increased with increase dwell time.

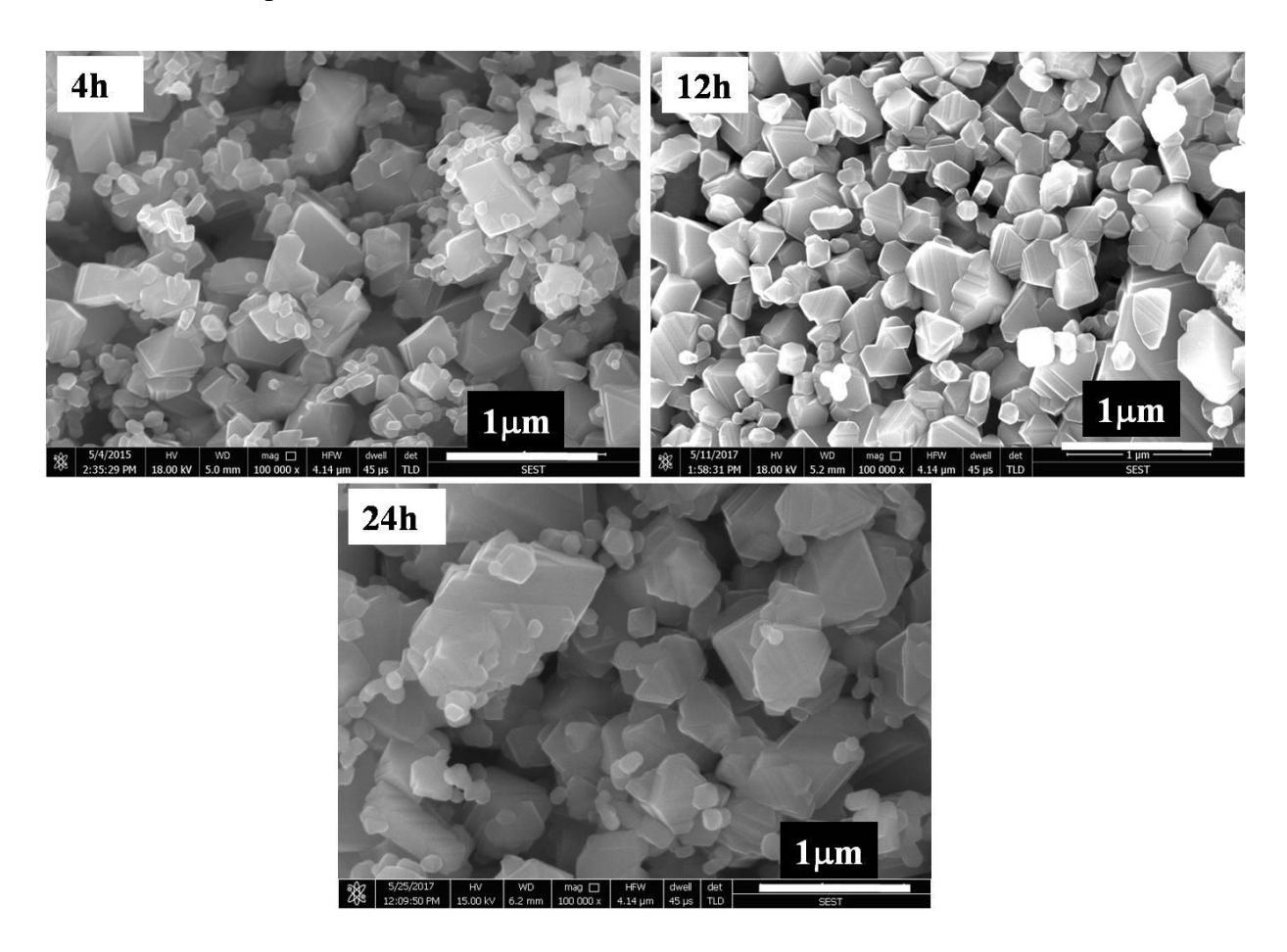


Figure 4.2.1.8 SEM micrographs of CFO powder prepared at 1000°C with different dwell time (4h, 12h, and 24h) and 1:1 salt to powder mass ratio.

Table 4.2.1.5 Average particle size of bigger particles and smaller particles calculated from SEM micrographs of CFO powder prepared at 1000°C with different dwell time (4h, 12h, and 24h) and 1:1 salt to powder mass ratio.

Sl. No	Sample	Average particle size of	Average particle size of
		larger particles (nm)	smaller particles (nm)
1	AC-1:1-1000°C-4h	335	90
2	AC-1:1-1000°C-12h	380	98
3	AC-1:1-1000°C-24h	565	100

#### 4.2.1.2.6 Magnetic properties of CFO prepared at different time intervals

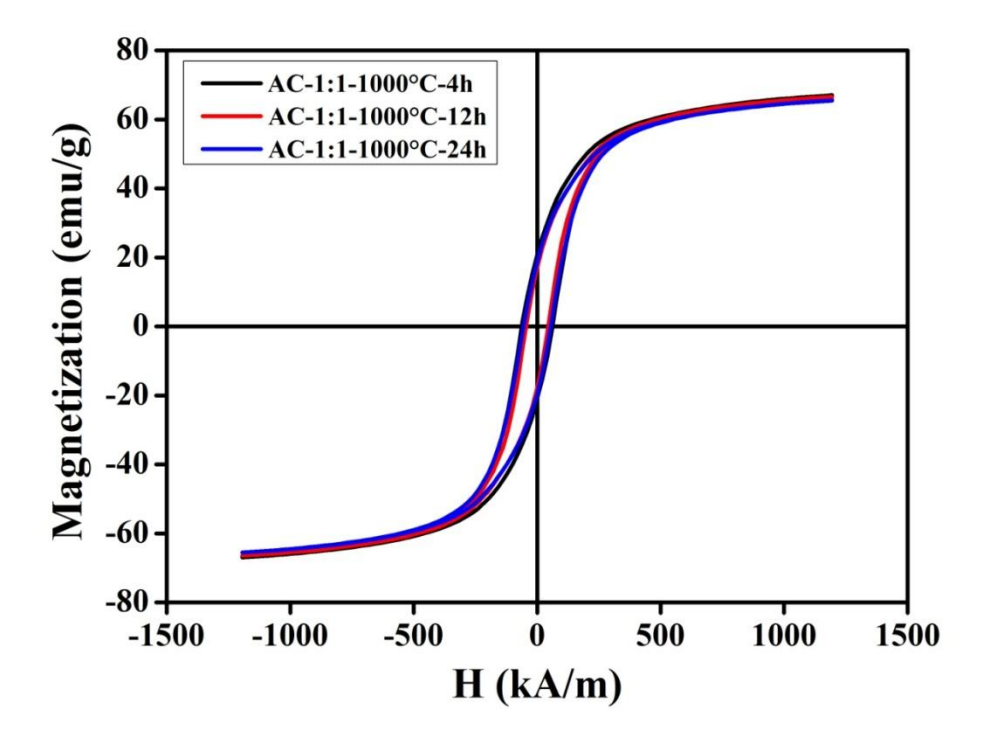


Figure 4.2.1.9 Room temperature M-H curve of CFO particles prepared at 1000°C with different dwell time (4h, 12h, and 24h) and 1:1 salt to powder mass ratio.

Room temperature M-H curves of CFO particles prepared at 1000°C with different dwell time is shown in figure 4.2.1.9. Magnetic properties of CFO particles have been obtained from hysteresis curves and the values are summarized in table 4.2.1.6. The saturation magnetization (M<sub>s</sub>) of CFO particles decreased slightly from 67 emu/g to 65.2 emu/g with increase in dwell time from 4h to 12h respectively. Similarly, a small decrease in remanence (M<sub>r</sub>) was from 20.7

emu/g to 17.2 emu/g with increase in dwell time from 4h to 24h has been observed. Notable decrease in coercivity from 62.5kA/m to 44.9 with increase in dwell time from 4h to 24h respectively has been observed.

Table 4.2.1.6 magnetic properties of CFO particles prepared at 1000°C with different dwell time (4h, 12h, and 24h) and 1:1 salt to powder mass ratio.

Sl. No	Sample	M <sub>s</sub> (emu/g)	M <sub>r</sub> (emu/g)	H <sub>c</sub> (kA/m)
1	AC-1:1-1000°C-4h	67	20.7	62.5
2	AC-1:1-1000°C-12h	66.4	18.8	55.1
3	AC-1:1-1000°C-24h	65.2	17.2	44.9

#### 4.2.1.2.7 Structural properties of CFO prepared at different salt to powder mass ratio

XRD patterns of CFO powders synthesized at 1000°C for24hwith different salt to powder ratio (1:1, 3:1, 5:1) are shown in figure 4.2.1.10, All samples are crystallized in pure cubic spinel phase (JCPDS file no. 22-1086). Lattice parameter of the samples was calculated from XRD using Nelson relay extrapolation plot and it was found be to 8.38Å for all three salt to powder ratio (1:1, 3:1, 5:1). Crystallite size has been calculated from sherrer's formula. The Crystallite size and lattice parameter values of CFO synthesized at 1000°C,24hwith different salt to powder ratio (1:1, 3:1, 5:1) are summarized in table 4.2.1.7. The crystallite size has been increased from 120 nm to 130 nm with increase in salt to powder ratio from 1:1 to 5:1 respectively.

Table 4.2.1.7 Crystallite size and lattice parameters of CFO particles prepared at 1000 °C, 24h with different salt to powder mass ratio (1:1, 3:1, 5:1)

Sl. No	Sample	Crystallite size (nm)	Lattice parameter (A°)
1	AC-1:1-1000°C-24h	120	8.38
2	AC-3:1-1000°C-24h	124	8.38
3	AC-5:1-1000°C-24h	130	8.38

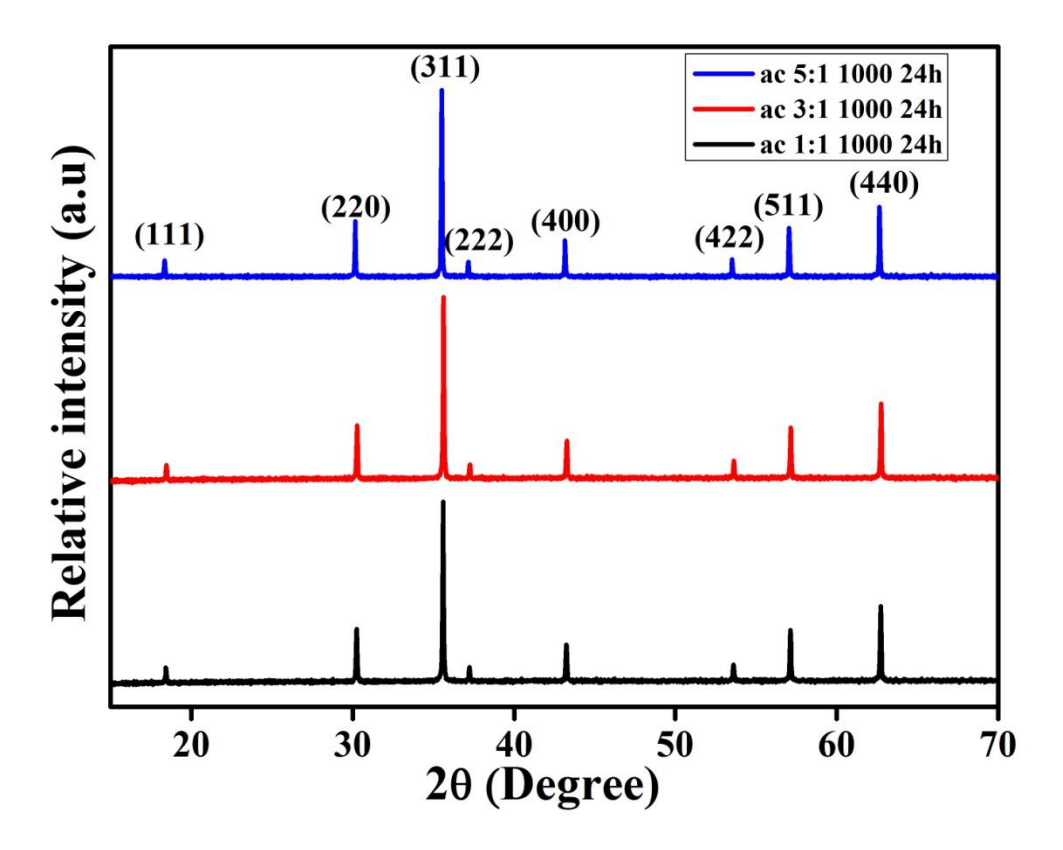


Figure 4.2.1.10 XRD pattern of CFO powder prepared at 1000°C, 24h with different salt to powder mass ratio (1:1, 3:1, 5:1)

#### 4.2.1.2.8 Microstructural properties of CFO prepared at different salt to powder mass ratio

SEM micrographs of CFO powder prepared at 1000°C for 24h with different salt to powder mass ratio are shown in figure 4.2.1.11. It has been observed from the micro images that the particle size of CFO particles has been increased with increase in salt to powder mass ratio. Micrographs of particles prepared at different salt to powder mass ratio contains two groups of particles with different size distributions such as particles of smaller size and particles of larger size. Average particle sizes of larger particles and smaller particles at different salt to powder mass ratio are summarized in table 4.2.1.7. Average particle size of small particles has been increased from 90 nm to 100 nm with an increase in salt to powder mass ratio from 1:1 to 5:1 respectively at 1000°C. Whereas, average particle size of larger particles has been increased from 565 nm to 915 nm with increased dwell time from 1:1 to 5:1 respectively at 1000°C for 24h. The larger particles are having triangular and octahedral shapes whereas smaller particles are having

distorted spherical shape. Numbers of particles with triangular and octahedral shapes were increased with increase in salt to powder mass ratio.

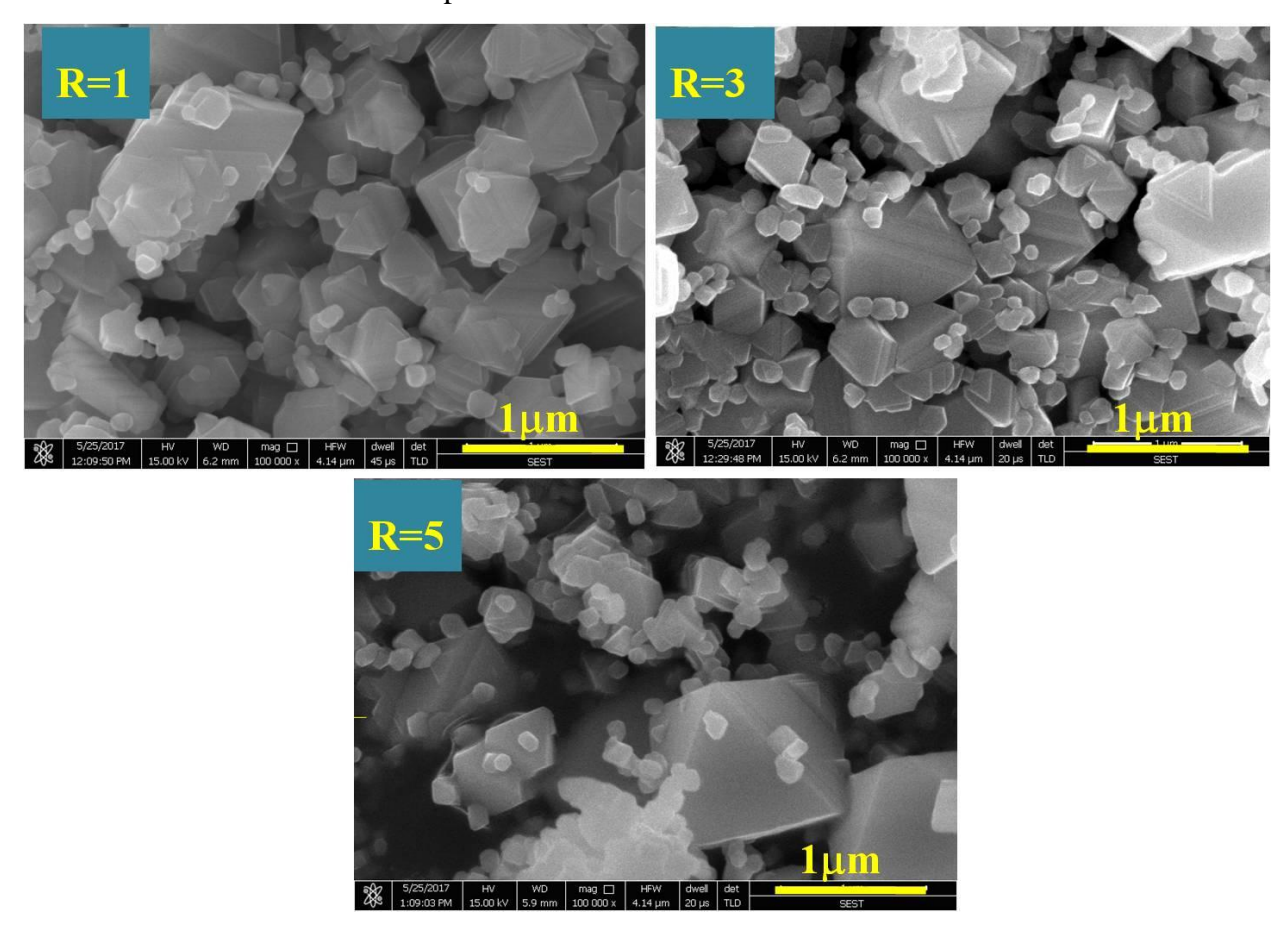


Figure 4.2.1.11 SEM micrographs of CFO powder prepared at 1000°C, 24h with different salt to powder mass ratio (1:1, 3:1, 5:1).

Table 4.2.1.8 Average particle size of bigger particles and smaller particles calculated from SEM micrographs of CFO powder prepared at 1000°C, 24h with different salt to powder mass ratio (1:1, 3:1, 5:1).

Sl. No	Sample	Average particle size of	Average particle size of
		larger particles (nm)	smaller particles (nm)
1	AC-1:1-1000°C-24h	565	100
2	AC-3:1-1000°C-24h	670	108
3	AC-5:1-1000°C-24h	915	140

#### 4.2.1.2.9 Magnetic properties of CFO prepared at different salt to powder mass ratio

Room temperature M-H curves of CFO particles prepared at 1000°C, 24hwith different salt to powder mass ratio are shown in figure 4.2.1.12. Magnetic properties of CFO particles have been obtained from hysteresis curves and the values are summarized in table 4.2.1.9. The Saturation magnetization (M<sub>s</sub>) values of CFO particles have been increased slightly from 65emu/g to71 emu/g with an increase in solid to powder mass ratio from 1:1 to 5:1 respectively. Likewise, a small decrease in remanence magnetization (M<sub>r</sub>) from 18.9emu/g to 16.emu/g with an increase in solid to powder mass ratio from 1:1 to 5:1 respectively has been observed. Notable decrease in coercivity from 55.5 kA/m to 30.7 has been observed with an increase in solid to powder mass ratio from 1:1 to 5:1 respectively.

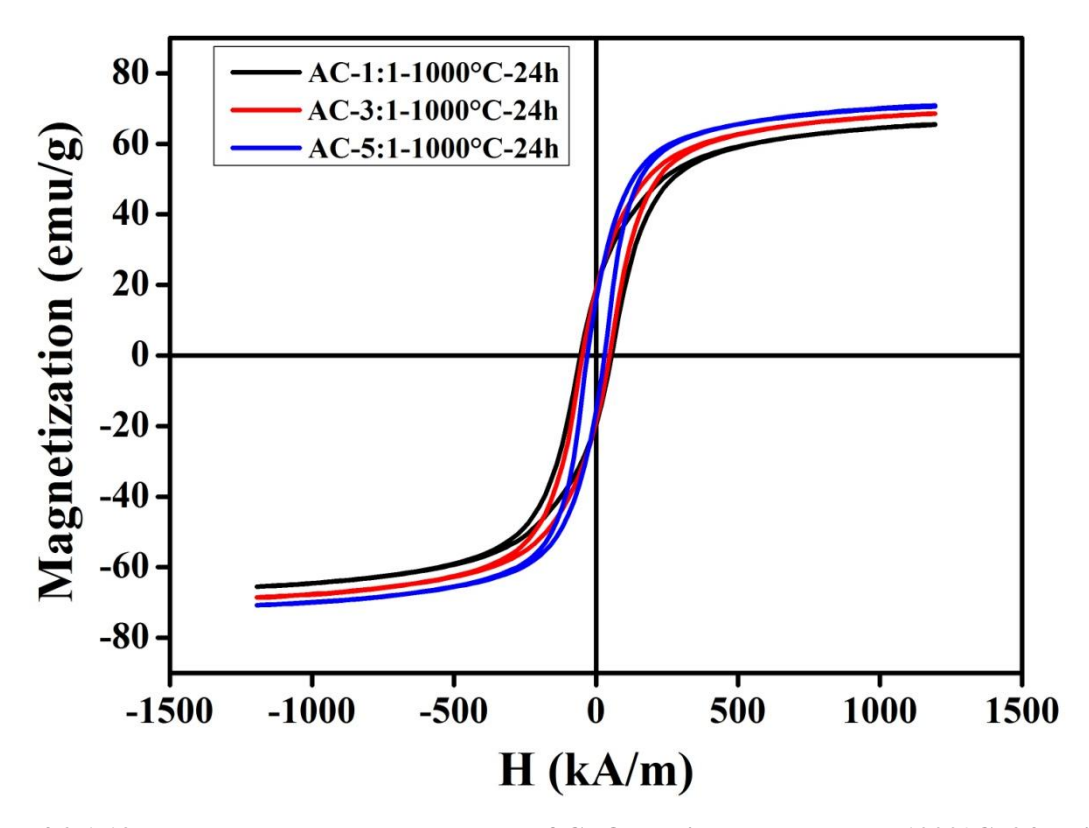


Figure 4.2.1.12 Room temperature M-H curve of CFO particles prepared at 1000°C, 24h with different salt to powder mass ratio (1:1, 3:1, 5:1).

Table 4.2.1.9 magnetic properties of CFO particles prepared at 1000°C, 24h with different salt to powder mass ratio (1:1, 3:1, 5:1).

Sl. No	Sample	M <sub>s</sub> (emu/g)	M <sub>r</sub> (emu/g)	H <sub>c</sub> (kA/m)
1	AC-1:1-1000°C-24h	65.5	18.9	55.5
2	AC-3:1-1000°C-24h	68.6	18.8	47.8
3	AC-5:1-1000°C-24h	70.9	16	30.7

#### 4.2.1.3 Conclusions

Phase pure CFO have been prepared by MSS using presynthesized CFO nano particles at different conditions uch as different temperatures (700°C, 800°C, 900°C, and 1000°C for 4h), different dwell time (4h, 12h, 24h), and different salt to powder ratios (1:1, 3:1, and 5:1). Particle size, saturation magnetization of CFO has been increased with increase in temparature, dwell time and salt to powder ratio. CFO particle morphology has been changed from distorted spherical to traingualr and octahedron shape with increase in temparature, dwell time and salt to powder ratio. Numbers of particles with triangular and octahedral shapes has been increased with increase in temperature, dwell time and powder to salt ratio.

## 4.2.2 Investigation of magnetic and magnetoelastic properties of textured CoFe<sub>2</sub>O<sub>4</sub> prepared by template grain growth (TGG) technique

CFO templates synthesized at different conditions (different temperatures, dwell time, salt to powder ratios) in Molten salt synthesis method. These templates were pressed into pellets and were sintered at 1350°C, 12h. the sintered pellets prepared from templates prepared at different temperatures such as 700°C, 800°C, 900°C and 1000°C for 4hwith 1:1 salt to powder mass ratios are referred as SP700, SP800, SP900 and SP1000 respectively. The sintered pellets prepared from powder synthesized at 1000°C, 1:1 mass ratio, and different dwell times such as 4h, 6h and 12h are referred as SP4h, SP12h, and SP24h respectively. And sintered pellets prepared from powder synthesized at 1000°C, 24h at different salt to powder mass ratios such as 1:1, 3:1, and 5:1 are referred as SPR1, SPR3, and SPR5 respectively. These sintered pellets were characterized for structural, morphological, magnetic and magnetoelastic properties by XRD, SEM, VSM and Magnetostriction setup respectively.

### 4.2.2.1 Characterization of CFO pellets prepared from CFO templates synthesized at different conditions

### 4.2.2.1.1 Structural properties of sintered pellets prepared from CFO templates synthesized at different temperatures

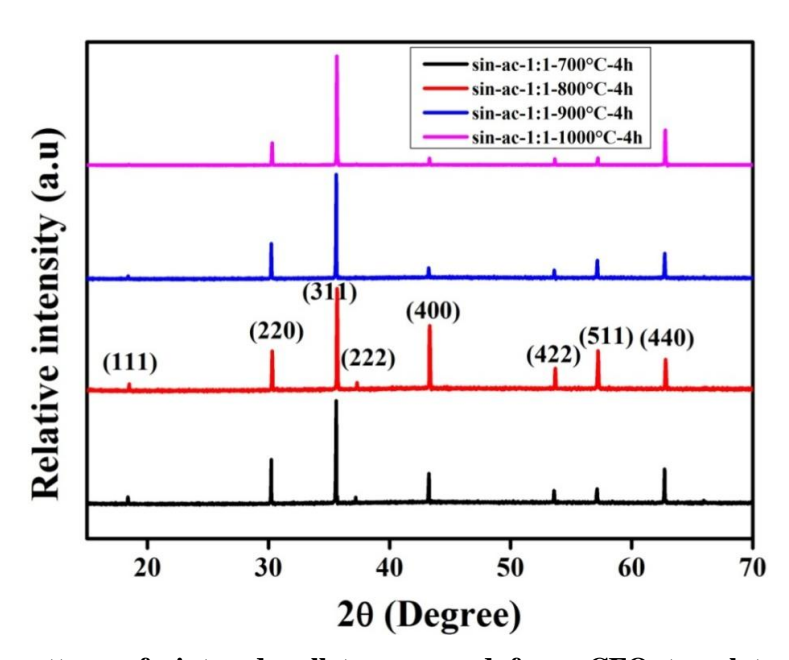


Figure 4.2.2.1 XRD pattern of sintered pellets prepared from CFO templates synthesized at different temperatures

XRD patterns of SP700, SP800, SP900 and SP1000 samples) are shown in figure 4.2.2.1. All the samples are in pure cubic spinel phase (JCPDS file no. 22-1086). Lattice parameter of the samples has been calculated using Nelson relay extrapolation plot from XRD. Lattice parameter of 8.38 Å has been calculated for all the sintered CFO samples prepared from CFO templates synthesized at different temperatures. No variation in lattice parameter has been observed for the sintered CFO samples prepared from CFO templates synthesized at different temperatures.

### 4.2.2.1.2 Microstructural properties of sintered pellets prepared from CFO templates synthesized at different temperatures

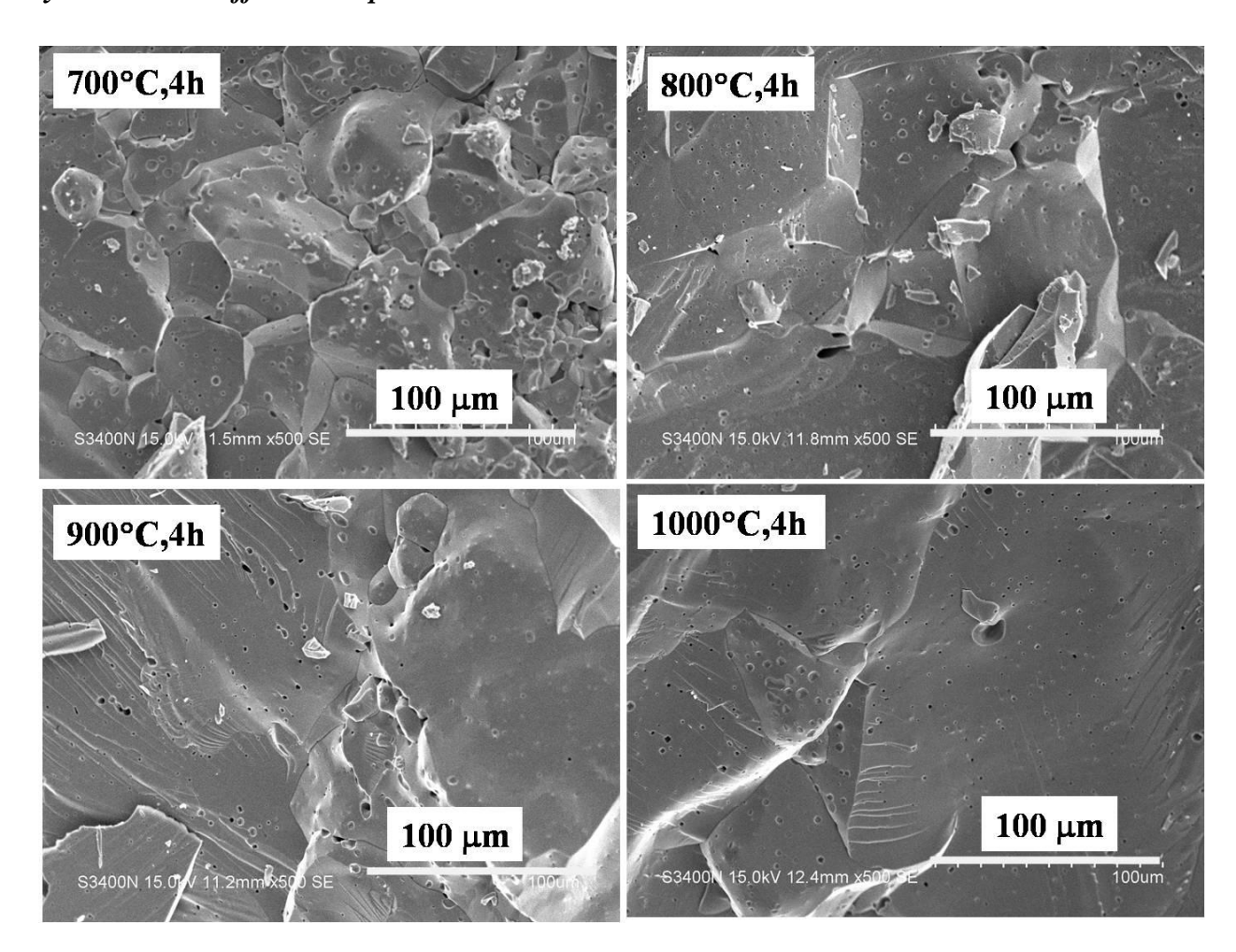


Figure 4.2.2.2 SEM micrographs of sintered pellets prepared from CFO templates synthesized at different temperatures (700°C, 800°C, 900°C and 1000°C for 4h)

Figure 4.2.2.2shows the SEM micrographs of SP700, SP800, SP900 and SP1000 samples. From SEM micrographs, it is observed that porosity is not present and complete densification of pellets

has taken place during sintering. Sintered density is calculated from Archimedes method following ASTM standard (C373-88) and it is found to be ~95% of the theoretical density for all CFO pellets, which is similar to the percent of theoretical density reported for CFO pellets synthesized by ceramic method [2]. Exaggerated grain growth has been observed for all CFO pellets prepared from CFO templates synthesized at different temperatures (700°C, 800°C, 900°C and 1000°C for 4h) with 1:1 salt to powder mass ratio.

# 4.2.2.1.3 Magnetic properties of sintered pellets prepared from CFO templates synthesized at different temperatures

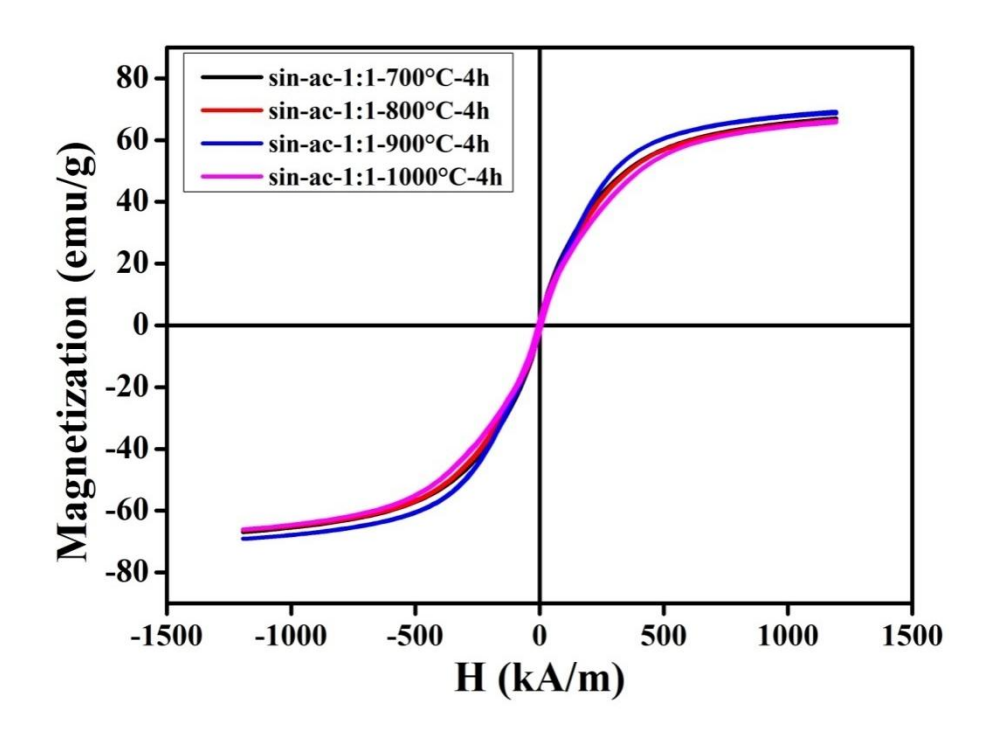


Figure 4.2.2.3 Room temperature M-H curve of sintered pellets prepared from CFO templates synthesized at different temperatures (700°C, 800°C, 900°C and 1000°C for 4h)

Room temperature M-H curves of sintered CFO pellets (SP700, SP800, SP900 and SP1000) are shown in figure 4.2.2.3. Magnetic properties of CFO particles have been obtained from hysteresis curves and shown in table 4.2.2.1. Small variation in saturation magnetization (65.7 emu/g to 68.7 emu/g), remanence (1.4 emu/g to 2.3 emu/g), and coercivity (4.9 kA/m to 7.4 kA/m) have been observed for sintered CFO samples pellets prepared from CFO templates synthesized at different temperatures.

Table 4.2.2.1 magnetic properties of sintered pellets prepared from CFO templates synthesized at different temperatures (700°C, 800°C, 900°C and 1000°C for 4h)

Sl. No	Sample	M <sub>s</sub> (emu/g)	M <sub>r</sub> (emu/g)	$H_c$ (kA/m)
1	sin-ac-1:1-700°C, 4h	66.4	1.7	5.4
2	sin-ac -1:1-800°C, 4h	66.1	1.8	6.2
3	sin-ac -1:1-900°C, 4h	68.7	1.4	4.9
4	sin-ac -1:1-1000°C, 4h	65.7	2.3	7.4

# 4.2.2.1.4 Magneto elastic properties of sintered pellets prepared from CFO templates synthesized at different temperatures

Magnetostriction has been measured on all CFO samples (SP700, SP800, SP900 and SP1000) and the curves are shown in figure 4.2.2.4. Strain gauges have been mounted along the diameter of the cylindrical sample. Parallel magnetostriction has been measured perpendicular to height of the cylindrical pellet and perpendicular magnetostriction has been measured along height of the cylindrical pellet. Variation of magnetostriction with temperature at which CFO templates are prepared is shown in figure 4.2.2.5. Among four samples, highest maximum parallel magnetostriction ( $\lambda_{\parallel}$ ) of 178 ppm has been observed at 300 kA/m magnetic field for SP700 and lowest  $\lambda_{\parallel}$  of 54 ppm has been obtained at 335 kA/m magnetic field for SP800. λ<sub>||</sub> values of 135 ppm at 355 kA/m magnetic field and 108 ppm at 477 kA/m magnetic field have been obtained for SP900 and SP1000 respectively. The magnetic field at which  $\lambda_{\parallel}$  is observed has been increased with the template synthesis temperature. Lowest maximum perpendicular magnetostriction ( $\lambda_{\perp}$ ) of 61 ppm has been obtained for SP700 and highest  $\lambda_{\perp}$  of 128 ppm has been obtained for SP800.  $\lambda_{\perp}$ values of 85 ppm and 106 ppm are obtained for SP900 and SP1000 respectively. Not a single report on magnetostriction of CFO prepared from MSS method is available in open literature. But,  $\lambda_{\parallel}$  values of SP700 and SP900 are better than the  $\lambda_{\parallel}$  value of 110 ppm reported for CFO prepared in ceramic route.

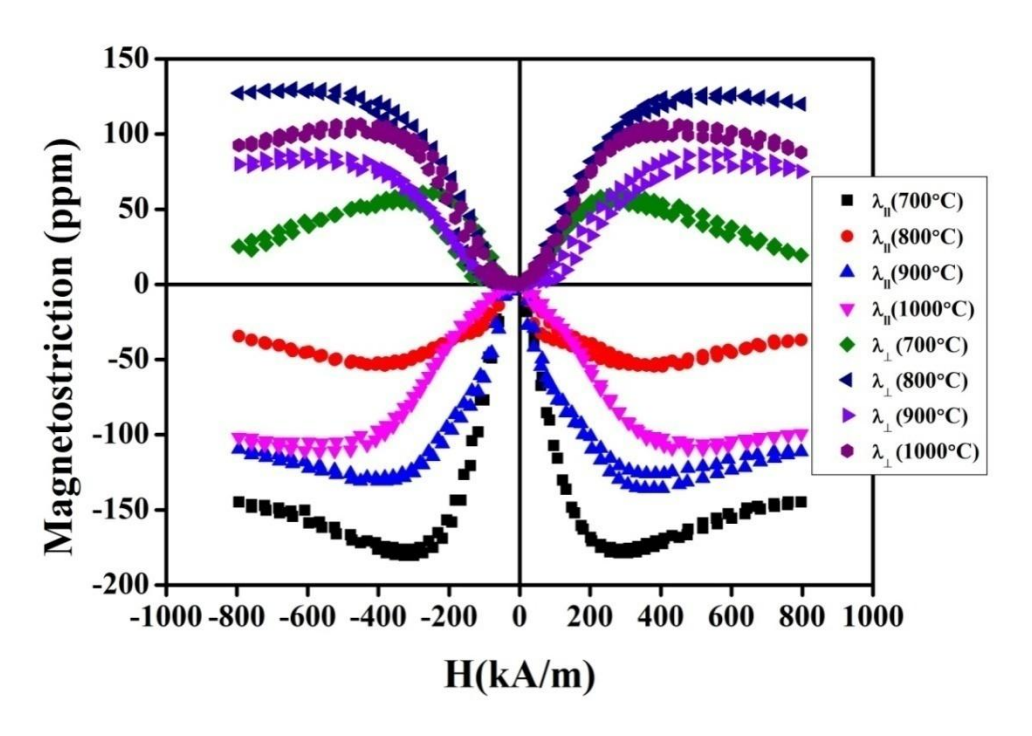


Figure 4.2.2.4 Magnetostriction curves of sintered pellets prepared from CFO templates synthesized at different temperatures (700°C, 800°C, 900°C and 1000°C for 4h)

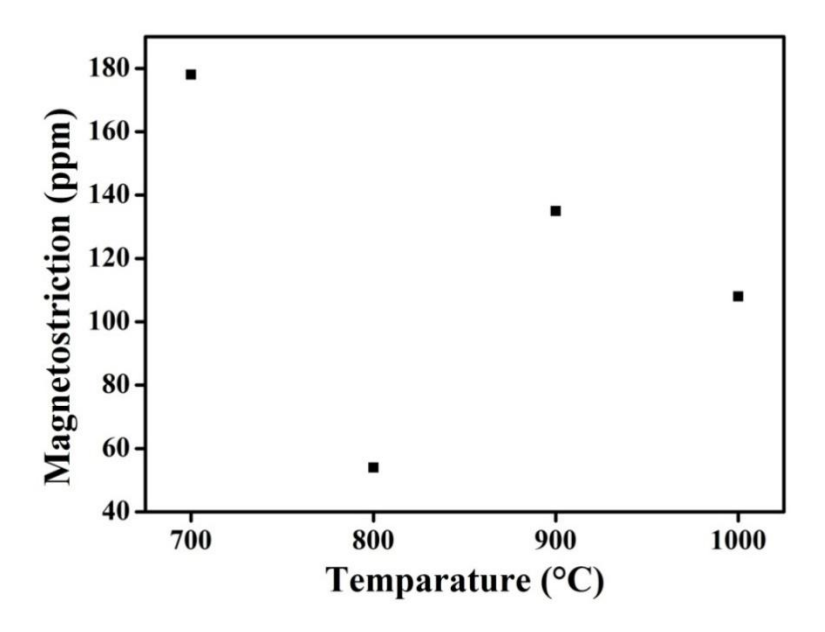


Figure 4.2.2.5 Variation of magnetostriction with temperature at which CFO templates have been prepared

For isotropic magnetostrictive material ratio between  $\lambda_{\perp}$  and  $\lambda_{\parallel}$  (Ratio of  $\lambda_{\perp}$ to  $\lambda_{\parallel}$ referred as  $\lambda_{r}$ ) should be 0.5. But here each sample has different  $\lambda_{r}$  value.  $\lambda_{r}$  values of 0.34, 2.37, 0.62, and 0.98 has been observed for SP700, SP800, SP900 and SP 1000 respectively. These  $\lambda_{r}$  values suggest that samples are not isotropic and some grain orientation might be possible in the samples. Since magnetostriction is a structure sensitive property, the magnetostriction values depends on thermal, magnetic and mechanical history of the samples. Here, each sample has different thermal history and hence variation in magnetostriction is expected.

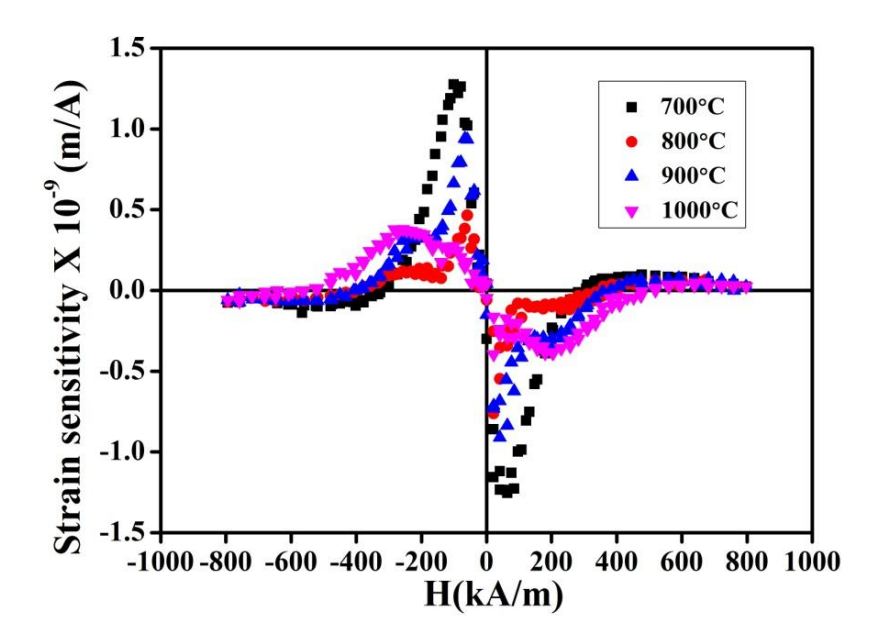


Figure 4.2.2.6 Strain sensitivity curves of sintered pellets prepared from CFO templates synthesized at different temperatures (700°C, 800°C, 900°C and 1000°C for 4h)

Strain sensitivity curves of SP700, SP800, SP900 and SP1000 shown in figure 4.2.2.6. Maximum strain sensitivity ( $d\lambda/dH$ ) of  $1.2\times10^{-9}$  m/A for SP700 and lowest  $d\lambda/dH$  of  $0.3\times10^{-9}$  m/A has been obtained for SP1000. Variation of maximum strain sensitivity with temperature at which CFO templates have been prepared is shown in figure 4.2.2.7. Strain sensitivity mainly depends on the slope of magnetostriction curve rather than the magnetostriction values. This is the reason why  $d\lambda/dH$  of SP800 is more than the  $d\lambda/dH$  of SP1000.

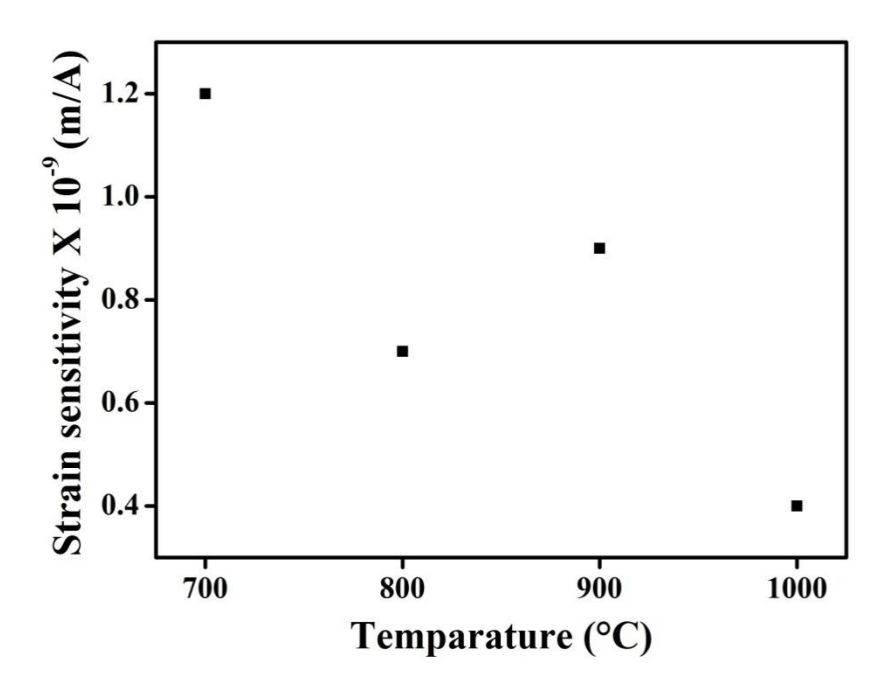


Figure 4.2.2.7 Variation of magnetostriction with temperature at which CFO templates have been prepared

# 4.2.2.1.5 Structural properties of sintered pellets prepared from CFO templates synthesized at different dwell time

XRD pattern of CFO sintered pellets (SP4h, SP12h, and SP24h) are shown in figure 4.2.2.8, which indicates all are in pure cubic spinel phase (JCPDS file no. 22-1086). Highest intensity has been observed for (511) peak for SP24h sample whereas (311) is the highest intensity peak for the isotropic CFO pellet. Texture coefficient of 1.8 has been observed for (511) peak for SP24h sample. High intensity has been observed for (400) peak for SP24h sample compare to the intensity of (440) peak observed for the isotropic CFO pellet. Texture coefficient of 1.2 has been observed for (440) peak for SP24h sample. Lattice parameter of the samples has been calculated using Nelson relay extrapolation plot from XRD. Lattice parameter of 8.38 Å has been calculated for all the sintered CFO samples prepared from CFO templates synthesized at 1000°C with 1:1 salt to powder mass ratio and different dwell times (4h, 12h, and 24h). No variation in lattice parameter has been observed for the sintered CFO samples prepared from CFO templates synthesized at different dwell time.

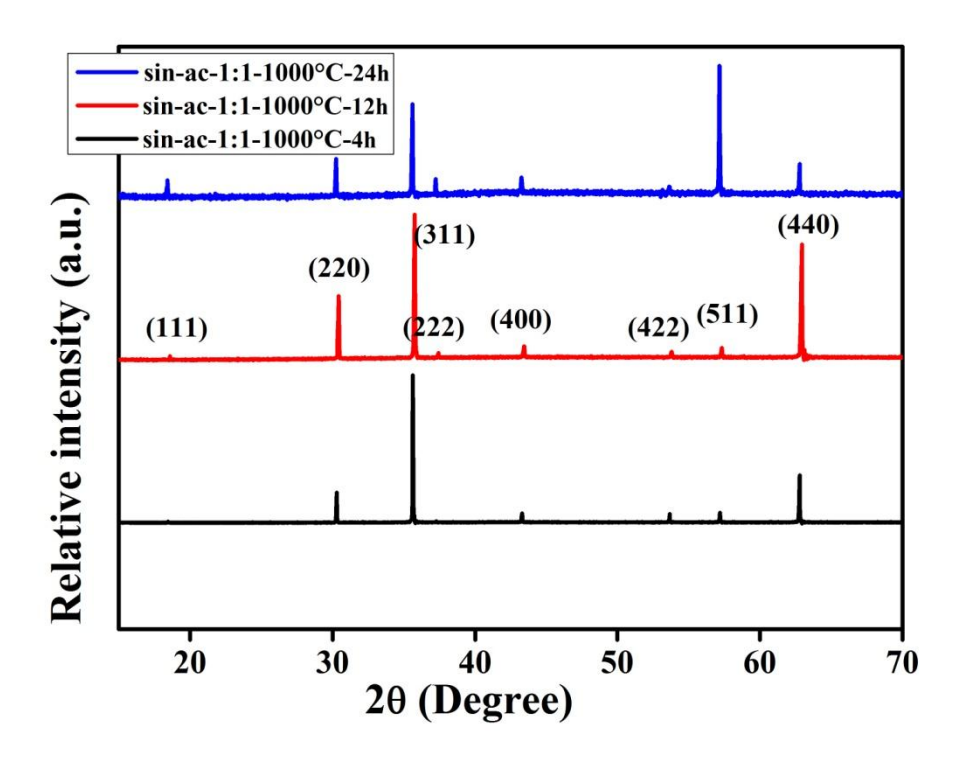


Figure 4.2.2.8 XRD pattern of sintered pellets prepared from CFO templates synthesized at 1000°C with 1:1 salt to powder mass ratio and different dwell time (4h, 12h, and 24h)

# 4.2.2.1.6 Microstructural properties of sintered pellets prepared from CFO templates synthesized at different dwell times

Figure 4.2.2.9shows the SEM micrographs of SP4h, SP12h, and SP24h samples. From SEM micrographs, it is observed that porosity is not present and complete densification of pellets has taken place during sintering. Sintered density is calculated from Archimedes method following ASTM standard (C373-88) and it is found to be ~95% of the theoretical density for all CFO pellets, which is similar to the percent of theoretical density reported for CFO pellets synthesized by ceramic method [2]. Exaggerated grain growth has been observed in SEM micrographs of SP4h, SP12h, and SP24h samples.

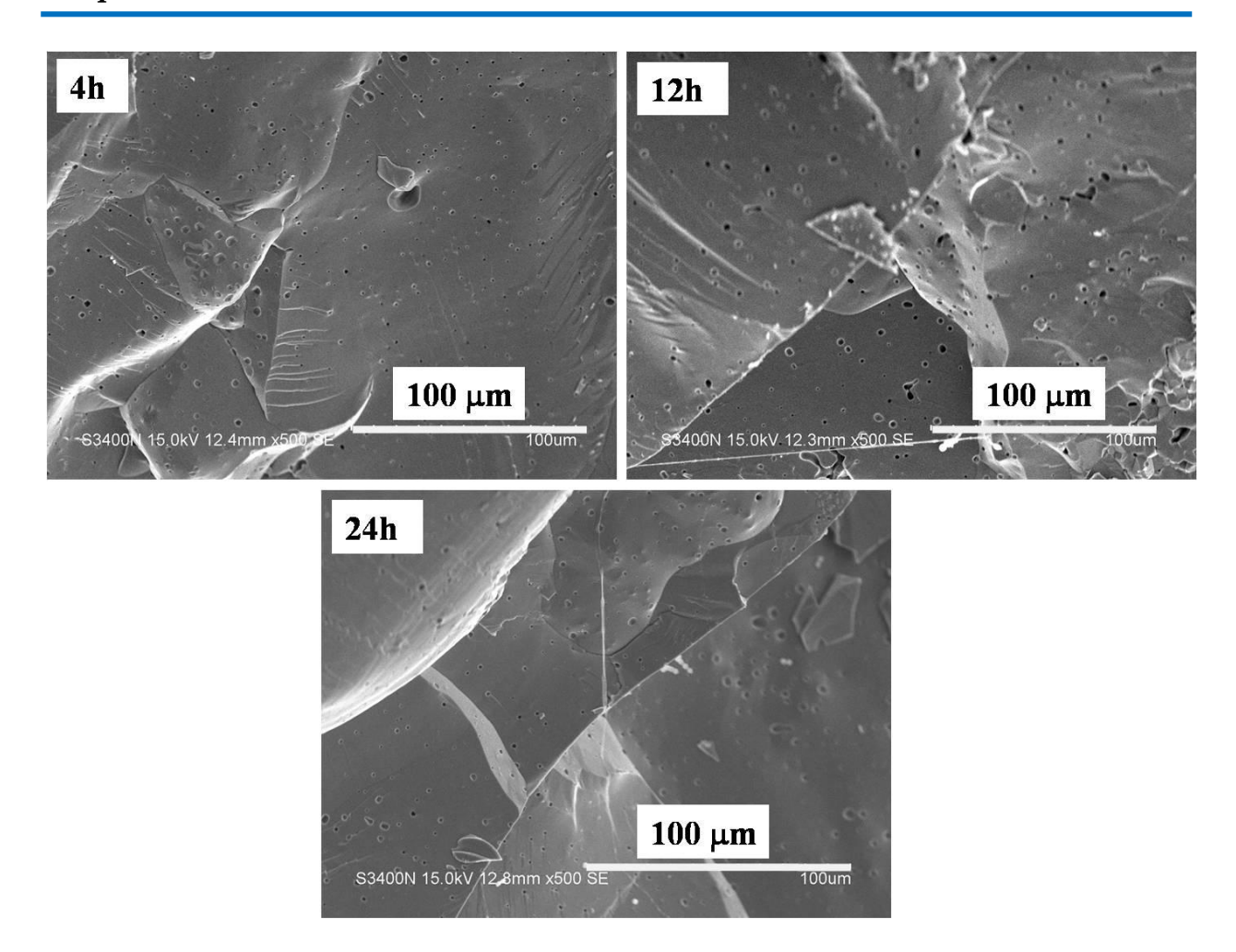


Figure 4.2.2.9 SEM micrographs of sintered pellets prepared from CFO templates synthesized at  $1000^{\circ}$ C with 1:1 salt to powder mass ratio and different dwell times (4h, 12h, and 24h)

# 4.2.2.1.7 Magnetic properties of sintered pellets prepared from CFO templates synthesized at different dwell times

Room temperature M-H curves of sintered CFO pellets (SP4h, SP12h, and SP24h) are shown in figure 4.2.2.10. Magnetic properties of CFO particles have been obtained from hysteresis curves and shown in table 4.2.2.2. Small variation in saturation magnetization (65.7 emu/g to 68.6 emu/g), remanence (1.8 emu/g to 2.2 emu/g), and coercivity (6.1 kA/m to 7.3 kA/m) have been observed for sintered CFO samples pellets prepared from CFO templates synthesized at different dwell time.

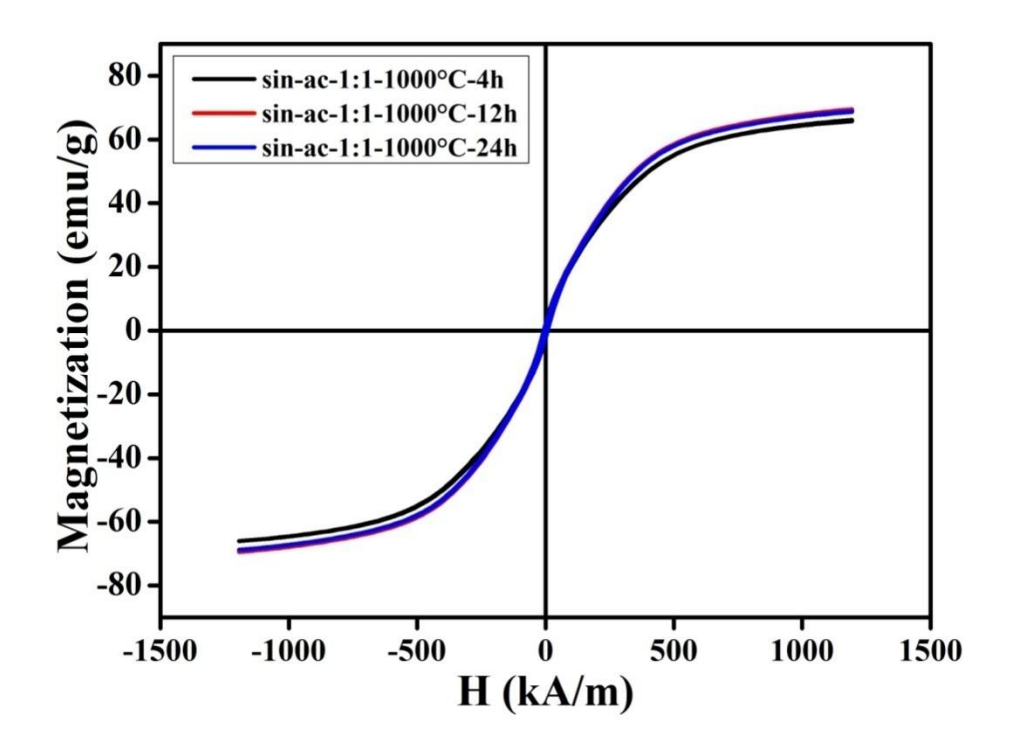


Figure 4.2.2.10 Room temperature M-H curve of sintered pellets prepared from CFO templates synthesized at 1000°C with 1:1 salt to powder mass ratio and different dwell times (4h, 12h, and 24h)

Table 4.2.2.2 magnetic properties of sintered pellets prepared from CFO templates synthesized at different temperatures (700°C, 800°C, 900°C and 1000°C for 4h)

Sl. No	Sample	M <sub>s</sub> (emu/g)	M <sub>r</sub> (emu/g)	$H_c$ (kA/m)
1	sin-ac -1:1-1000°C-4h	65.7	2.2	7.3
2	sin-ac -1:1-1000°C-12h	69.3	1.8	6.1
3	sin-ac -1:1-1000°C-24h	68.6	1.8	6.1

# 4.2.2.1.8 Magneto elastic properties of sintered pellets prepared from CFO templates synthesized at different dwell times

Magnetostriction has been measured on all sintered (SP4h, SP12h, and SP24h) and the data is shown in figure 4.2.2.11. Strain gauges have been mounted along the diameter of the cylindrical sample. For samples, parallel and perpendicular magnetostriction has been measured perpendicular and parallel to the height of the cylindrical pellet. Variation of magnetostriction with dwell time at which CFO templates have prepared has been shown in figure 4.2.2.5. Among three

samples, highest Maximum parallel magnetostriction ( $\lambda_{\parallel}$ ) of 163 ppm has been observed at 355 kA/m magnetic field for SP12h and lowest  $\lambda_{\parallel}$  of 111 ppm has been obtained at 477 kA/m magnetic field for SP4h.  $\lambda_{\parallel}$ values of 145 ppm at 331 kA/m magnetic field have been obtained for SP24h. The magnetic field at which  $\lambda_{\parallel}$ has been decreased (from 477 kA/m to 331 kA/m) with increase in dwell time. Lowest maximum perpendicular magnetostriction ( $\lambda_{\perp}$ ) of 71 ppm for SP24h and highest  $\lambda_{\perp}$  of 106 ppm has been obtained for SP4h.  $\lambda_{\perp}$ value of 85 ppm and 106 ppm are obtained for SP12h.  $\lambda_{\parallel}$ values of SP4h, SP12h and SP24h are better than the  $\lambda_{\parallel}$  value of 110 ppm reported for CFO prepared in ceramic route.

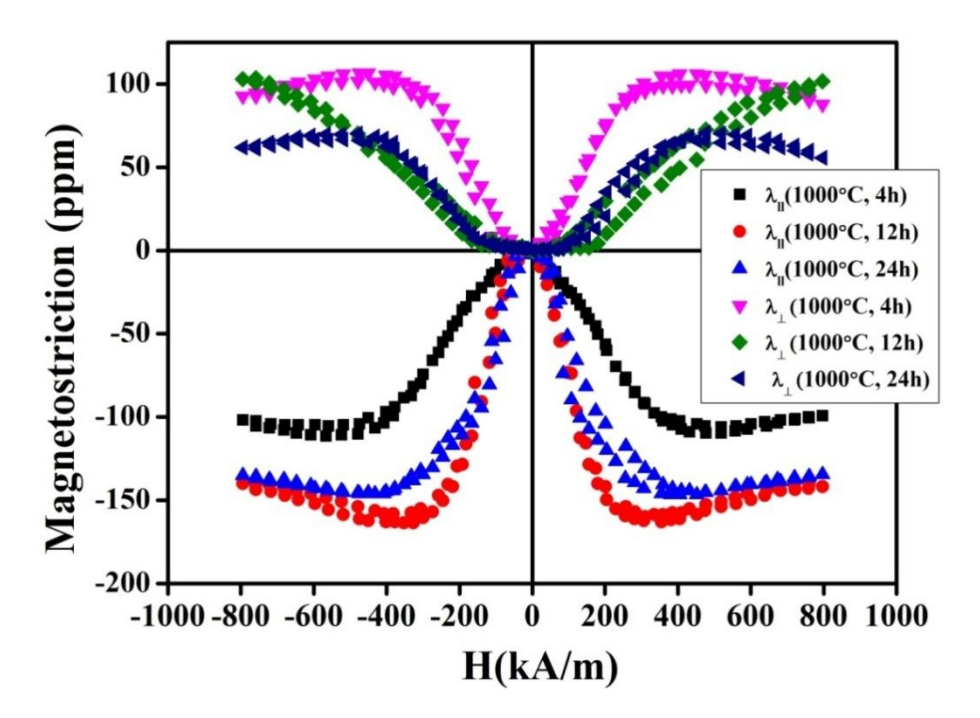


Figure 4.2.2.11 Magnetostriction curves of sintered pellets prepared from CFO templates synthesized at 1000°C with 1:1 salt to powder mass ratio and different dwell times (4h, 12h, and 24h)

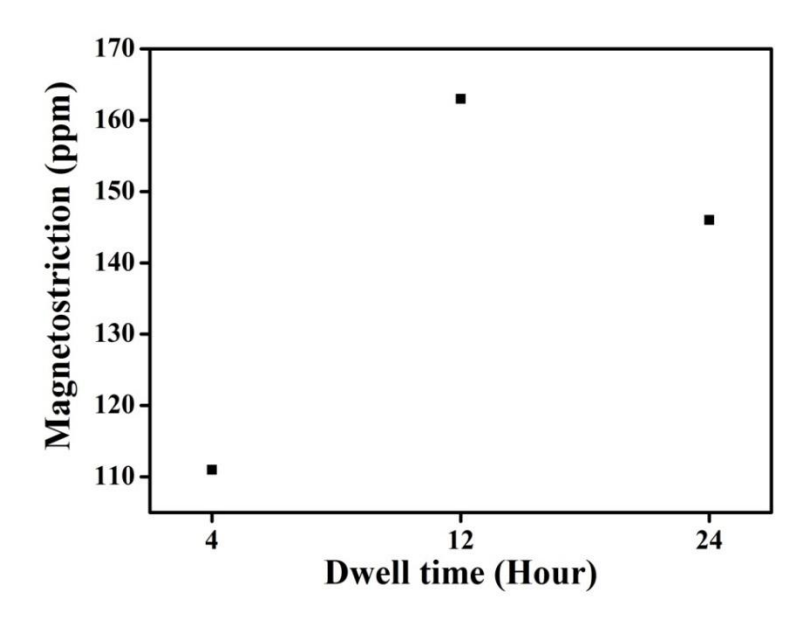


Figure 4.2.2.12 Variation of magnetostriction with dwell time at which CFO templates have been prepared

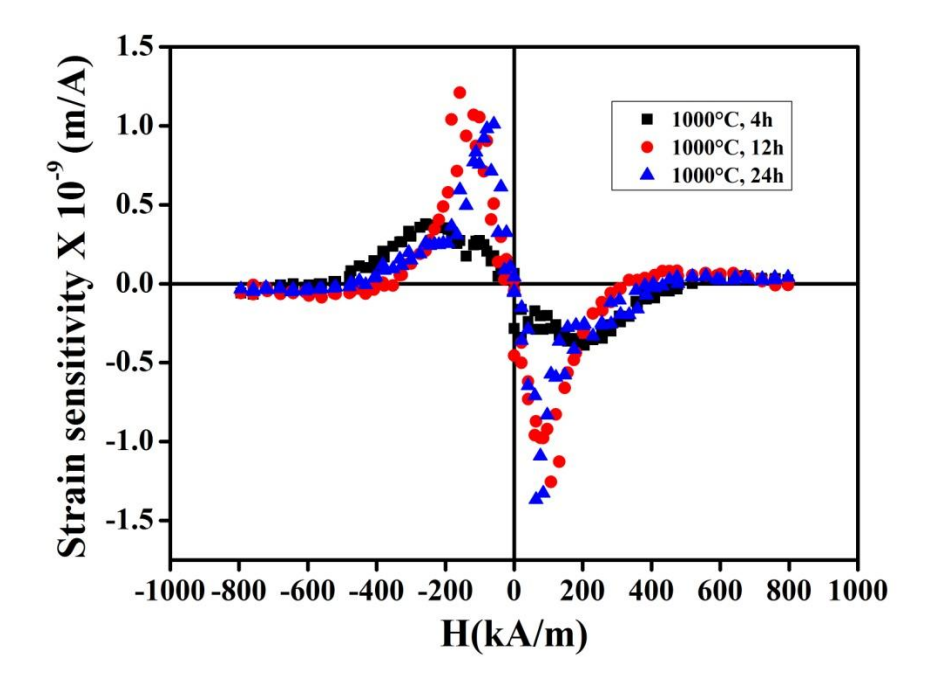


Figure 4.2.2.13 Magnetostriction curves of sintered pellets prepared from CFO templates synthesized at 1000°C with 1:1 salt to powder mass ratio and different dwell times (4h, 12h, and 24h)

For isotropic magnetostrictive material ratio between  $\lambda_{\perp}$  and  $\lambda_{\parallel}$  (Ratio of  $\lambda_{\perp}$ to  $\lambda_{\parallel}$ referred as  $\lambda_{r}$ ) should be 0.5. But here each sample has different  $\lambda_{r}$  value.  $\lambda_{r}$  values of 0.95, 0.63, and 0.48 has been observed for SP4h, SP12h, and SP24h respectively. These  $\lambda_{r}$  values suggest that samples are not isotropic and some grain orientation might be possible in the samples. Since magnetostriction is a structure sensitive property, the magnetostriction values depends on thermal, magnetic and mechanical history of the samples. Here, each sample has different thermal history and hence variation in magnetostriction is expected.

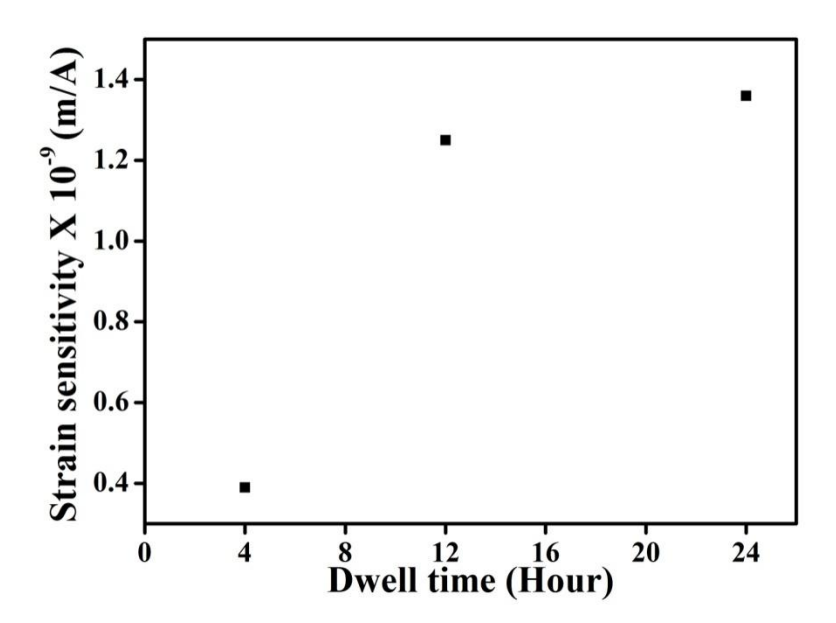


Figure 4.2.2.14 Variation of strain sensitivity with dwell time at which CFO templates have been prepared

Strain sensitivity curves of SP4h, SP12h, and SP24h are shown in figure 4.2.2.13. Maximum strain sensitivity ( $d\lambda/dH$ ) of  $1.4\times10^{-9}$  m/A for SP24h and lowest  $d\lambda/dH$  of  $0.4\times10^{-9}$  m/A has been obtained for SP4h. Variation of maximum strain sensitivity with temperature at which CFO templates have been prepared has been shown in figure 4.2.2.14. Strain sensitivity values increased linearly with increase in dwell time.

### 4.2.2.1.9 Structural properties of sintered pellets prepared from CFO templates synthesized at different salt to powder mass ratios

XRD pattern of CFO sintered pellets of SPR1, SPR3, and SPR5 samples are shown in figure 4.2.2.15, which resulted in pure cubic spinel phase (JCPDS file no. 22-1086). Highest intensity has been observed for (511) peak for SPr1 and SPr3 sample whereas (311) is the highest intensity peak for the isotropic CFO pellet. Texture coefficients of 1.8 and 1.2 have been observed for (511) SPr1 and SPr3 samples respectively. Lattice parameter of the samples has been calculated using Nelson relay extrapolation plot from XRD. Lattice parameter of 8.38 Å has been calculated for all the sintered CFO samples prepared from CFO templates synthesized at different temperatures. No variation in lattice parameter has been observed for the sintered CFO samples prepared from CFO templates synthesized at different salt to powder mass ratios.

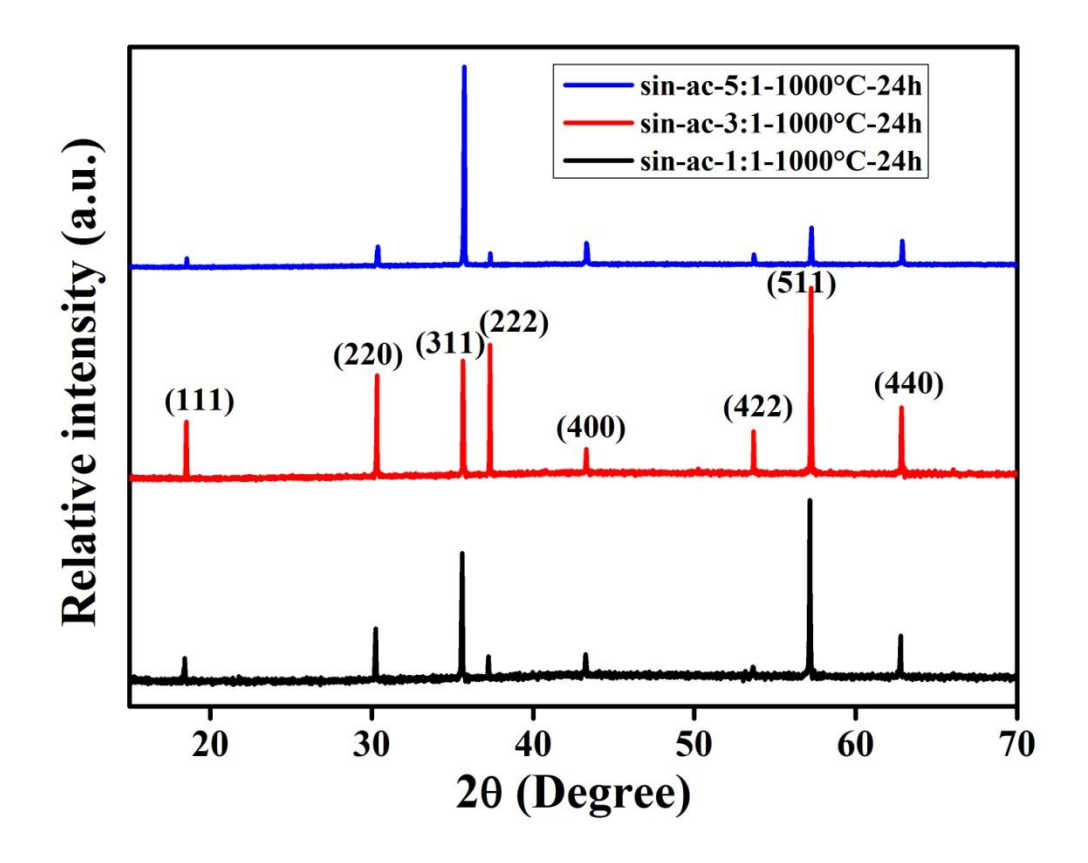


Figure 4.2.2.15 XRD pattern of sintered pellets prepared from CFO templates synthesized at 1000°C, 24h with different salt to powder mass ratios (1:1, 3:1, and 5:1)

4.2.2.1.10. Microstructural properties of sintered pellets prepared from CFO templates synthesized at different salt to powder mass ratios

Figure 4.2.2.16 shows the SEM micrographs of sintered CFO pellets (SPR1, SPR3, and SPR5). From SEM micrographs, it is observed that porosity is not present and complete densification of pellets has taken place during sintering. Sintered density is calculated from Archimedes method following ASTM standard (C373-88) and it is found to be ~95% of the theoretical density for all CFO pellets, which is similar to the percent of theoretical density reported for CFO pellets synthesized by ceramic method [2]. Exaggerated grain growth has been observed for all CFO pellets prepared from CFO templates synthesized at 1000°C, 24hwith different salt to powder mass ratios (1:1, 3:1, and 5:1).

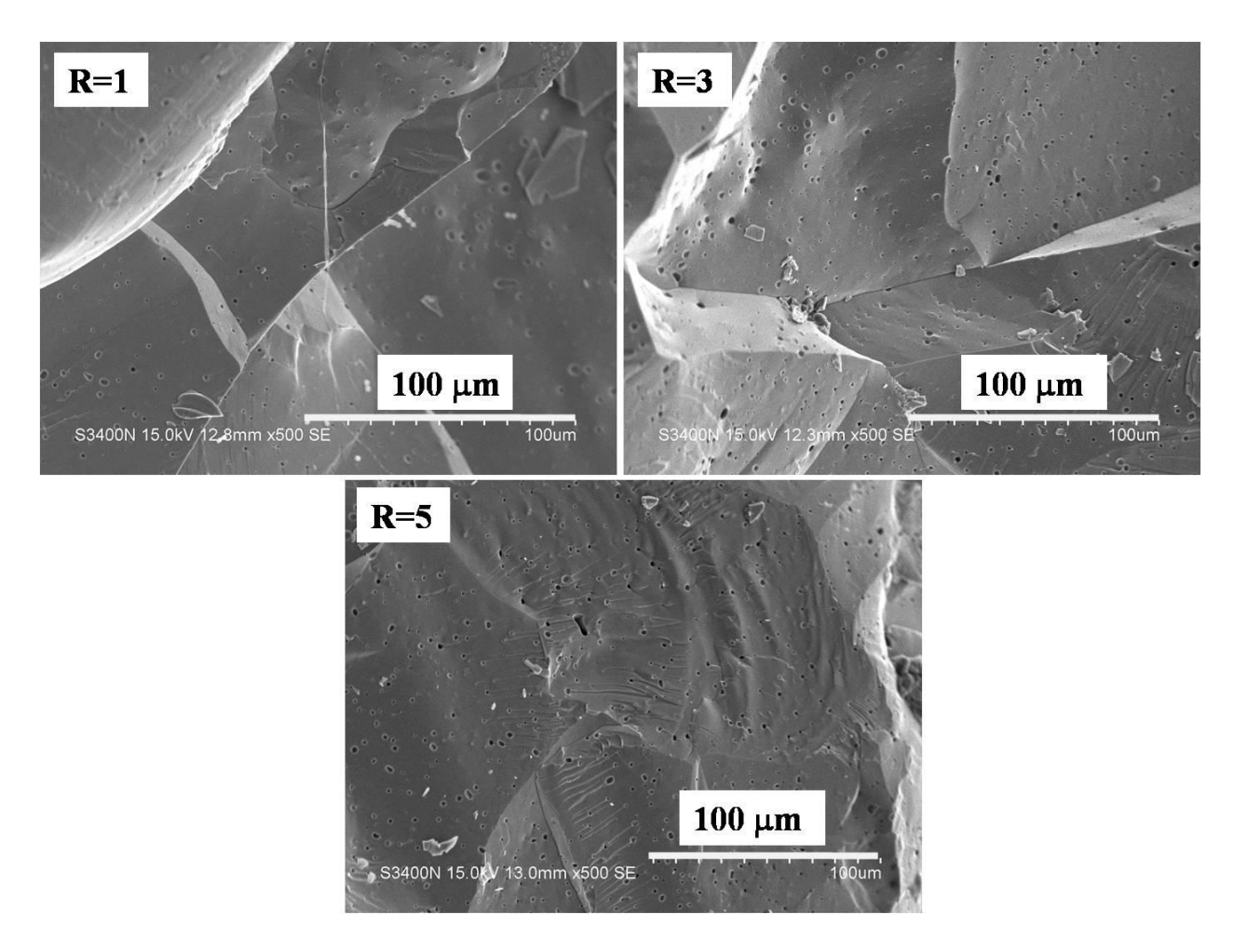


Figure 4.2.2.16 SEM micrographs of sintered pellets prepared from CFO templates synthesized at 1000°C, 24h with different salt to powder mass ratios (1:1, 3:1, and 5:1)

4.2.2.1.11. Magnetic properties of sintered pellets prepared from CFO templates synthesized at different salt to powder mass ratios

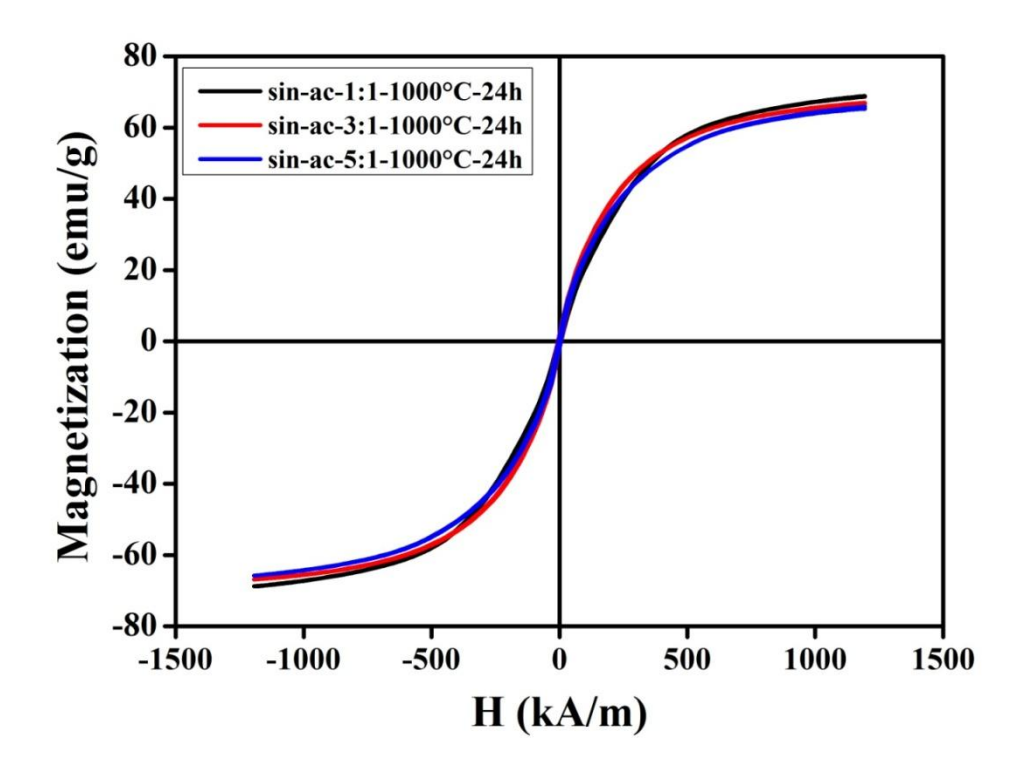


Figure 4.2.2.17 Room temperature M-H curve of sintered pellets prepared from CFO templates synthesized at 1000°C, 24h with different salt to powder mass ratios (1:1, 3:1, and 5:1)

Room temperature M-H curves of sintered CFO pellets (SPR1, SPR3, and SPR5) have been shown in figure 4.2.2.17. Magnetic properties of CFO particles have been obtained from hysteresis curves and shown in table 4.2.2.3. Small variation in saturation magnetization (66.6 emu/g to 68.6 emu/g), remanence (1.8 emu/g to 2.2 emu/g), and coercivity (4.5 kA/m to 6.4 kA/m) have been observed for sintered CFO samples pellets prepared from CFO templates synthesized at different dwell time.

Table 4.2.2.3 magnetic properties of sintered pellets prepared from CFO templates synthesized at  $1000^{\circ}$ C, 24h with different salt to powder mass ratios (1:1, 3:1, and 5:1)

Sl. No	Sample	M <sub>s</sub> (emu/g)	M <sub>r</sub> (emu/g)	H <sub>c</sub> (kA/m)
1	sin-ac -1:1-1000°C-24h	68.6	1.8	6
2	sin-ac -3:1-1000°C-24h	66.6	2.2	6.4
3	sin-ac -5:1-1000°C-24h	68.2	1.6	4.5

4.2.2.1.12 Magneto elastic properties of sintered pellets prepared from CFO templates synthesized at different salt to powder mass ratios

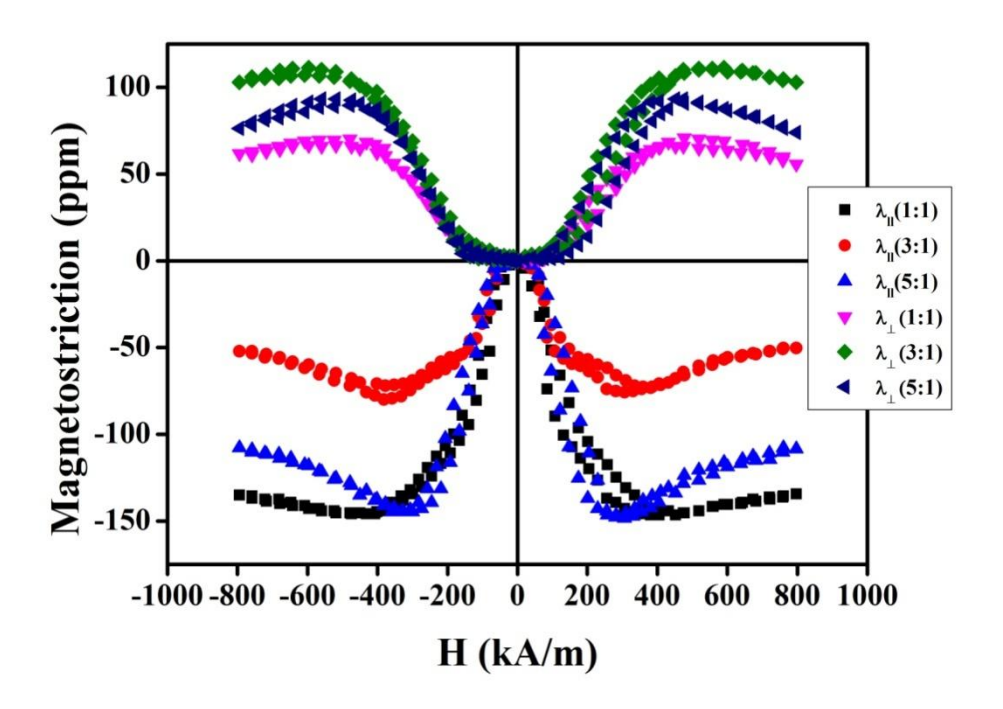


Figure 4.2.2.18 Magnetostriction curves of sintered pellets prepared from CFO templates synthesized at 1000°C, 24h with different salt to powder mass ratios (1:1, 3:1, and 5:1)

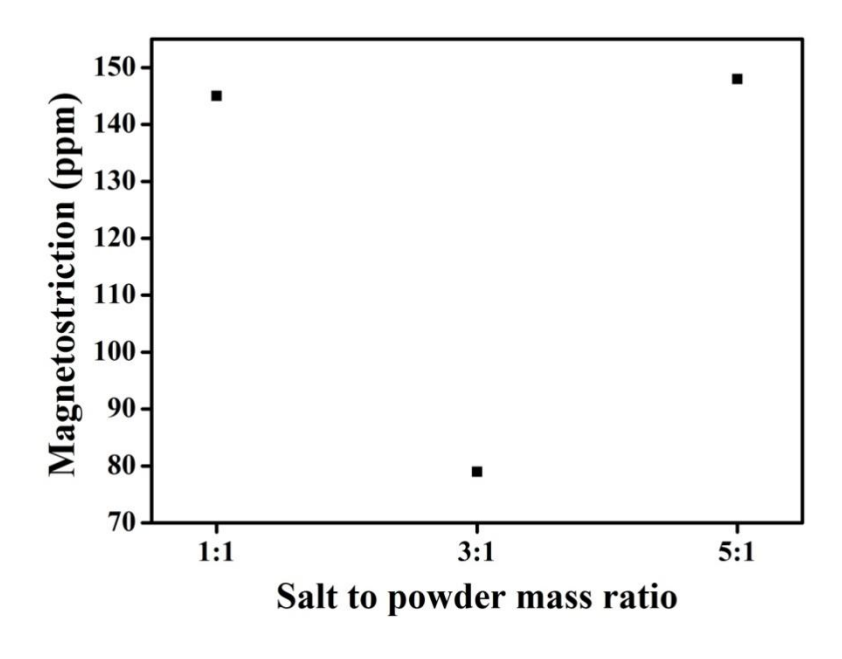


Figure 4.2.2.19 Variation of magnetostriction with salt to powder mass ratio

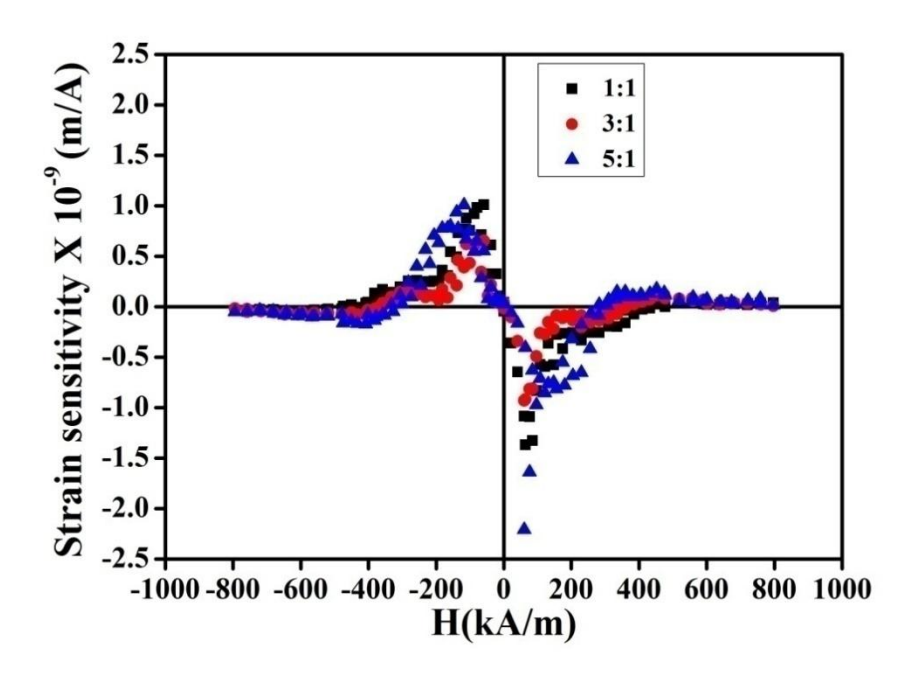


Figure 4.2.2.20 Strain sensitivity curves of sintered pellets prepared from CFO templates synthesized at 1000°C, 24h with different salt to powder mass ratios (1:1, 3:1, and 5:1)

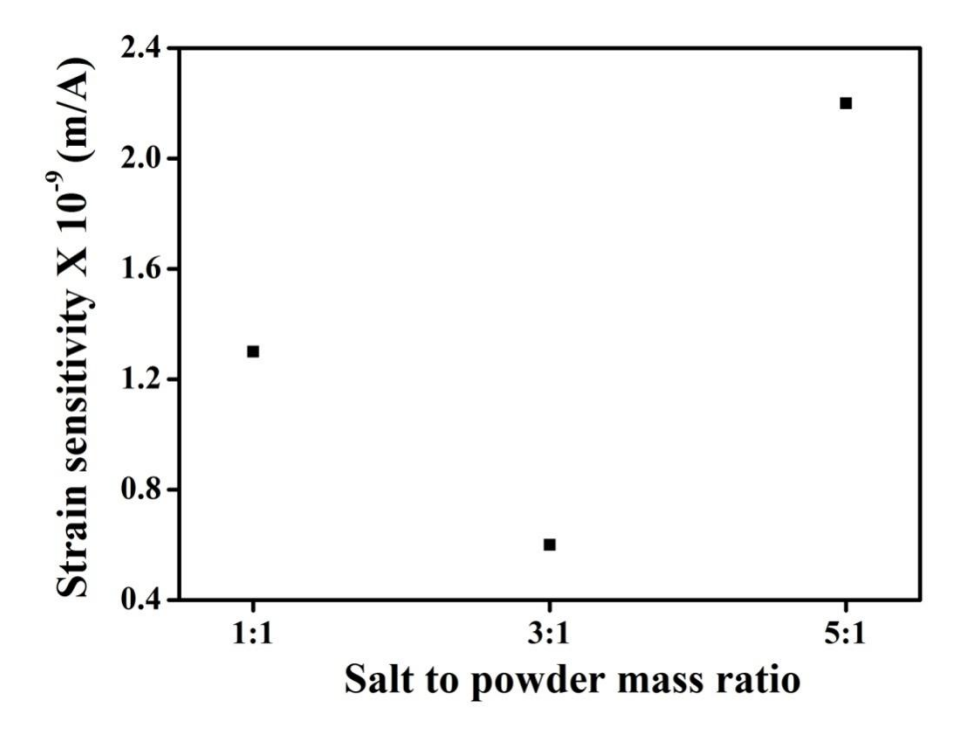


Figure 4.2.2.21 Variation of strain sensitivity with salt to powder mass ratio

Magnetostriction has been measured on all sintered CFO pellets (SPR1, SPR3, and SPR5) and the data is shown in figure 4.2.2.18. Strain gauges have been mounted along the diameter of the cylindrical sample. For samples, parallel and perpendicular magnetostriction has been measured perpendicular and parallel to the height of the cylindrical pellet. Variation of magnetostriction with salt to powder mass ratio at which CFO templates were prepared has been shown in figure 4.2.2.19. Among three samples, highest Maximum parallel magnetostriction ( $\lambda_{\parallel}$ ) of 148 ppm has been observed at 281 kA/m magnetic field for SPr5 and lowest  $\lambda_{\parallel}$  of 69 ppm has been obtained at 382 kA/m magnetic field for SPr3.  $\lambda_{\parallel}$ values of 145 ppm at 331 kA/m magnetic field have been obtained for SPr2. Lowest maximum perpendicular magnetostriction ( $\lambda_{\perp}$ ) of 71 ppm has been obtained for SPr1 and highest  $\lambda_{\perp}$  of 108 ppm has been obtained for SPr3.  $\lambda_{\perp}$ value of 93 ppm has been obtained for SPr5. $\lambda_{\parallel}$  values of SPr1 and SPr5 were better than the  $\lambda_{\parallel}$  value of 110 ppm reported for CFO prepared in ceramic route.

For isotropic magnetostrictive material ratio between  $\lambda_{\perp}$  and  $\lambda_{\parallel}$  (Ratio of  $\lambda_{\perp}$ to  $\lambda_{\parallel}$ referred as  $\lambda_{r}$ ) should be 0.5. But here each sample has different  $\lambda_{r}$  value.  $\lambda_{r}$  values of 0.48, 1.36, and 0.62 has been observed for SPr1, SPr3, and SPr5 respectively. These  $\lambda_{r}$  values suggest that samples are not isotropic and some grain orientation might be possible in the samples. Since magnetostriction is a structure sensitive property, the magnetostriction values depends on thermal, magnetic and mechanical history of the samples. Here, each sample has different thermal history and hence variation in magnetostriction is expected for each sample.

Strain sensitivity curves of SPr1, SPr3, and SPr5 are shown in figure 4.2.2.20. Maximum strain sensitivity ( $d\lambda/dH$ ) of  $2.2\times10^{-9}$  m/A for SPr5 and lowest  $d\lambda/dH$  of  $0.9\times10^{-9}$  m/A has been obtained for SPr3.  $d\lambda/dH$  of  $1.4\times10^{-9}$  m/A has been obtained for SPr1. Variation of maximum strain sensitivity with temperature at which CFO templates have been prepared has been shown in figure 4.2.2.21. Strain sensitivity values decreases initially and increases with increase in salt to powder mass ratio.

#### **4.2.2.2 Conclusions**

Phase pure CFO pellets have been prepared from CFO powder synthesized at different conditions such as different temperature, dwell time, and salt to powder ratio. Preferential

orientation has been observed for (511) peak for SPr1, SPr3 and SP24h samples. A small variation in magnetic properties has been observed for CFO pellets prepared at different conditions.  $\lambda_r$  values suggest that samples are not isotropic and some grain orientation might be possible for the pellets prepared at different temperatures, dwell time and salt to powder ratio.

### **References:**

- 1. K. Zhang, T. Holloway, A.K. Pradhan, J. Magn. Magn. Mater, 323 (2011) 1619.
- 2. S. D. Bhame, P. A. Joy, Sens. Actuators, A, 137 (2007) 256.
- 3. W. jiquan, G. Xuexu; Y. Chao, L. Jiheng, B. Xiaoqian, J. Magn. Magn. Mater. 401 (2016) 662-666.
- 4. R. M. Bozorth, E. F. Tilden, A. J. Williams, Phys. Rev. 99 (1955) 1788.
- 5. V. R. Monaji, L. Abdellah, P. Sabin, D. Dibakar, Sci.rep. 7 (2017) 7395.
- 6. A. Muhammad, R. S. Turtelli, M. Kriegisch, R. Grossinger, F. Kubel, T. Konegger, J. Appl. Phys., 111 (2012) 013918.
- 7. I. C. Nlebedim, N. Ranvah, P. I. Williams, Y. Melikhov, J. E. Snyder, A. J. Moses, D. C. Jiles, J. Magn. Magn. Mater. 322 (2010) 1929–1933.
- 8. K. K. Mohaideen, P. A Joy, ACS Appl. Mater., 4 (2012) 6421–6425.
- 9. C. C. H. Lo; A. P. Ring, J. E. Snyder, D. C. Jiles, IEEE Trans. Magn., 41 (2005) 3676 -3678.
- 10. A. Rafferty, T. Prescott, D. Brabazon, Ceram. Int. 34 (2008) 15–21.

# CHAPTER 5 SUMMARY & CONCLUSIONS

### Chapter 5

### **Summary & Conclusions**

This chapter gives summary and conclusions of the results of the present work and also the scopes for future research in this area

### **Summary and conclusions:**

- ➤ Pure cubic spinel of AC-CFO, SS-CFO has been prepared in different magnetic fields of both parallel and perpendicular magnetic field assisted compaction.
- Average grain size of 3 μm to 5 μm has been observed for all AC-CFO samples prepared at different magnetic fields of both parallel and perpendicular magnetic field assisted compaction.
- ➤ Enhancement in magnetostriction, 33% (139 ppm to 185 ppm) and strain sensitivity, 40% (0.5×10<sup>-9</sup> m/A to 0.7×10<sup>-9</sup> m/A) have been observed for AC-CFO samples prepared by parallel magnetic field assisted compaction.
- ➤ A significant enhancement in magnetostriction, 89% (110 ppm to 207 ppm) and strain sensitivity, 141% (1.1×10<sup>-9</sup> m/A to 2.8×10<sup>-9</sup> m/A) have been observed for SS-CFO samples prepared by parallel magnetic field assisted compaction.
- ➤ Enhancement in magnetostriction, 22% (137 ppm to 167 ppm) and strain sensitivity, 40% (0.5×10<sup>-9</sup> m/A to 0.7×10<sup>-9</sup> m/A) have been observed for AC-CFO samples prepared by parallel magnetic field assisted compaction.
- ➤ A significant enhancement in magnetostriction, (113 ppm to 209 ppm) ~85% and strain sensitivity, 185% (0.9×10<sup>-9</sup> m/A to 2.5×10<sup>-9</sup> m/A) have been observed for SS-CFO samples prepared by parallel magnetic field assisted compaction.
- > Texture Coefficient of 2.2has been observed for (511) plane in cobalt ferrite sintered sample prepared at 1T parallel field.
- > Texture Coefficient of 1.6 has been observed for (440) plane in cobalt ferrite sintered sample prepared at 1.5T parallel field.

- ➤ CFO templates have been synthesized at different temperatures (700°C, 800°C, 900°C, 1000°C for 4h), different dwell time (4h, 12h and 24h) at 1000°C, and different ratios (1:1, 3:1, 5:1) for 1000°C, 24h.
- ➤ Preferential orientation of (511) plane has been observed for XRD pattern of SPR1 and SPR3 pellets.
- ➤ Oriented CFO can be prepared in both TGG and MAC techniques.
- > Oriented CFO can be prepared in both parallel and perpendicular MAC.
- ➤ Oriented CFO can be prepared with CFO synthesized by solid state method but not with the CFO synthesized by autocombustion method.
- > Small variation in magnetic properties has been observed for both AC-CFO and SS-CFO samples compacted under parallel and perpendicular MAC.
- ➤ Good magnetoelastic properties can be obtained for SS-CFO compacts synthesized in perpendicular MAC.
- ➤ Better magnetoelastic properties can be obtained for CFO samples, synthesized in MSS method followed by perpendicular MAC.
- ➤ In magnetic field assisted compaction, threshold magnetic field is required to impart orientation during compaction. Any magnetic field less than the threshold magnetic field cannot impart orientation in the CFO compact.

### **Future scope of work**

- > Texture analysis of SS-CFO textured samples by EBSD and XRD will be planned for future.
- > Investigation of magnetic and magneto elastic properties of oriented CFO prepared by gel casting and screen printing will be planned for future.
- ➤ Molten salt synthesis of CFO followed by magnetic field assisted compaction will be planned for future.



# Investigation of Magnetic and Magnetoelastic Properties of Oriented Cobalt Ferrite

by Srinivas Indla

Submission date: 29-Mar-2021 09:56AM (UTC+0530)

Submission ID: 1545082651

File name: Srinivas\_Indla.pdf (7.2M)

Word count: 20380 Character count: 105218

# Investigation of Magnetic and Magnetoelastic Properties of Oriented Cobalt Ferrite

ORIGINA	LITY REPORT			
2 SIMILA	2% RITY INDEX	5% INTERNET SOURCES	20% PUBLICATIONS	2% STUDENT PAPERS
PRIMAR	Y SOURCES			
1	Dibakar I propertie assisted	Indla, Arout Chel Das. "Enhanceme s of cobalt ferrite compaction tech d Compounds, 2	ent in magneto by magnetic nique", Journa	ostrictive field al of
2	scholarba	ank.nus.edu.sg	O v	School of Engineering Sciences and Ted  School of Engineering Sciences and Ted  University of Hyderabad 500 0
3	mafiadoo			1%
4	www.md			<1%
5	link.sprin			<1%
6	Shara So "Magneto	initha Reddy, J. I owmya, A. Sriniva o-electric propert O 4 -(1-x)(Ba 0.8	as, Dibakar Da ies of in-situ p	as. repared

# 0.9 )O 3 particulate composites", Ceramics International, 2016

Publication

7	Grunwald, A "Design of a magnetostrictive (MS) actuator", Sensors & Actuators: A. Physical, 20080528	<1%
8	MUKHLIS M. ISMAIL, NASMA A. JABER. "INFLUENCES OF CATION DISTRIBUTION OF ZINC SUBSTITUTED ON INVERSE SPINEL NICKEL FERRITE NANOPARTICLE FOR SUPERPARAMAGNETIC APPROACH", Surface Review and Letters, 2018 Publication	<1%
9	"Advanced Nanomaterials and Nanotechnology", Springer Science and Business Media LLC, 2013	<1%
10	Submitted to Savitribai Phule Pune University Student Paper	<1%
11	Monaji V. Reddy, Tanjore V. Jayaraman, Neeraj Patil, Dibakar Das. "Giant magnetoelastic properties in Ce-substituted and magnetic field processed cobalt ferrite", Journal of Alloys and Compounds, 2020	<1%

12	Dibakar Das. "Enhancement in magnetostrictive properties of cobalt ferrite by magnetic field assisted compaction technique", Journal of Alloys and Compounds, 2018 Publication	<1%
13	R.D Purohit, B.P Sharma, K.T Pillai, A.K Tyagi. "Ultrafine ceria powders via glycine-nitrate combustion", Materials Research Bulletin, 2001	<1%
14	Guangbin Ji, Xiaohui Lin, Yanyan Sun, Syed Ahmed Ali Trimizi, Hailin Su, Youwei Du. "Molten salt growth and magnetic properties of octahedral CoFe2O4 crystals: effects of synthesis conditions", CrystEngComm, 2011 Publication	<1%
15	T MAKAROVA. "Ferromagnetic Carbonaceous Compounds", Carbon Based Magnetism, 2006 Publication	<1%
16	baadalsg.inflibnet.ac.in Internet Source	<1%
17	etheses.whiterose.ac.uk Internet Source	<1%
18	S. Yuvaraj, N. Manikandan, G. Vinitha. "Influence of copper ions on structural and non-linear optical properties in manganese ferrite nanomaterials", Optical Materials, 2017 Publication	<1%

19	"The Earth's Magnetism", Springer Science and Business Media LLC, 2006 Publication	<1%
20	"Advances in Nanoscale Magnetism", Springer Science and Business Media LLC, 2009	<1%
21	Bhaskar B. Ghate, Alex Goldman. "Ferrimagnetic Ceramics", Wiley, 2006 Publication	<1%
22	Submitted to Jawaharlal Nehru Technological University Student Paper	<1%
23	Jun Sik Kim, Bhaskar Chandra Mohanty, Chan Su Han, Seung Jun Han, Gwang Heon Ha, Liwei Lin, Yong Soo Cho. "In Situ Magnetic Field-Assisted Low Temperature Atmospheric Growth of GaN Nanowires via the Vapor–Liquid–Solid Mechanism", ACS Applied Materials & Interfaces, 2013	<1%
24	Monaji Vinitha Reddy, Abdellah Lisfi, Sabin Pokharel, Dibakar Das. "Colossal piezomagnetic response in magnetically pressed Zr+4 substituted cobalt ferrites", Scientific Reports, 2017 Publication	<1%

25	N.M. Deraz. "Glycine-assisted fabrication of nanocrystalline cobalt ferrite system", Journal of Analytical and Applied Pyrolysis, 2010	<1%
26	www.freepatentsonline.com Internet Source	<1%
27	R. Blum, M. Audier, Y. Bréchet, F. Weiss, J. P. Sénateur, A. Rouault. "Decorations of magnetic flux pinning positions on the (001) face of a single crystal of high- superconductor YBa (Cu, Au) O ", Philosophical Magazine Letters, 1992	<1%
28	Engineering Ceramics '96 Higher Reliability through Processing, 1997.  Publication	<1%
29	G. L. Messing, S. Trolier-McKinstry, E. M. Sabolsky, C. Duran et al. "Templated Grain Growth of Textured Piezoelectric Ceramics", Critical Reviews in Solid State and Materials Sciences, 2004	<1%
30	Patil, B.B., and S. Basu. "Synthesis and Characterization of PdO-NiO-SDC Nano-powder by Glycine-Nitrate Combustion Synthesis for Anode of IT-SOFC", Energy Procedia, 2014. Publication	<1%